501394 1N-02
MF A08 CSCL 20N
175541
P122

NASA
Technical
Paper
3355

July 1993

Supersonic Aerodynamic Characteristics of an Advanced F-16 Derivative Aircraft Configuration

Mike C. Fox
and Dana K. Forrest

(NASA-TP-3355) SUPERSONIC AERODYNAMIC CHARACTERISTICS OF AN ADVANCED F-16 DERIVATIVE AIRCRAFT CONFIGURATION (NASA) 122 p

N93-31733

Unclas

H1/02 0175541

NASA

NASA Technical Paper 3355

1993

Supersonic Aerodynamic Characteristics of an Advanced F-16 Derivative Aircraft Configuration

Mike C. Fox
ViGYAN, Inc.
Hampton, Virginia

Dana K. Forrest
Langley Research Center
Hampton, Virginia

National Aeronautics and Space Administration
Office of Management
Scientific and Technical Information Program

Acknowledgments

The authors greatly appreciate the contributions of C. S. Stewart, B. W. Townsend, and A. J. Wood of the General Dynamics Corporation for their geometric definitions, reference information, and general technical insight concerning this investigation.

Contents

Summary

An investigation has been made at Mach numbers of 1.60 to 2.16 to determine the longitudinal and lateral-directional characteristics of an advanced aircraft configuration. The aircraft concept is a derivative of the United States Air Force F-16C multirole fighter. The basic (baseline) configuration concept incorporates the F-16 fuselage with a fixed-geometry inlet, single engine, single vertical tail, and modified wing. The F-16 40° trapezoidal wing has been replaced with a 50°, clipped-delta wing that features an integrated forebody strake and no horizontal tail. The wing camber surface was designed to provide optimized drag due to lift at transonic speeds while minimizing trim drag at supersonic speeds for efficient cruising capability. Aerodynamic comparisons are presented between the baseline configuration and the F-16C model and between the baseline configuration and a generic configuration that employs a similarly cambered wing. Several external store carriage options and two sensor fairings were also evaluated during the test.

The results indicate that the baseline configuration possessed linear pitching-moment characteristics and remained laterally stable through the Mach numbers and angles of attack tested. Directional stability is reduced at higher Mach numbers, but the stability is regained when lower surface ventral fins are added. Control surfaces that were incorporated in the model proved effective throughout the test range. Deflecting the inboard, multipurpose flaps improved the trimmed lift-drag ratio; and deflecting the leading-edge flaps 2° up lowered the minimum drag. Also, the baseline complement of simulated air-to-air missiles increased the minimum drag, but the lift and pitching-moment characteristics remained unchanged.

The derivative configuration showed the potential for increased sustained-g maneuvering capability in relation to the F-16C model because of the improved lift/drag; the derivative configuration also maintained comparable lateral-directional stability characteristics. Comparison of the data for the derivative configuration with those from a previously tested generic wing model indicated that the data trends agreed well—the differing aerodynamic characteristics were consistent with configuration differences.

Introduction

To support advanced military aircraft technology, the National Aeronautics and Space Administration (NASA) has conducted research related to highly maneuverable fighter aircraft. This report presents results of a supersonic wind tunnel investigation of the Falcon 21 configuration, which is an advanced derivative concept of the United States Air Force (USAF) F-16C fighter aircraft. Research was performed under a cooperative program between the NASA Langley Research Center and the General Dynamics Corporation, the original developer of the F-16 aircraft. The Falcon 21, referred to in this report as the baseline configuration, incorporates an F-16 fuselage with a new wing and blended forebody strake. The wing planform is a clipped delta with a leading-edge sweep of 50° and a trailing-edge sweep of −25°. The wing camber, in combination with scheduled leading- and trailing-edge control surfaces, was designed to minimize lift-dependent drag at a Mach number M of 0.90 for sustained-g maneuvering, while minimizing trimmed drag at supersonic cruise conditions. (A more detailed wing design criteria description was obtained from J. J. Azevedo and A. E. Sheridan, General Dynamics Corporation, Ft. Worth, Texas.) The research effort succeeded previous studies of a generic wing model with an identical planform shape and similar twist distribution (research performed by G. Hernandez, R. M. Wood, and P. F. Covell of the Langley Supersonic/Hypersonic Aerodynamics Branch). The aerodynamic characteristics of the baseline model were compared with those of the generic wing model to evaluate the aerodynamic effects of integrating the advanced generic wing planform into a realistic fighter aircraft configuration.

Longitudinal and lateral-directional force and moment data were obtained on a 1/15-scale model tested in the Langley Unitary Plan Wind Tunnel at Mach numbers of 1.60 to 2.16. These data were obtained to evaluate the basic performance parameters and control effectiveness of the configuration. Low-drag store carriage options and advanced sensor fairings were also investigated. The aerodynamic data for the baseline configuration were compared with those for the F-16C and generic wing models. The results from the wind tunnel investigation are summarized herein.

Symbols

The longitudinal aerodynamic coefficients are referenced to the stability-axis system and the lateral-directional coefficients are referenced to the body-axis system. Data coefficients for each model are reduced on their respective wing reference areas, unless otherwise noted. The data were reduced about

a moment reference center at 30 percent of the mean aerodynamic chord for the baseline configuration, 35 percent for the F-16C model, and 30 percent for the generic wing model. (See figs. 1–3.)

b	wingspan, in. (fig. 1)
BL	buttock line, in.
C_A	axial-force coefficient
C_D	drag coefficient, $\frac{\text{Drag}}{qS}$
C_{D_i}	internal drag coefficient, $\frac{\text{Internal drag}}{qS}$
ΔC_D	drag increment
CG	center-of-gravity location
C_L	lift coefficient, $\frac{\text{Lift}}{qS}$
C_{L_α}	lift-curve slope at $C_L = 0$
C_l	rolling-moment coefficient, $\frac{\text{Rolling moment}}{qSb}$
C_{l_β}	lateral stability derivative, $\frac{\partial C_l}{\partial \beta}, \frac{C_{l_{(\beta=+2°)}} - C_{l_{(\beta=-2°)}}}{4°}$, per deg
C_m	pitching-moment coefficient, $\frac{\text{Pitching moment}}{qS\bar{c}}$
C_N	normal-force coefficient
C_n	yawing-moment coefficient, $\frac{\text{Yawing moment}}{qSb}$
C_{n_β}	directional stability derivative, $\frac{\partial C_n}{\partial \beta}, \frac{C_{n_{(\beta=+2°)}} - C_{n_{(\beta=-2°)}}}{4°}$, per deg
C_Y	side-force coefficient, $\frac{\text{Side force}}{qS}$
C_{Y_β}	side-force derivative due to sideslip, $\frac{\partial C_Y}{\partial \beta}, \frac{C_{Y_{(\beta=+2°)}} - C_{Y_{(\beta=-2°)}}}{4°}$, per deg
c	streamwise local chord length, in.
$\bar{c}$	wing mean aerodynamic chord, in.
FS	fuselage station, in.
g	acceleration due to gravity, 32.17 ft/sec^2
HT	horizontal tail deflection angle measured parallel to free stream, positive (table V) trailing edge down, deg
INV	model inverted for flow angularity runs (table V)
IRST	infrared search and track sensors
LEF	leading-edge flap deflection angle measured parallel to free stream, positive leading edge down, deg
L	left side
L/D	lift-drag ratio
M	Mach number
MRC	moment reference center (fig. 1)
PF	pitch flap deflection angle measured normal to hinge line, positive trailing edge down, deg
p_o	stagnation pressure, psf
q	free-stream dynamic pressure, psf
R	right side
Re	unit Reynolds number, per ft
RUD	rudder deflection angle measured normal to hinge line, positive trailing edge left, deg
S	wing reference area, ft^2 (fig. 1)
TEF	trailing-edge flap (inboard and outboard) deflection angle measured normal to hinge line, positive trailing edge down, deg
TEFi	inboard trailing-edge flap deflection angle measured normal to hinge line, positive trailing edge down, deg
TEFo	outboard trailing-edge flap deflection angle measured normal to hinge line, positive trailing edge down, deg
T_o	stagnation temperature, °F
t/c	airfoil thickness-to-chord ratio
V.T.	vertical tail
v	variable angle of attack, table V
WL	waterline, in.
x/d	longitudinal spacing parameter for store carriage, calculated by $\frac{\text{Longitudinal distance between stores}}{\text{Diameter of store}}$
y	distance along wing semispan, in.
α	angle of attack, deg
β	angle of sideslip, deg

$\delta_{\text{FLAP}_{\text{req}}}$	trailing-edge flap deflection required for trim, positive trailing edge down, deg
η	fraction of wing semispan, $y/(b/2)$
Subscripts:	
max	maximum
min	minimum
ref	reference
tr	trimmed

Test Information

Description of Models

Two 1/15-scale models were tested during this investigation. The models were scaled representations of a USAF F-16C aircraft and an advanced derivative called Falcon 21 and referred to as the baseline model in this report. Three-view drawings of the models are shown in figures 1 and 2 and characteristic descriptions are given in tables I and II to illustrate the geometric differences between the two configurations. Photographs of the baseline model (Falcon 21) installed in the Unitary Plan Wind Tunnel are found in figure 4.

The baseline model incorporated a cambered fuselage with a normal shock inlet, flow-through duct, clipped-delta wing, and single vertical tail. A zero-boattail nozzle position provided adequate clearance for the internal balance and sting arrangement without the need to distort the external geometry of the model. The configuration employed a constant-chord, full-span leading-edge flap bounded between the fraction of the wing semispan $\eta = 0.264$ and $\eta = 1.0$ and trailing-edge inboard and outboard flaps. Fuselage shelf-mounted pitch flaps were available for either speedbrake or pitch control. All aft control surfaces could be deflected from $-30°$ to $30°$, and the leading-edge flaps could be deflected from $-2°$ to $25°$.

The baseline model can simulate external store carriage options. This configuration carried four semisubmerged AIM-120 advanced medium-range air-to-air missile (AMRAAM) models on the lower fuselage/wing blend at buttock line BL 2.767. The mounting incorporated the low-drag, tandem-carriage concept similar to that described in reference 1. Because the model did not have cavities for the AIM-120 missiles, the simulated missiles represented only the exposed portion of the missiles and were mounted flush to the bottom of the model. The forward AIM-120 missiles had larger frontal areas than the aft missiles because of the waterline orientation of the missiles and the receding strake contour design. The configuration also carried a permanent, dual-purpose pylon at 63 percent of the wing semispan (BL 8.800) that would house the outboard flap actuator for the actual aircraft in addition to carrying external stores. The baseline configuration also carried a simulated AIM-9L Sidewinder missile on each permanent pylon. The investigation also included the effect of two 600-gal fuel tanks under the wing at 37 percent of the wing semispan, as illustrated in figure 5.

The F-16C wind tunnel model (fig. 2) used the same fuselage and vertical tail as the baseline model. The ventral fin, located on the fuselage lower surface of the F-16C, was also tested on the baseline model. The trapezoidal wing for the F-16C model employed full-span leading-edge flaps and a single-surface trailing-edge flap. The trailing-edge flap was capable of being deflected from $-20°$ to $20°$, and the leading-edge flap was capable of being deflected from $-2°$ to $25°$. The F-16C configuration carried a simulated AIM-9J Sidewinder missile and launcher on each wing tip.

The baseline model was similar to the previously tested generic wing model shown in figure 3. The geometry of the two configurations is compared in figure 6. The wings have an identical planform shape with similar camber-twist distributions. The cambered wing geometry for the generic wing model was derived by a supersonic optimal camber design procedure that uses linear lifting-surface theory to compute a self-trimming camber shape with minimum lift-dependent drag (ref. 2). The baseline model used the same wing geometry as the generic wing model but with reduced spanwise twist to maintain the two-segment trailing-edge flap hinge lines within the wing contour. The generic wing configuration could accommodate the original twist distribution because it used a three-segment trailing-edge flap system. The trailing-edge flap hinge-line sweeps were equal for both models, the trailing-edge flap area for the baseline configuration constituted 11.14 percent of its reference planform area compared with 12.2 percent for the generic wing model. Another configuration difference was a blended forebody strake for the baseline rather than the $65°$ swept inboard wing extension for the generic model. The most pronounced difference between models was the fuselage. The Falcon 21 incorporated the F-16C fuselage model with a flow-through duct, whereas the fuselage for the generic wing model did not have an inlet, duct, canopy, or vertical tail. However, the generic fuselage did

contain a forebody camber that represents typical fighter aircraft.

Wind Tunnel Facility and Test Conditions

The test was conducted in the Unitary Plan Wind Tunnel. The tunnel is a continuous-flow, supersonic tunnel in which Mach number and pressure can be varied and has test section dimensions of approximately 4 by 4 ft. A comprehensive description of this facility is presented in reference 3. Test section 1 was used for this test to obtain data at $M = 1.60$, 1.80, 2.00, and 2.16. The primary Reynolds number Re was 2.0×10^6/ft; however, selected runs were made at $Re = 1.5 \times 10^6$ and 4.0×10^6/ft. A complete listing of the wind tunnel test conditions is contained in table III.

The angle of attack α was varied from $-4°$ to 20° at sideslip angles $\beta = -2°$, 0°, 2°, 5°, and 7.5°. Also, β was varied from $-7.5°$ to 7.5° at selected angles of attack. To ensure fully turbulent boundary-layer flow conditions, transition strips composed of No. 60 sand were applied on the upper and lower lifting surfaces of each model and on the nose, nacelle, vertical tail, and ventral fins, as illustrated in figure 7. The transition particle size and location were selected according to the methods discussed in references 4–6.

Aerodynamic forces and moments on the models were measured with an internal six-component strain gauge balance, which was attached to a sting that was rigidly fastened to the tunnel support system. Coefficient accuracies for the six balance components at the Mach numbers tested and the primary Reynolds number are contained in table IV. Balance chamber static pressures were measured concurrently with force data by pressure tubes at fore and aft positions in the balance cavity. The drag data have been corrected to the condition of free-stream static pressure in the balance chamber. Internal flow corrections from a previous F-16 test entry were applied directly to the F-16C drag data. For the baseline model, the same internal drag coefficients were re-referenced to the proper wing area and applied. Values of the internal drag coefficients, shown in figure 8, were used to correct the drag data. No base drag corrections were made for either model. Angle-of-attack corrections for each model have been made for tunnel flow angularity and for balance and sting deflections under aerodynamic load.

Discussion of Results

The technical discussion is divided into three major sections. The first section covers the basic aerodynamic characteristics for the baseline model (Falcon 21), including effects of store carriage and sensor fairings. This section is the primary portion of the results and is more detailed than the other two sections. The second section addresses the comparison of the baseline model configuration with the F-16C model. The third section compares the longitudinal characteristics of the baseline model with those of the cambered generic wing model.

The results presented in the following figures are for $Re = 2.0 \times 10^6$/ft; however, aerodynamic coefficient data for all test conditions are tabulated in the supplement, which is recorded on microfiche and attached to the inside back cover. The nomenclature definitions for the tabulated coefficient data are also included in the supplement. The test run log, table V, lists all the configurations tested and their associated run numbers for the baseline model and F-16C experimental investigation.

Baseline Model Characteristics

Longitudinal aerodynamic characteristics. Longitudinal aerodynamic characteristics at various trailing-edge flap deflections are shown in figure 9. The configuration exhibits a nearly linear pitching-moment variation at all Mach numbers. The lift curves are also linear for $\alpha \leq 6°$; however, a negative gradient in the lift-curve slope is evident for $\alpha > 6°$, which indicates the beginning of flow separation on the wing.

The trimmed aerodynamic characteristics for the baseline configuration are found in figure 10. The data were trimmed about a center-of-gravity location of 0.30 of the mean aerodynamic chord $\bar{c}$. This location corresponds to a subsonic static margin of -3.2 percent $\bar{c}$, which is reasonable for a current fighter design. For the specified reference point, the analysis shows that the configuration is trim limited at $\alpha = 11°$ to 13°, depending on Mach number. To determine whether the trim limit would hinder the performance envelope of the aircraft, a simple calculation of maximum attainable g units was made. If a typical mid-combat weight for this class of vehicle is 30 000 lb, for flight at 30 000 ft the trimmed wind tunnel data for the Falcon 21 configuration show a capability of $9.0g$ at $M = 1.60$, which would approach the structural limit of current fighters. Therefore, based on the rigid model data, the aircraft would have more than adequate trim control power for symmetric maneuvers in this Mach number range.

Pitch flap effectiveness. The baseline configuration incorporates trailing-edge control surfaces referred to as pitch flaps. (See fig. 1.) These pitch

flaps can be scheduled independently or in conjunction with the other trailing-edge surfaces or can be used as a clamshell speedbrake similar to that used on the F-16. For this investigation, both upper and lower surfaces of the pitch flaps were deflected as a unit. These control surfaces were tested to determine whether their use, in conjunction with the trailing-edge flaps, benefited supersonic trim characteristics. Two combinations of pitch flap/trailing-edge flaps (both of which are for PF/TEF = $-10°$ to $-30°$) were tested to evaluate the longitudinal effects.

The effect of augmenting the trailing-edge flaps with pitch flap deflection is shown in figure 11. The plotted untrimmed data show effects in lift, drag, and pitching moment for all Mach numbers. The deflection of the pitch flaps caused a decrease in lift at all Mach numbers tested. As expected, the pitch flap deflection produced a positive pitching-moment increment that remained linear for the angles of attack tested. The effect on drag was small for PF = $-10°$ and remained essentially constant throughout the lift range. For PF = $-30°$, the drag increment was larger and increased with lift. The pitching-moment, lift, and drag increments that resulted from pitch flap deflection decreased slightly with increased Mach number.

Although the untrimmed drag characteristics showed a slight increase in drag with pitch deflection, the trimmed results presented in figure 12 show that the positive shift in zero-lift pitching moment resulted in a lower required flap deflection for trim and in a slight reduction in drag; however, no change in lift was evident compared with use of the trailing-edge flaps alone. The maximum pitch flap deflection tested expanded the trim envelope, which allowed higher trimmed lift through the increased moment generated by the control surfaces. All data contained in figure 12 are trimmed values; however, because of the limited data acquired when the pitch flaps were deflected in conjunction with the trailing-edge flaps, those discrete trim points are illustrated by symbols. The test results indicate that deflection of pitch flaps might be advantageous on this configuration, but further investigation is needed to determine the optimal deflection schedule relative to the trailing-edge flap position.

Uprigged leading-edge flap. As discussed earlier, the wing camber distribution was designed to provide the best compromise between transonic sustained-g maneuver capability and minimum supersonic trim drag at cruise conditions. To further minimize cruise drag, uprigged leading-edge flaps (i.e., leading edge up) were explored based on positive results for the previously tested generic wing model. In the earlier tests, the generic wing model was evaluated with the leading-edge flaps deflected at $-2°$ and $-4°$, and the deflection setting of $-2°$ was more beneficial than the settings of $0°$ and $-4°$. Because of the similar camber distributions between the baseline configuration and the generic wing model, the leading-edge deflection angle LEF = -2 was chosen to test on the baseline. Results from this test indicated that uprigging the leading-edge flaps for the baseline model reduced the minimum drag by 5 to 7 counts (i.e., $\Delta C_D = 0.0005$ to 0.0007) across the supersonic Mach number range. (See fig. 13.) Data for the uprigged flap configuration presented in figure 14 show a slight lift increase with a corresponding nose-up pitching moment at lift coefficient $C_L \leq 0.40$. The lift-curve slope remained unchanged, but a translation of lift curves occurred. The trimmed longitudinal characteristics, shown in figure 15, illustrate that the reduction in drag at low lift conditions that resulted from the uprigged leading-edge flaps was retained for the selected trim condition.

Lateral-directional aerodynamic characteristics. Figure 16 shows the variation of the yawing-moment, rolling-moment, and side-force coefficients with sideslip angle at selected angles of attack and free-stream Mach numbers of 1.60, 1.80, and 2.00. Variations of rolling moment and side force are small with respect to α for the Mach numbers tested. The yawing moment shows a destabilizing trend with increasing α and M. For the angles of attack tested, the configuration remains directionally stable except at $\alpha = 15°$ for $M = 1.80$ and 2.00. (See figs. 16(b) and 16(c).)

During this investigation, the vertical tail was removed to determine the contribution of that component to the lateral-directional characteristics of the baseline configuration. Lower surface ventral fins, identical in size and location to those of the F-16C model, were also tested to determine the effect on directional stability. The contribution of the vertical tail and the ventral fins at $\alpha = 0°$ to the yawing-moment, rolling-moment, and side-force coefficients as a function of sideslip angle is shown in figure 17. Figure 18 shows the data as derivatives reduced for $\beta = \pm 2°$ at selected angles of attack. The data are sufficiently linear in the selected sideslip range to provide accurate derivative calculations. Symbols were included in this figure because the derivatives were obtained from data taken at the indicated angles of attack. Figures 17 and 18 clearly show that the vertical tail-off configuration is directionally unstable and has nearly neutral lateral stability at all Mach numbers and angles of attack.

The baseline configuration becomes directionally unstable at $\alpha > 15°$ for $M = 1.80$ and at $\alpha > 10°$ for $M = 2.00$. The addition of the ventrals to the baseline configuration shows an increase in directional stability at all Mach numbers and angles of attack with little or no effect on lateral stability. With the lower surface ventral fins, the configuration remains directionally stable throughout the tested range.

Differential flap effectiveness. The variation of yawing-moment, rolling-moment, and side-force coefficients with α for the baseline configuration at selected trailing-edge flap roll-control deflection combinations is shown in figure 19. The results indicate adverse yaw with rolling moment when the trailing-edge surfaces are deflected in the positive direction and favorable yaw when they are deflected in the negative direction. Deflections were made on one side only to reduce the rolling-moment load on the balance. In actual flight, the trailing-edge flaps would be scheduled for both sides. The roll-control effectiveness of the baseline configuration can be approximated by the superposition of the moments in figure 19.

External Store Carriage

Air-to-air missile carriage. The baseline model was tested with four semisubmerged AIM-120 AMRAAM missiles and two AIM-9L Sidewinder missiles. The perceived advantages for this primary missile carriage option and the evaluation of a forward missile fairing are discussed in this section. The effects on the longitudinal aerodynamic characteristics of adding these simulated missiles to the clean (i.e., no stores) aircraft are shown in figure 20. The addition of either set of missiles is shown not to affect the lift and pitching-moment characteristics for the Mach numbers tested. However, the drag of the configuration, especially the minimum drag, is increased when the missiles are added. Because the missiles have no significant effects on the other parameters, only the effects on minimum drag will be presented for the remaining missile data. The baseline model with the missiles is illustrated in figure 21 and the increments in minimum drag associated with these missiles added to a clean aircraft for supersonic Mach numbers are shown in figure 22.

The Falcon 21 configuration was designed to carry the AIM-120 missiles in a manner that submerged a large portion of missile volume within the aircraft; also, much of the exposed volume of the missile is submerged in the aircraft boundary layer to reduce drag. The drag at low lift conditions is an important parameter because the increased drag will decrease the cruising range. Data from other investigations (refs. 7 and 8) confirm that the drag can be significantly reduced if the semisubmerged carriage option is used. Other advantages or possible disadvantages to this type of carriage are discussed in references 7 and 8.

In addition to being semisubmerged, the missiles were mounted in tandem to provide aerodynamic shielding. (See refs. 7 and 8.) The AIM-120 missiles were installed in a closely spaced ($x/d = 0.345$), inline arrangement (fig. 23) to maximize the shielding from the blunt aft end of the forward store and maintain adequate clearance to operationally launch the missiles from the full-scale aircraft. The increments in minimum drag are shown in figure 24 for the forward AIM-120 missiles alone and with the addition of the aft AIM-120 missiles. The shielding clearly allows the aft missiles to be carried at a significantly smaller penalty than would occur for unshielded aft missiles.

As mentioned earlier, the forward-mounted AIM-120 missiles had larger exposed frontal areas than the aft-mounted missiles. The waterline orientation of the missiles, in combination with the receding strake contour, created a gap between the front portion of the missiles and the lower contour of the model. The gap exposed the entire missile circumference for 37 percent of the length of the forward missiles. Fairings, shown in figure 25, were installed to fill the gap between the missiles and the lower wing-shelf contour and to assess the impact on drag. Similar fairings were tested in an earlier low-speed wind tunnel entry and results showed that the addition of the fairings had a negligible effect on drag at subsonic conditions (private communication from M. E. Jacobson, General Dynamics Corporation, Ft. Worth, Texas). The supersonic results (fig. 26) showed an increase in minimum drag of approximately 2 to 4 counts ($\Delta C_D = 0.0002$ to 0.0004) for the fairings in the Mach number range tested. The measured drag increments were only slightly larger than the balance accuracy quoted in table IV but are adverse. Because the fairings were constructed to only roughly simulate a feasible design, a more refined aerodynamic design or reorientation of the forward missiles might reduce the drag by reducing the frontal area or improving the adjacent flow patterns.

600-gal fuel tanks. The model was tested with two simulated 600-gal fuel tanks installed at BL 5.1333 (fig. 5) to assess their influence on the aerodynamic characteristics at supersonic speeds. The fuel tanks would extend the mission range significantly and could be carried with a complement of air-to-air or air-to-ground stores. For current

aircraft, the tanks are generally flown subsonically to obtain the best range but are rated to fly supersonically (to $M = 1.60$) if needed.

The longitudinal test results (fig. 27) show that lift, drag, and pitching moment are significantly affected by the tanks because they cause a lift loss that increases slightly as α increases. The lift loss is nearly a constant increment for low angles of attack (i.e., $\alpha < 7$ for $M = 1.60$ and $\alpha < 5$ for $M = 1.80$), whereas the lift more rapidly decreases for higher angles of attack. A positive shift in zero-lift pitching moment and a decrease in static longitudinal stability are associated with the tanks. This reduction in stability is likely a result of flow separation on the wing. The supersonic drag increment for the tanks is nearly 40 percent of the minimum drag for the baseline configuration.

Sensor Fairings

Two sensor fairings (fig. 28) were investigated to assess their effect on the longitudinal aerodynamic characteristics. The fairings simulated two possible Infrared Search and Track (IRST) sensor housings and locations for the Falcon 21 aircraft. The wind tunnel data showed no change in lift or pitching moment, but did show a small increase in minimum drag, as illustrated in figure 29. The drag increase was smaller than expected, which suggests that local flow interactions, such as with the canopy, could minimize the drag of the fairings. Further studies are needed to understand the flow mechanisms present.

Comparison of Baseline Model With F-16C Model

Longitudinal aerodynamic characteristics. This section briefly compares the untrimmed longitudinal aerodynamic characteristics of the baseline configuration with the F-16C model in figures 30–33. The data shown in figures 30 and 31 have been reduced about their respective reference wing areas (see tables I and II) and expected operational center-of-gravity (CG) locations (i.e., Falcon 21: 30 percent $\bar{c}$; F-16C: 35 percent $\bar{c}$). Data for both configurations are with the leading-edge flaps deflected 2° up and data for the F-16C model are with the trailing-edge flap deflected 2° up, also. These settings were chosen because of the aerodynamic improvement shown for the baseline configuration (figs. 13–15) and because the standard operational flap setting for the F-16C aircraft during supersonic flight is LEF = −2° and TEF = −2°. The baseline configuration was tested with AIM-9L missiles. The F-16C model was tested with the AIM-9J missiles to maintain a consistent tie-in configuration with previous tests.

The basic aerodynamic characteristics of the two configurations at a representative $M = 1.60$ are shown in figure 30; the minimum drag, maximum lift-drag ratio L/D, and lift-curve slope trends with Mach number are summarized in figure 31. The F-16C configuration has a higher lift-curve slope and a lower lift-dependent drag coefficient (i.e., $C_D - C_{D_{min}}$) mainly because of its lower wing sweep and higher aspect ratio. Minimum drag coefficient for the baseline configuration is lower than for the F-16C model, offsetting the lower lift and higher lift-dependent drag coefficients to give the baseline configuration a substantially higher lift-drag ratio than the F-16C model for $C_L < 0.4$. As mentioned previously, each set of data was referenced on its own wing reference area. The F-16C model has other lifting surfaces (i.e., horizontal tails, forebody, and shelf areas) that are not included in the reference area. If the data were reduced about a weighted planform area reference for each configuration, the magnitudes of lift-curve slope and drag differences discussed above would likely be smaller.

Whereas the data in figures 30 and 31 show aerodynamic comparisons, the data in figures 32 and 33 show a comparison of the two aircraft configurations on a performance basis. To compare the configurations consistently, the F-16C data were re-referenced to the Falcon 21 geometry. The basic aerodynamic characteristics of the two configurations reduced with a common reference geometry are shown in figure 32 for $M = 1.60$. Minimum drag, maximum L/D, and lift-curve slope trends with Mach number for the configurations are summarized in figure 33. The data reduced with the common reference geometry show that the F-16C configuration now has a lower lift-curve slope and higher lift-dependent drag coefficient (i.e., $C_D - C_{D_{min}}$) relative to the baseline configuration. Although the baseline configuration has a higher minimum drag coefficient than that of the F-16C because of skin friction associated with the larger wing and shelf area, it generates greater lift and L/D than the F-16C for $C_L > 0.15$ for $M = 1.60$.

Lateral-directional comparisons. The static lateral-directional stability characteristics of the baseline configuration are compared with those of the F-16C in figure 34. As reported earlier, the configurations are quite similar with a common fuselage and vertical tail. To compare the configurations on a consistent basis, the F-16C data were re-referenced to the baseline model geometry and the data for both configurations were reduced about the body-axis system at a common moment reference location. The moment reference location (fuselage station FS 21.683) relates to $0.30\bar{c}$ for the baseline

configuration and $0.384\bar{c}$ for the F-16C model. The data were reduced at a common fuselage location to show the direct influence of the wing on the static stability characteristics. The sensitivity of the moment reference location for the F-16C model at the operational CG of $0.35\bar{c}$ versus the common reference location of $0.384\bar{c}$ was evaluated; however, the effects on stability characteristics were negligible.

As illustrated in figure 34, the baseline configuration has slightly more lateral stability than does the F-16C model at $\alpha = 0°$ and $M = 1.60$ and has nearly the same level of stability as the F-16C at $M = 2.00$. The directional stability level for the baseline configuration is slightly lower than that of the F-16C for both Mach numbers examined. The difference in stability can be attributed to the fact that the F-16C has lower surface ventral fins. Addition of ventrals to the baseline model (also see figs. 17 and 18) provides a comparable level of directional stability.

Comparison of Baseline Model With Generic Wing Model

This section presents a comparison of the untrimmed and trimmed longitudinal aerodynamic characteristics of the baseline configuration with those of the generic wing model. The configurations have identical wing planforms, in addition to other similarities, as discussed in "Description of Models." The objective of this comparison was to determine the effects of integrating the generic wing planform onto a realistic fighter aircraft fuselage. Because of the small differences in the spanwise twist distribution between the two wings, the results reflect wing twist differences along with other integration effects. These integration effects are representative of typical design compromises but do not necessarily reflect all trades that must be addressed in design optimization.

The data for both configurations are presented for a moment reference center at 30 percent of their individual mean aerodynamic chords so that pitching-moment characteristics could be compared. The leading-edge flaps for both models were deflected up 2° while the trailing-edge flaps remained undeflected.

Untrimmed comparisons. The lift, pitching-moment, and lift-dependent drag characteristics of the two configurations at the tested Mach numbers are compared in figure 35. A translation of lift curves is evident there, as well as a zero-lift pitching-moment shift between the two models that is likely attributable to the wing twist and body camber differences. The baseline configuration exhibits slightly higher lift-curve slopes and slightly more stable pitching-moment characteristics than does the generic wing model. The lift-dependent drag curves show little difference between the configurations at $M = 1.60$; however, at higher Mach numbers the baseline configuration shows lower untrimmed lift-dependent drag than the generic wing model.

Trimmed comparisons. The trimmed aerodynamic characteristics for the baseline configuration and the generic wing model are shown in figure 36. The baseline configuration exhibited higher trimmed lift-dependent drag because of the larger pitching-moment increment required to trim at a given lift condition. A larger trailing-edge flap deflection was required for the baseline configuration not only to counter the larger pitching moment, but also to compensate for the baseline model having a 10-percent smaller ratio of trailing-edge flap area to wing area than the other model. (See "Description of Models.")

Concluding Remarks

An experimental investigation was conducted in the NASA Langley Unitary Plan Wind Tunnel to evaluate the supersonic characteristics of an advanced F-16 derivative aircraft concept designated Falcon 21. Force and moment data were obtained at Mach numbers of 1.60 to 2.16 and angles of attack of −4° to 20°. The baseline configuration was tested with various control surface deflections in addition to selected external store loadings and other configuration variables. The baseline configuration was also compared with test results from the United States Air Force F-16C model and the previously tested generic wing research model.

The results indicate that the baseline configuration possessed linear pitching-moment characteristics and remained laterally stable throughout the range of Mach numbers and angles of attack tested. Directional stability was reduced at higher Mach numbers, but the stability was regained when lower surface ventral fins were added.

Deflection of various control surfaces was shown to benefit aerodynamic performance of the baseline configuration. Deflecting the pitch flap surfaces to aid in trimming improved the lift-drag ratio by reducing trim drag while minimally affecting lift. In addition, the pitch flaps can provide higher trimmed lift because the flap surfaces increase the generated pitching moment. Deflection of the leading-edge flaps 2° up reduced the minimum drag.

Several air-to-air external store carriage options and two sensor fairings were examined on the baseline model during this study. The data indicated that the addition of the simulated missiles increased minimum drag but did not change the lift and pitching-moment

characteristics. The AIM-120 missiles were mounted in tandem to provide aerodynamic shielding. The results showed that the shielding allowed the aft missiles to be carried at a significantly smaller penalty to the minimum drag than would occur for unshielded aft missiles. One forward missile fairing was evaluated and found not to be aerodynamically beneficial. Two protuberances, representing possible sensor fairing geometries and locations, were tested on the baseline configuration. The fairings showed smaller drag penalties than expected. However, additional study is needed to understand the local flow mechanisms present.

A comparison of the untrimmed supersonic aerodynamic characteristics of the baseline model with those of the F-16C configuration showed that the F-16C has a higher lift-curve slope and lower lift-dependent drag mainly because of the lower wing sweep and higher aspect ratio. However, the minimum drag for the Falcon 21 is lower, offsetting the lower lift and higher lift-dependent drag, which gives the baseline configuration a substantially higher lift-drag ratio than that of the F-16C for lift coefficients below 0.4. When the two configurations are reduced on common reference geometry, the baseline configuration shows higher lift/drag than the F-16C after the effects of the lower minimum drag coefficient for the F-16C are surpassed. The lateral-directional data indicate that both aircraft configurations possess similar lateral stability levels and, when ventral fins are added to the baseline configuration, the directional stability level is comparable to that of the F-16C model.

Comparison of the baseline model data with those from the previously tested generic wing model to evaluate effects of integrating a generic wing planform into a realistic fighter concept indicated that the data trends agreed well. The differences in the aerodynamic characteristics were consistent with the modifications to the wing twist distribution and to other configuration differences.

NASA Langley Research Center
Hampton, VA 23681-0001
April 21, 1993

References

1. Finley, D. B.: *Final F-16XL Aerodynamic Status Report and Flight Test Results.* 400 PR 139 (Contract F33657-78G-0004-0009), General Dynamics, Fort Worth Div., Sept. 1985.

2. Kulakowski, L. J.; Stancil, R. T.; Dansby, T.; and Stewart, J. D.: Design of Efficient, Self-Trimming Wing Mean Surfaces for Conventional Supersonic Aircraft. IAS Paper No. 59-116, June 1959.

3. Jackson, Charlie M., Jr.; Corlett, William A.; and Monta, William J.: *Description and Calibration of the Langley Unitary Plan Wind Tunnel.* NASA TP-1905, 1981.

4. Braslow, Albert L.; Hicks, Raymond M.; and Harris, Roy V., Jr.: *Use of Grit-Type Boundary-Layer-Transition Trips on Wind-Tunnel Models.* NASA TN D-3579, 1966.

5. Stallings, Robert L., Jr.; and Lamb, Milton: *Effects of Roughness Size on the Position of Boundary-Layer Transition and on the Aerodynamic Characteristics of a 55° Swept Delta Wing at Supersonic Speeds.* NASA TP-1027, 1977.

6. Wassum, Donald L.; and Hyman, Curtis E., Jr.: *Procedures and Requirements for Testing in the Langley Research Center Unitary Plan Wind Tunnel.* NASA TM-100529, 1988.

7. Wilcox, Floyd J., Jr.: Tangential, Semisubmerged, and Internal Store Carriage and Separation at Supersonic Speeds. AIAA-91-0198, Jan. 1991.

8. Frost, R. C.; and Miles, J. B.: *Effects of External Stores on the Aerodynamic Characteristics of Aircraft.* FZM-5044, General Dynamics, Fort Worth Div., Mar. 12, 1968.

Table I. Geometric Characteristics of Baseline Model

(a) Component geometry

Wing:	
Theoretical area (reference), ft^2	2.800
Span, in.	27.753
Aspect ratio	1.910
Taper ratio	0.1168
Mean aerodynamic chord, in.	17.555
Leading-edge sweep, deg	50.000
Trailing-edge sweep, deg	−25.000
Airfoil section	NACA 64A modified biconvex
Airfoil thickness-to-chord ratio t/c (root/tip), percent	2.5/4.5
Vertical tail:	
Area, ft^2	0.243
Exposed span, in.	6.733
Aspect ratio	1.294
Mean aerodynamic chord, in.	5.470
Leading-edge sweep, deg	47.500
Airfoil section	Biconvex
Airfoil thickness-to-chord ratio t/c (root/tip), percent	5.3/3.0
Ventral fins (tested, but not baseline):	
Area, ft^2 (both sides)	0.071
Exposed span, in. (actual)	1.833
Aspect ratio (theoretical)	0.472
Mean aerodynamic chord, in.	3.321
Leading-edge sweep, deg	30.000
Vertical cant angle (tip outboard)	15.000
Airfoil section	3.89-percent modified wedge/constant 0.004 radius
Inlet area, in^2	3.674
Exit area, in^2	2.766
Chamber area, in^2	3.243

(b) Wetted areas and reference lengths

Component	Wetted area, ft^2	Reference length, in.
Fuselage	3.814	38.013
Wing	3.360	17.555
Vertical tail	0.572	5.470

Table II. Geometric Characteristics of F-16C Model

(a) Component geometry

Wing:	
Theoretical area (reference), ft^2	1.3333
Span, in.	24.000
Aspect ratio	3.000
Taper ratio	0.2275
Mean aerodynamic chord, in.	9.056
Leading-edge sweep, deg	40.000
Trailing-edge sweep, deg	0.000
Airfoil section	NACA 64A204
Airfoil thickness-to-chord ratio t/c (root/tip), percent	4.000
Horizontal tails (exposed):	
Area, ft^2 (both sides)	0.283
Semispan, in.	4.642
Aspect ratio (each side)	1.058
Mean aerodynamic chord, in.	4.725
Leading-edge sweep, deg	40.000
Dihedral angle, deg	−10.000
Airfoil section	Biconvex
Airfoil thickness-to-chord ratio t/c (root/tip), percent	6.00/3.50
Vertical tail:	
Area, ft^2	0.243
Exposed span, in.	6.733
Aspect ratio	1.294
Mean aerodynamic chord, in.	5.470
Leading-edge sweep, deg	47.500
Airfoil section	Biconvex
Airfoil thickness-to-chord ratio t/c (root/tip), percent	5.30/3.00
Ventral fins:	
Area, ft^2 (both sides)	0.071
Exposed span, in. (actual)	1.833
Aspect ratio (theoretical)	0.472
Mean aerodynamic chord, in.	3.321
Leading-edge sweep, deg	30.000
Vertical cant angle (tip outboard), deg	15.000
Airfoil section	3.89-percent modified wedge/constant 0.004 radius
Inlet area, in^2	3.674
Exit area, in^2	2.766
Chamber area, in^2	3.243

(b) Wetted areas and reference lengths

Component	Wetted area, ft^2	Reference length, in.
Fuselage	3.448	38.013
Wing	1.516	9.056
Horizontal tails	0.568	4.725
Vertical tail	0.572	5.470
Ventral fins	0.136	3.321

Table III. Wind Tunnel Test Conditions

[$T_o = 125°F$ for all runs]

M	p_o, lb/ft^2	Re, ft^{-1}
1.60	809	1.5×10^6
1.80	866	1.5×10^6
2.00	940	1.5×10^6
1.60	1079	2.0×10^6
1.80	1154	↓
2.00	1253	↓
2.16	1349	↓
1.60	2157	4.0×10^6
1.80	2308	↓
2.00	2507	↓
2.16	2699	↓

Table IV. Coefficient Accuracy[a]

[$Re = 2.0 \times 10^6$/ft]

	Nominal error for—					
M	C_N	C_A	C_m	C_l	C_n	C_Y
1.60	0.0009	0.0002	0.0021	0.0004	0.0006	0.0004
1.80	0.0009	↓	0.0021	↓	↓	↓
2.00	0.0010	↓	0.0022	↓	↓	↓
2.16	0.0010	↓	0.0022	↓	↓	↓

[a]The nominal error of the force and moment coefficients obtained from the six-component strain gauge balance measurements is based on a statistical average of balance calibration loads; however, based on limited data repeatability checks and data trends, the incremental accuracy of the data is believed to be better than that indicated by these nominal values.

Table V. Wind Tunnel Test Run Log

Configuration			Control surface deflections					Model attitude		Run number at M—				Notes
Config.	Batch	Description	LEF	TEFi (L/R)	TEFo (L/R)	PF	RUD	α	β	1.60	1.80	2.00	2.16	
F-16C baseline with AIM-9J missiles on wingtip launchers (1 per side); BL 8.800[a]														
1	1	F-16C baseline	−2	−2		HT = 0	0	v	0	1	4	6	9	
1	1		−2	−2		HT = 0	0	0	v	12		8		
1	2		−2	−2		HT = 0	0	v	0	2	5	7	10	Model inverted
Falcon 21 baseline with AIM-120 missiles at BL 2.767 and AIM-9L (1 per side); BL 8.800[b]														
2	6	Falcon 21 baseline	−2	0	0	0	0	v	0	35	36	37	38	
3	3		↓	10	10	↓	↓	↓	↓	23	24	25	26	
4	4		↓	−10	−10	↓	↓	↓	↓	27	28	29	30	
5	5		↓	−20	−20	↓	↓	↓	↓	31	32	33	34	
6	7		0	0	0	↓	↓	↓	↓	39	49	59	69	
6	8		↓	↓	↓	↓	↓	↓	↓	40	50	60	70	Model inverted
7	18		↓	↓	↓	↓	↓	↓	↓	107	108	109	110	Repeat configuration
7	18		↓	↓	↓	↓	↓	↓	↓	111	112	113	114	$Re = 4.0 \times 10^6$
6	7		↓	↓	↓	↓	↓	↓	−2	41	51	61		
6	7		↓	↓	↓	↓	↓	↓	2	42	52	62		
6	7		↓	↓	↓	↓	↓	↓	5	43	53	63		
6	7		↓	↓	↓	↓	↓	↓	7.5	44	54	64		
6	7		↓	↓	↓	↓	↓	0	v	45	55	65		
6	7		↓	↓	↓	↓	↓	5	↓	46	56	66		
6	7		↓	↓	↓	↓	↓	10	↓	47	57	67		
6	7		↓	↓	↓	↓	↓	15	↓	48	58	68		$M = 1.60$; $\alpha = 12°$
8	19		↓	↓	↓	↓	10	v	0	115	116	117		
9	20		↓	↓	↓	↓	20	↓	↓	118	119	120		
10	29		↓	↓	↓	↓	30	↓	↓	173	174	175		
11	14		↓	−10	−10	↓	0	↓	↓	90	91	92	93	
12	30		↓	−10	−10	−10	↓	↓	↓	176	177	178	179	
13	15		↓	−20	−20	0	↓	↓	↓	94	95	96	97	
14	16		↓	−30	−30	0	↓	↓	↓	98	99	100	101	

[a] F-16C baseline (information supplied by the Model Test and CFD Group, General Dynamics Corporation, Ft. Worth, Texas) B76, E14, F86, F87, N4, P89, R3, V18a[a], W25, X49, X52, X69, X182, X183, X184, X187, X189, and X232.

[b] Falcon 21 baseline (information supplied by the Model Test and CFD Group, General Dynamics Corporation, Ft. Worth, Texas) F-16C fuselage with baseline Falcon 21 wing and strake: B258, E52, E82a, F336, F337, F338, F339, N4, P159, R3, V18a[a], W103, X49, X52, X69, X182, X183, X184, X187, X189, and X232.

Table V. Concluded

Configuration			Control surface deflections					Model attitude		Run number at M—				Notes
Config.	Batch	Description	LEF	TEFi (L/R)	TEFo (L/R)	PF	RUD	α	β	1.60	1.80	2.00	2.16	
15	17		0	−30	−30	−30	0	v	0	104	103	105	106	
16	13		↓	10	10	0	↓	↓	↓	86	87	88	89	
17	11		↓	0	+20/0	↓	↓	↓	↓	80	81	82		
18	10		↓	0	−20/0	↓	↓	↓	↓	77	78	79		
19	12		↓	+20/0	+20/0	↓	↓	↓	↓	83	84	85		
20	9		↓	−20/0	−20/0	↓	↓	↓	↓	71	74	75		$Re = 1.5 \times 10^6$
20	9		↓	−20/0	−20/0	↓	↓	↓	↓	72	73	76		
21	31	With AIM-120 fairing	↓	0	0	↓	↓	↓	↓	180	181	182		
22	23	With 2 AIM-120 forward (1/side)	↓	↓	↓	↓	↓	↓	↓	148	149	150	151	
23	24	Without (4) AIM-120	↓	↓	↓	↓	↓	↓	↓	152	153	154	155	
24	25	Without (4) AIM-120; without AIM-9L	↓	↓	↓	↓	↓	↓	↓	156	157	158	159	
25	26	With 600-gal tanks (BL = 5.133; 1 per side)	↓	↓	↓	↓	↓	↓	↓	160	161			
26	22	With ventrals	↓	↓	↓	↓	↓	↓	↓	133	138	143		
26	22	With ventrals	↓	↓	↓	↓	↓	0	v	134	139	144		
26	22	With ventrals	↓	↓	↓	↓	↓	5	↓	135	140	145		
26	22	With ventrals	↓	↓	↓	↓	↓	10	↓	136	141	146		
26	22	With ventrals	↓	↓	↓	↓	↓	15	↓	137	142	147		$M = 1.60$; $\alpha = 12°$
27	21	Without vertical tail	↓	↓	↓	↓	Off	0	↓	121	125	129		
27	21	Without vertical tail	↓	↓	↓	↓	↓	5	↓	122	126	130		
27	21	Without vertical tail	↓	↓	↓	↓	↓	10	↓	123	127	131		
27	21	Without vertical tail	↓	↓	↓	↓	↓	15	↓	124	128	132		$M = 1.60$; $\alpha = 12°$
28	27	With IRST 1	↓	↓	↓	↓	0	v	0	162	165	167		
28	27	With IRST 1	↓	↓	↓	↓	↓	v	0	164				
28	27	With IRST 1	↓	↓	↓	↓	↓	v	0	169				Repeat configuration
28	27	With IRST 1	↓	↓	↓	↓	↓	5	v	163	166	168		
29	28	With IRST 2	↓	↓	↓	↓	↓	A3	0	170	171		172	$M = 2.16$; $Re = 1.9 \times 10^6$

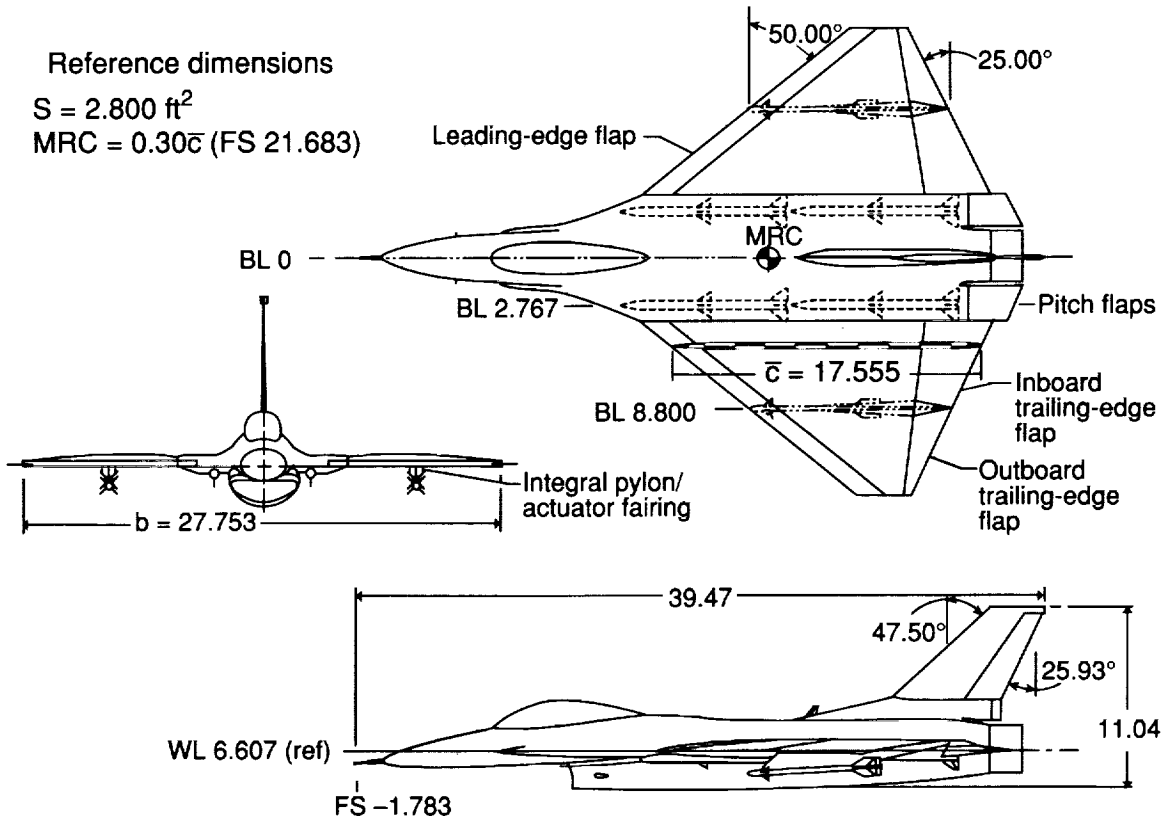

Figure 1. Three-view illustration of baseline wind tunnel model. All linear dimensions are in inches.

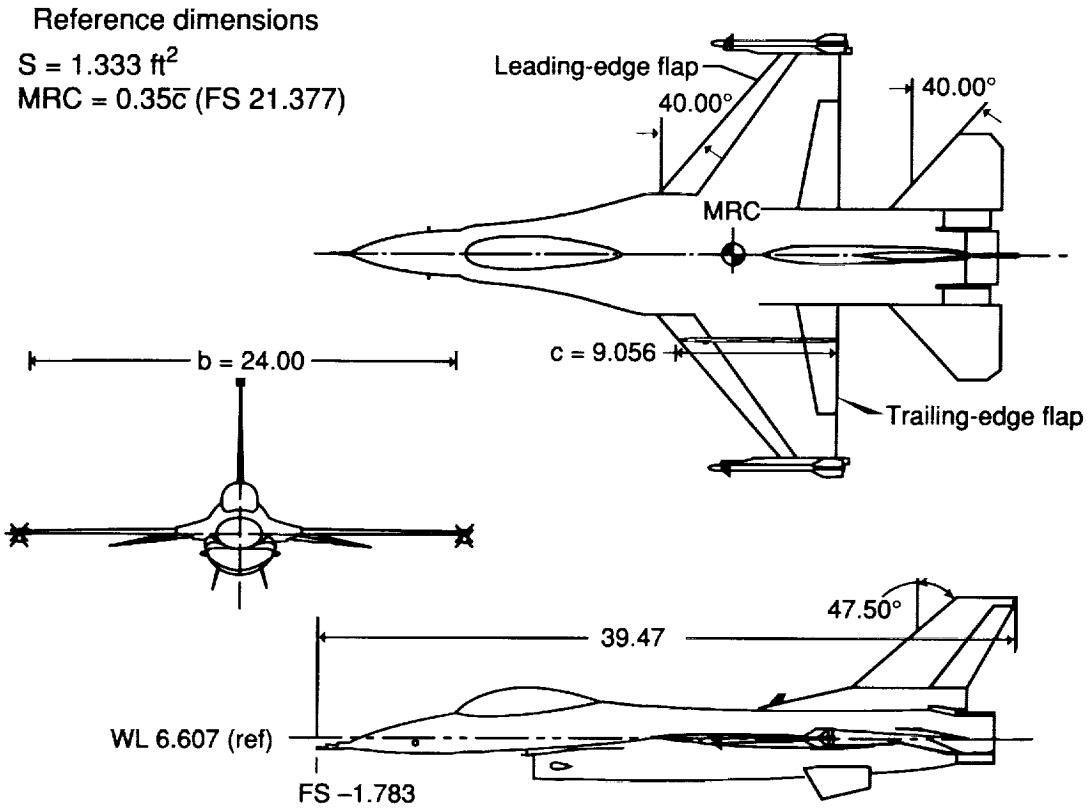

Figure 2. Three-view illustration of F-16C wind tunnel model. All linear dimensions are in inches.

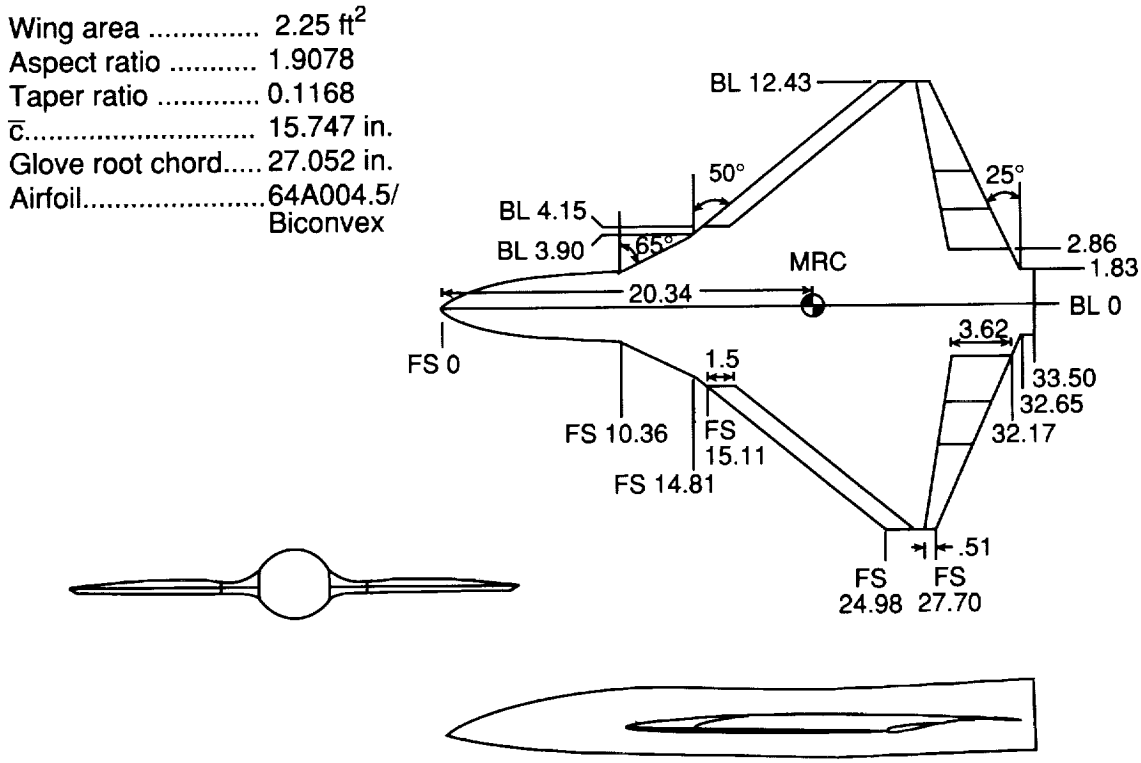

Figure 3. Three-view illustration of generic wing wind tunnel model.

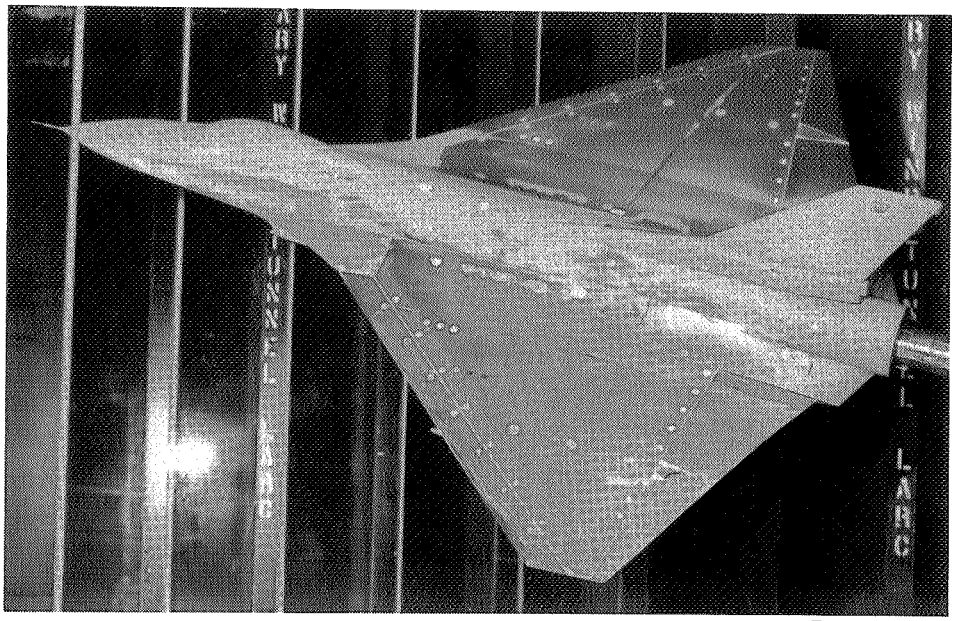

L-91-14753

(a) Top view.

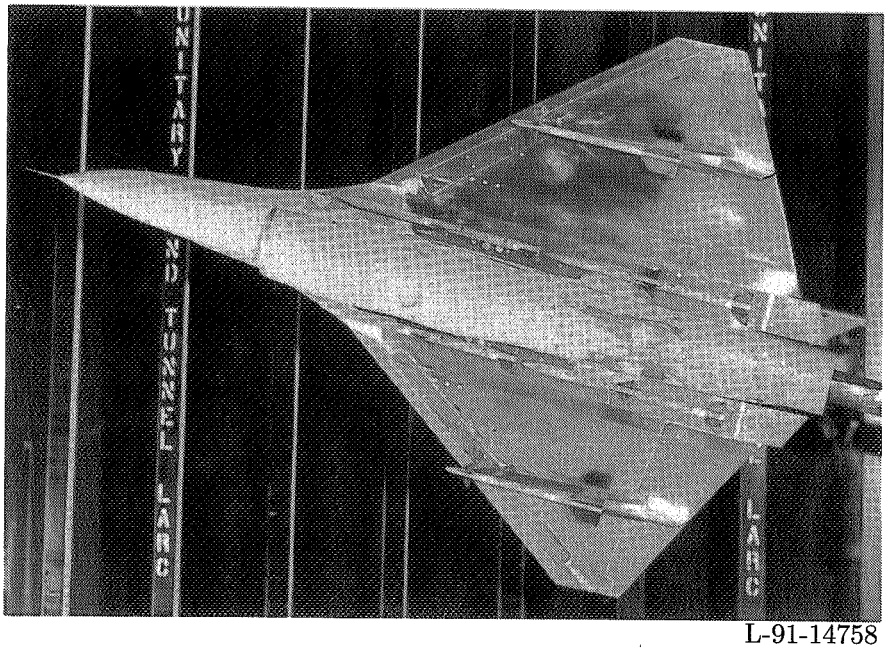

L-91-14758

(b) Bottom view.

Figure 4. Advanced F-16 derivative model in Unitary Plan Wind Tunnel.

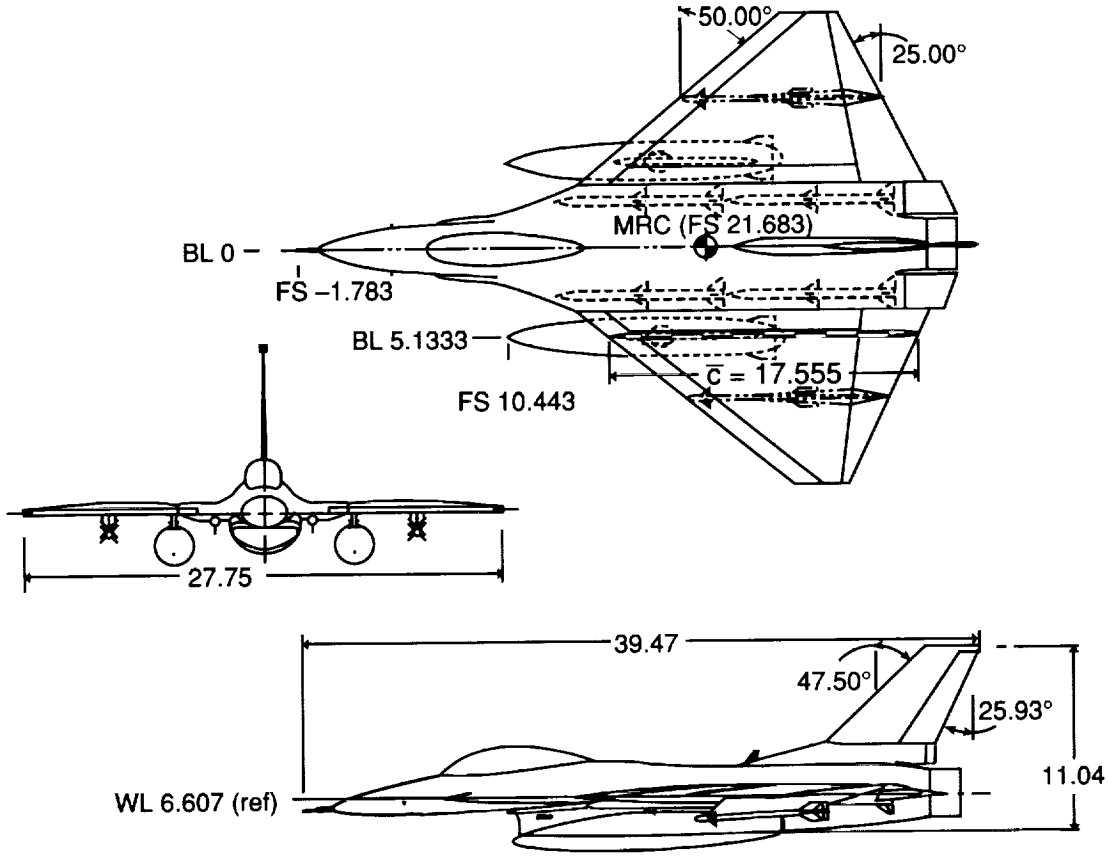

Figure 5. Simulated 600-gal fuel tanks on baseline model. All linear dimensions are in inches.

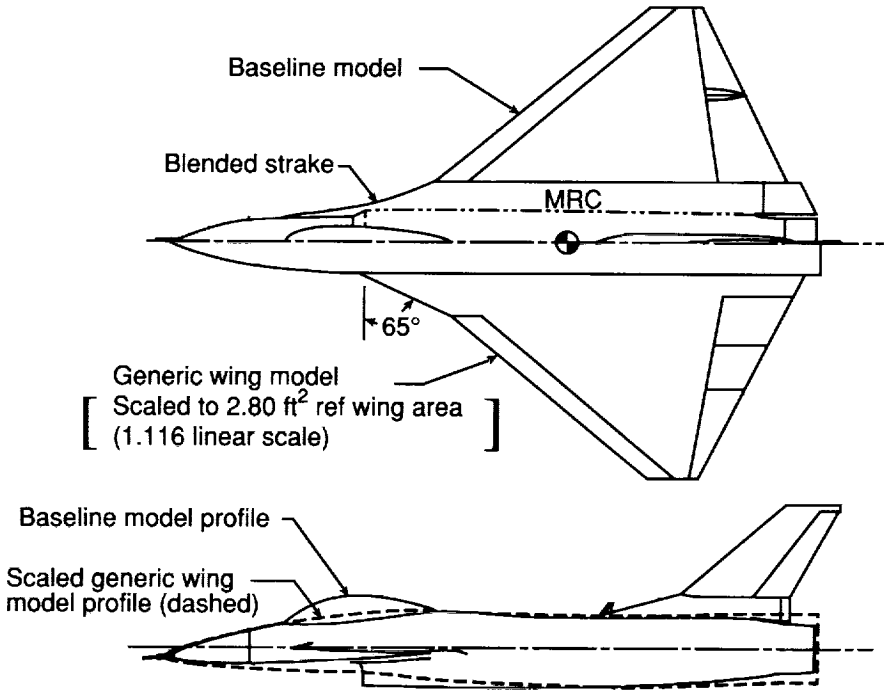

Figure 6. Baseline configuration geometry compared with generic wing model. MRC = $0.30\,\bar{c}$ for both configurations.

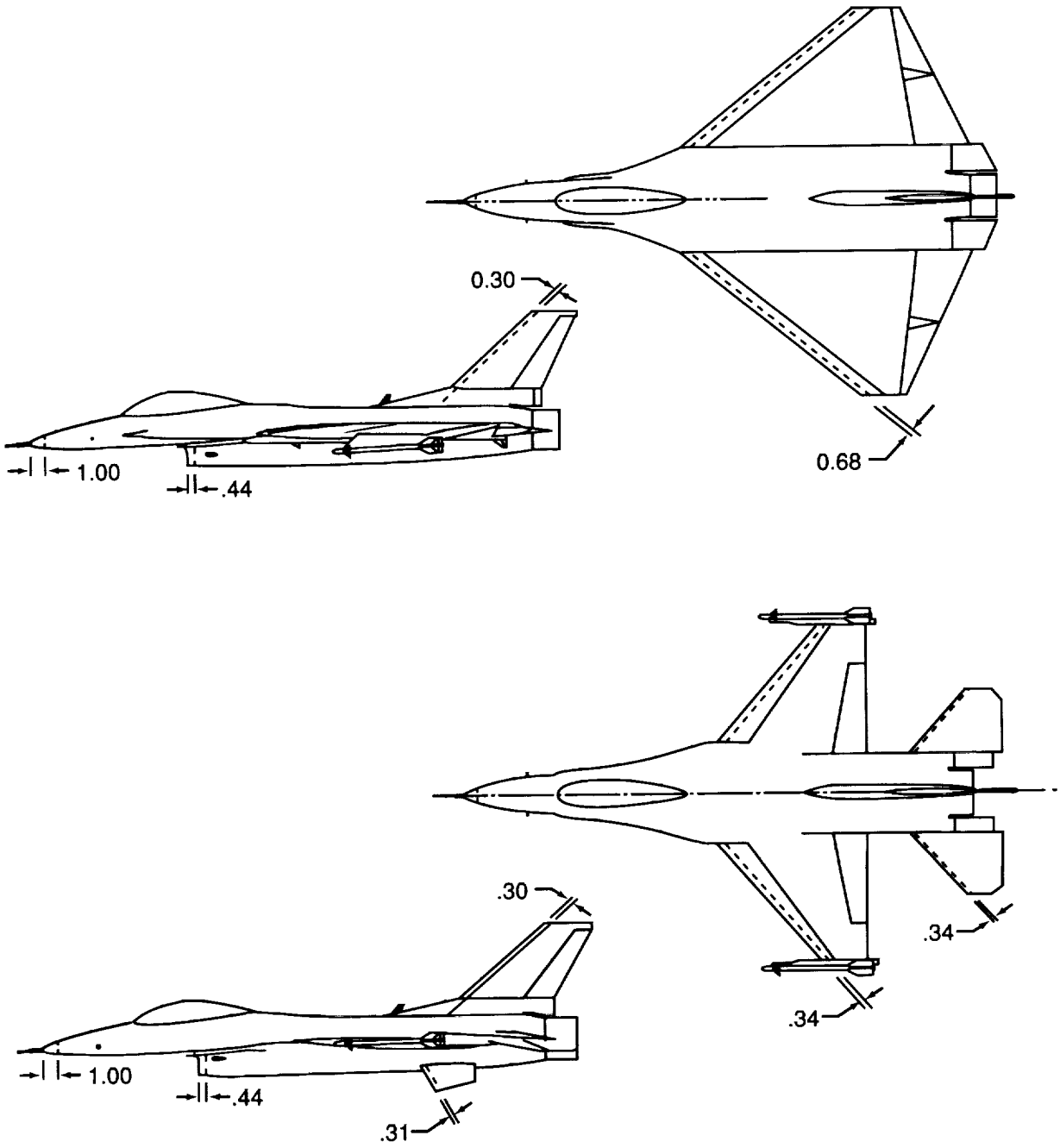

Figure 7. Transition strip locations for baseline and F-16C models. All dimensions are in inches.

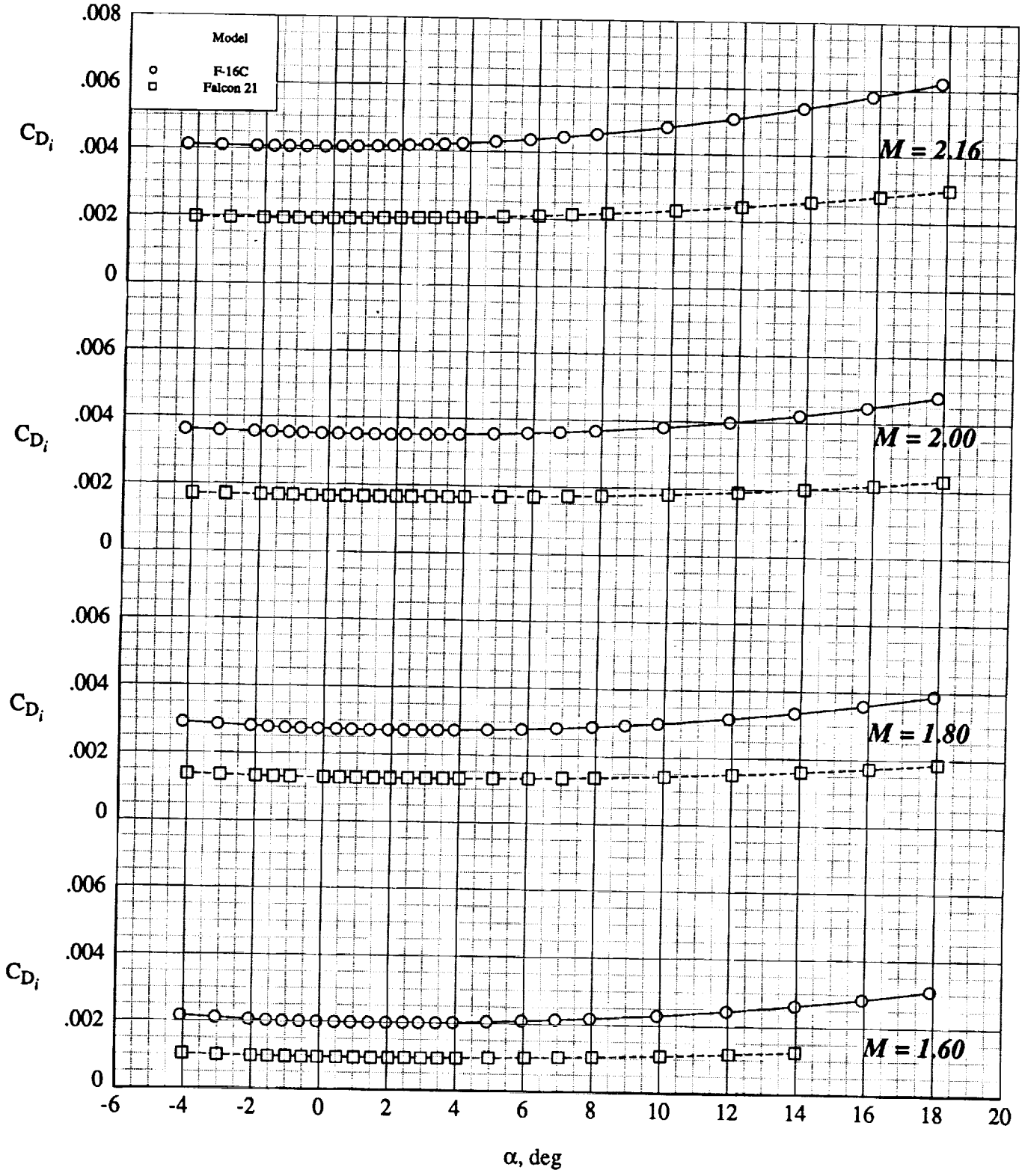

Figure 8. Internal drag corrections for F-16C and baseline models.

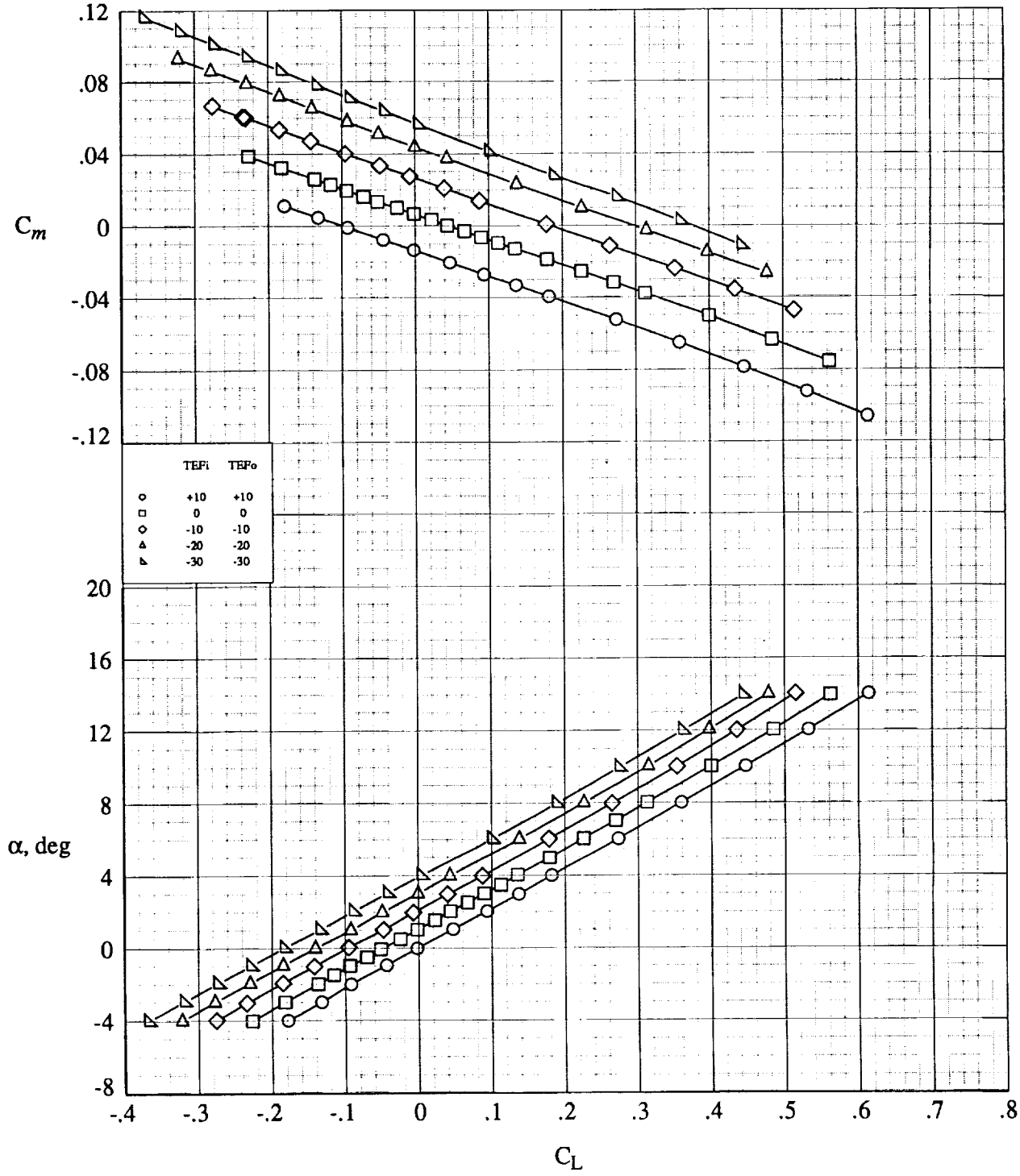

(a) $M = 1.60$.

Figure 9. Longitudinal aerodynamic characteristics for baseline model. LEF = 0°; $CG_{ref} = 0.30\bar{c}$.

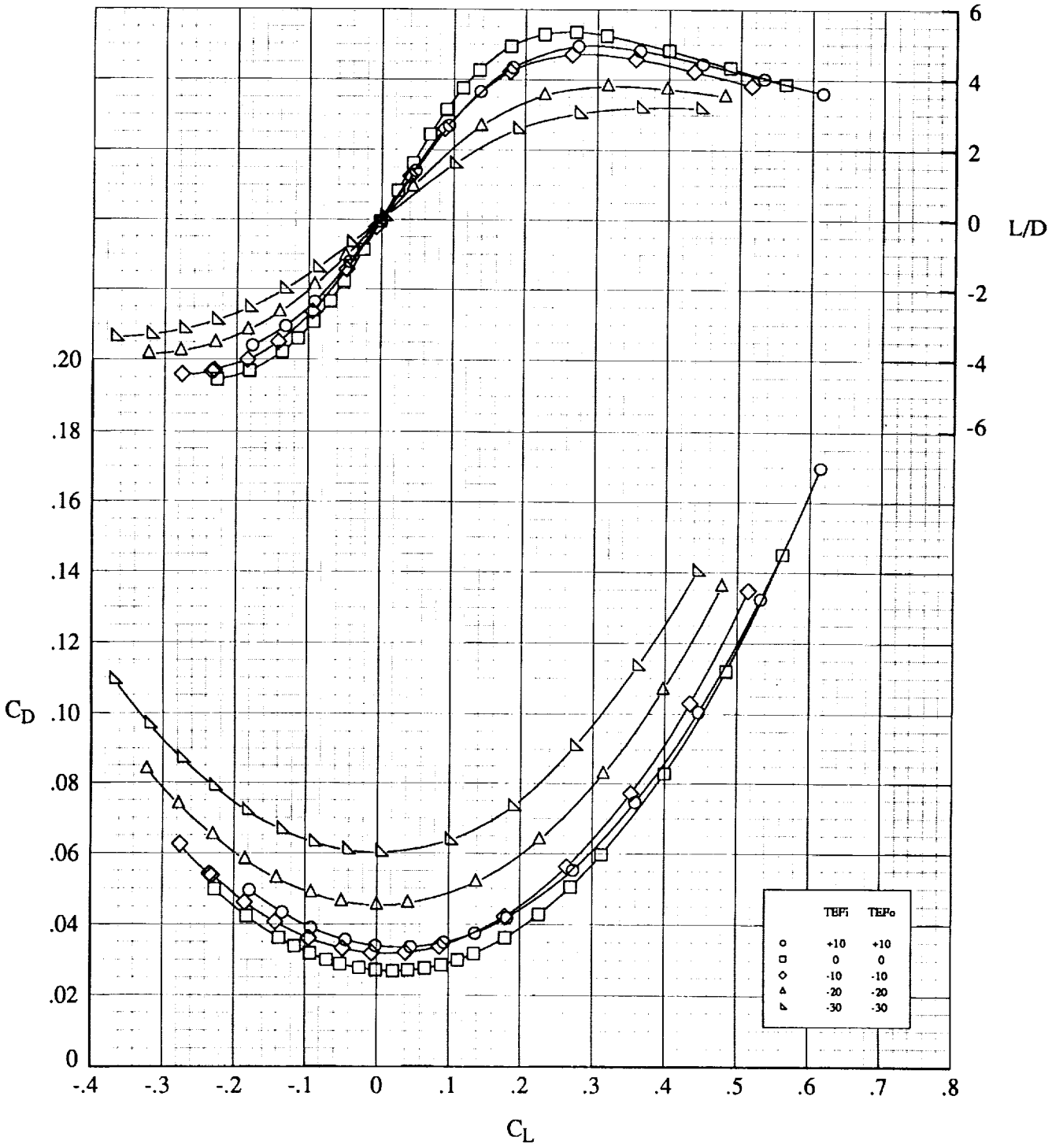

(a) Concluded.

Figure 9. Continued.

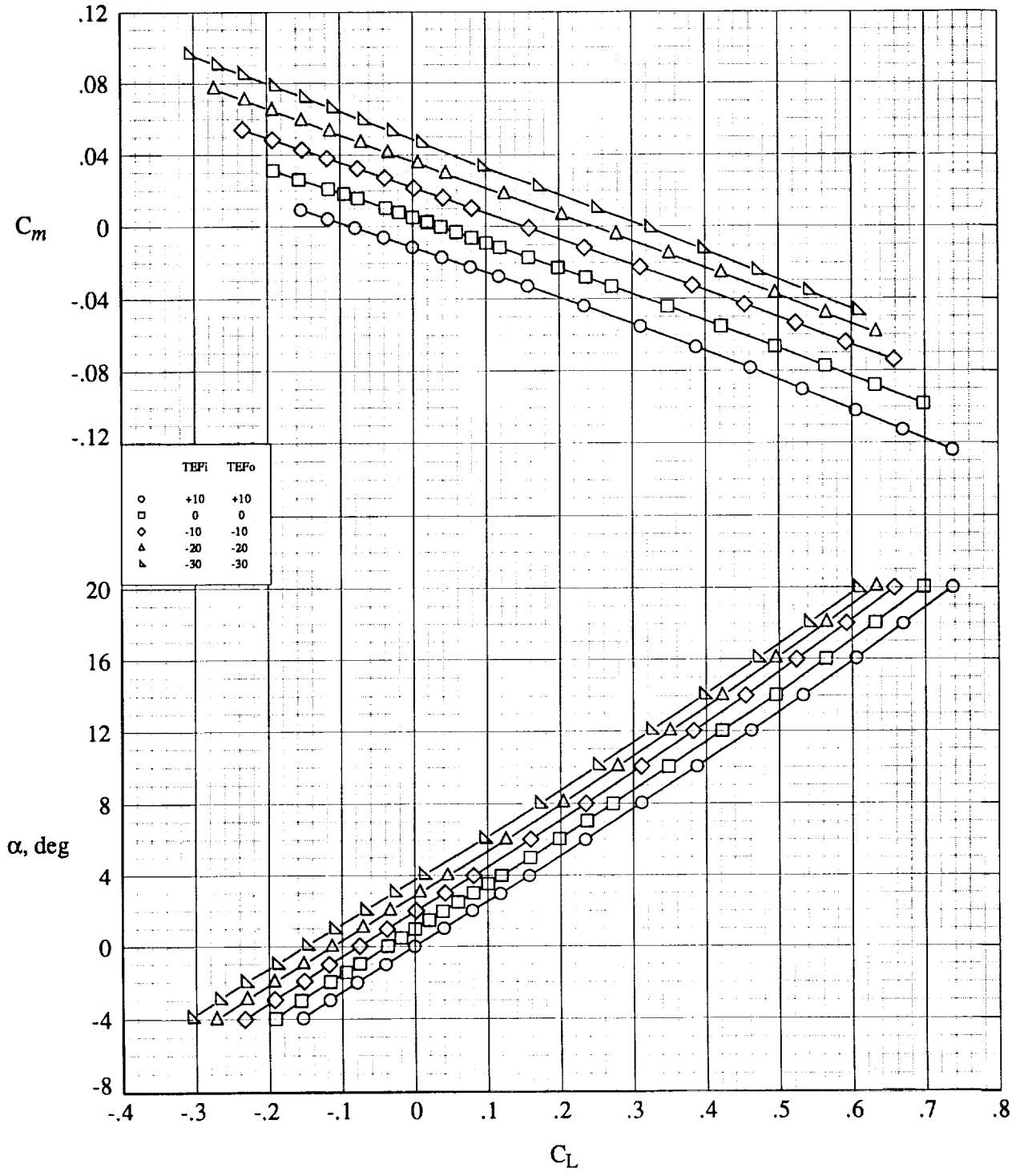

(b) $M = 1.80$.

Figure 9. Continued.

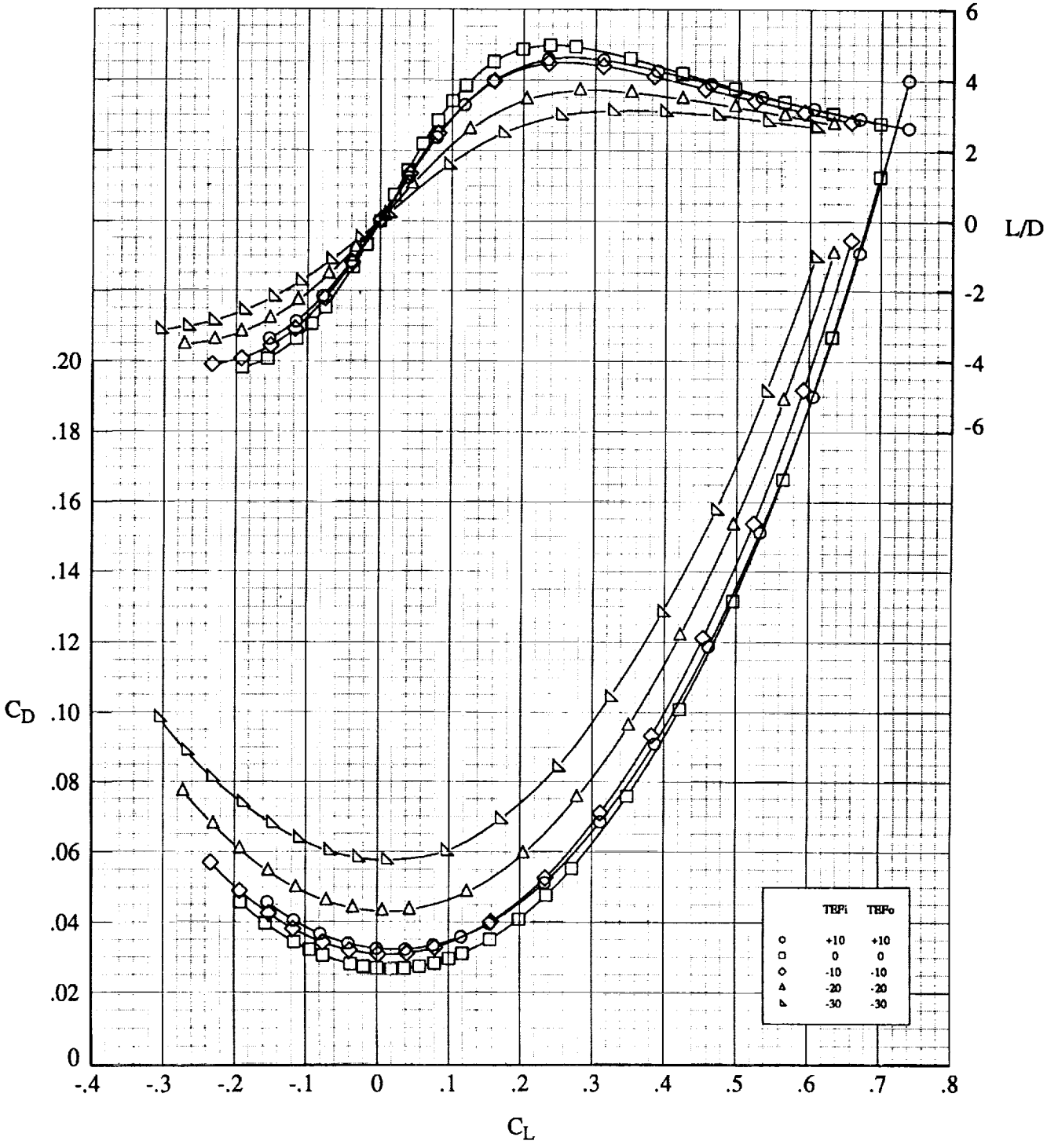

(b) Concluded.

Figure 9. Continued.

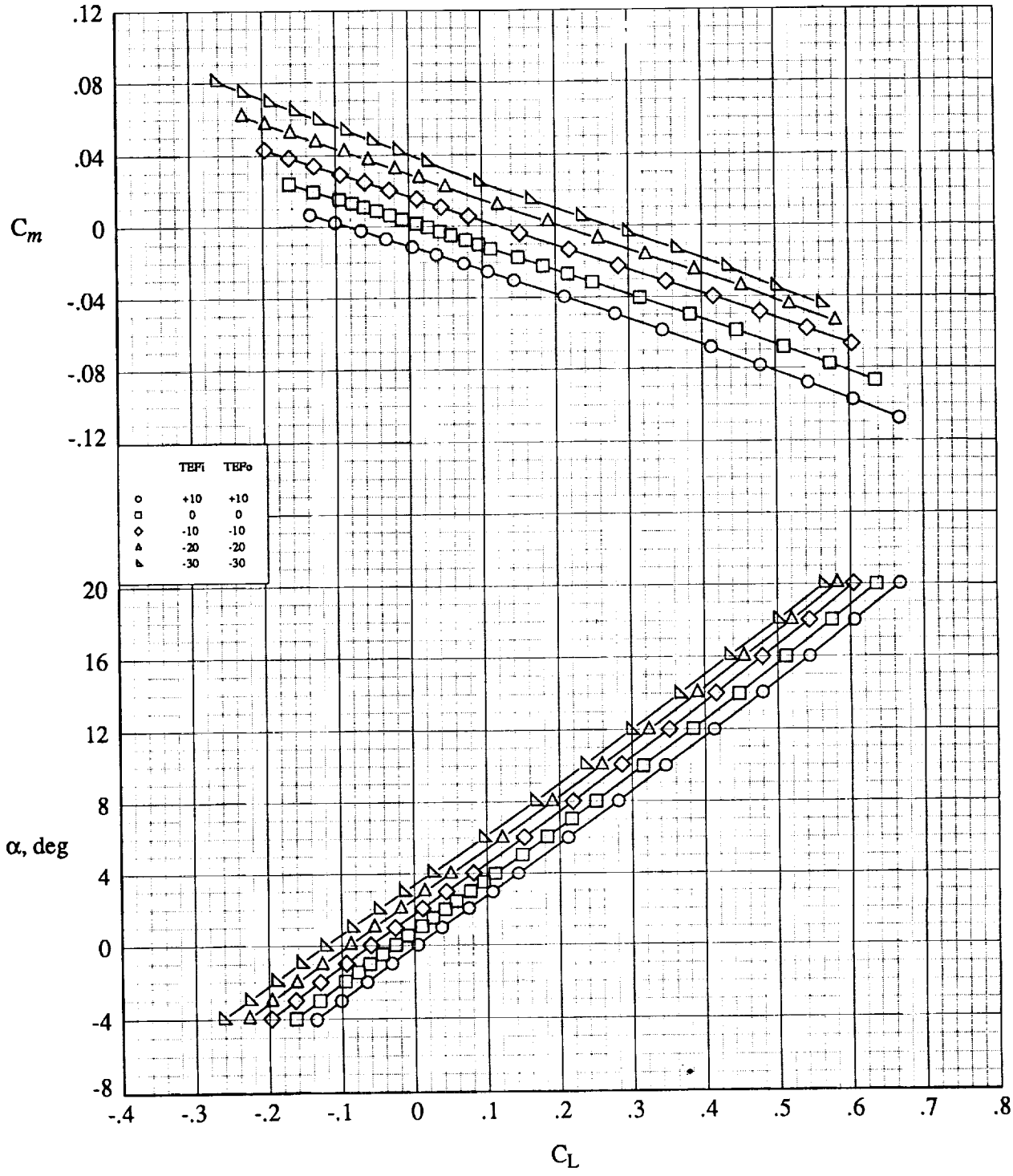

(c) $M = 2.00$.

Figure 9. Continued.

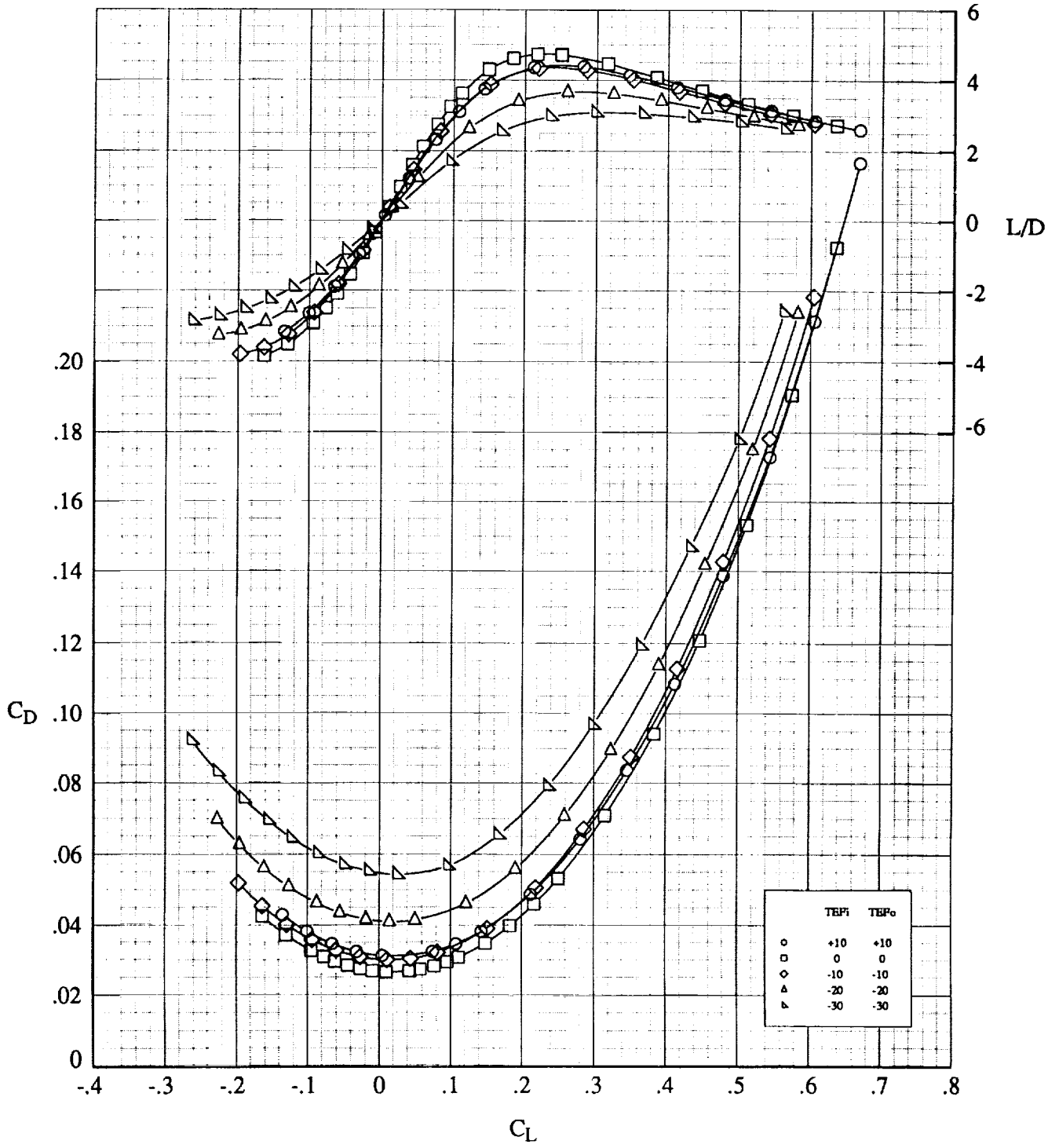

(c) Concluded.

Figure 9. Continued.

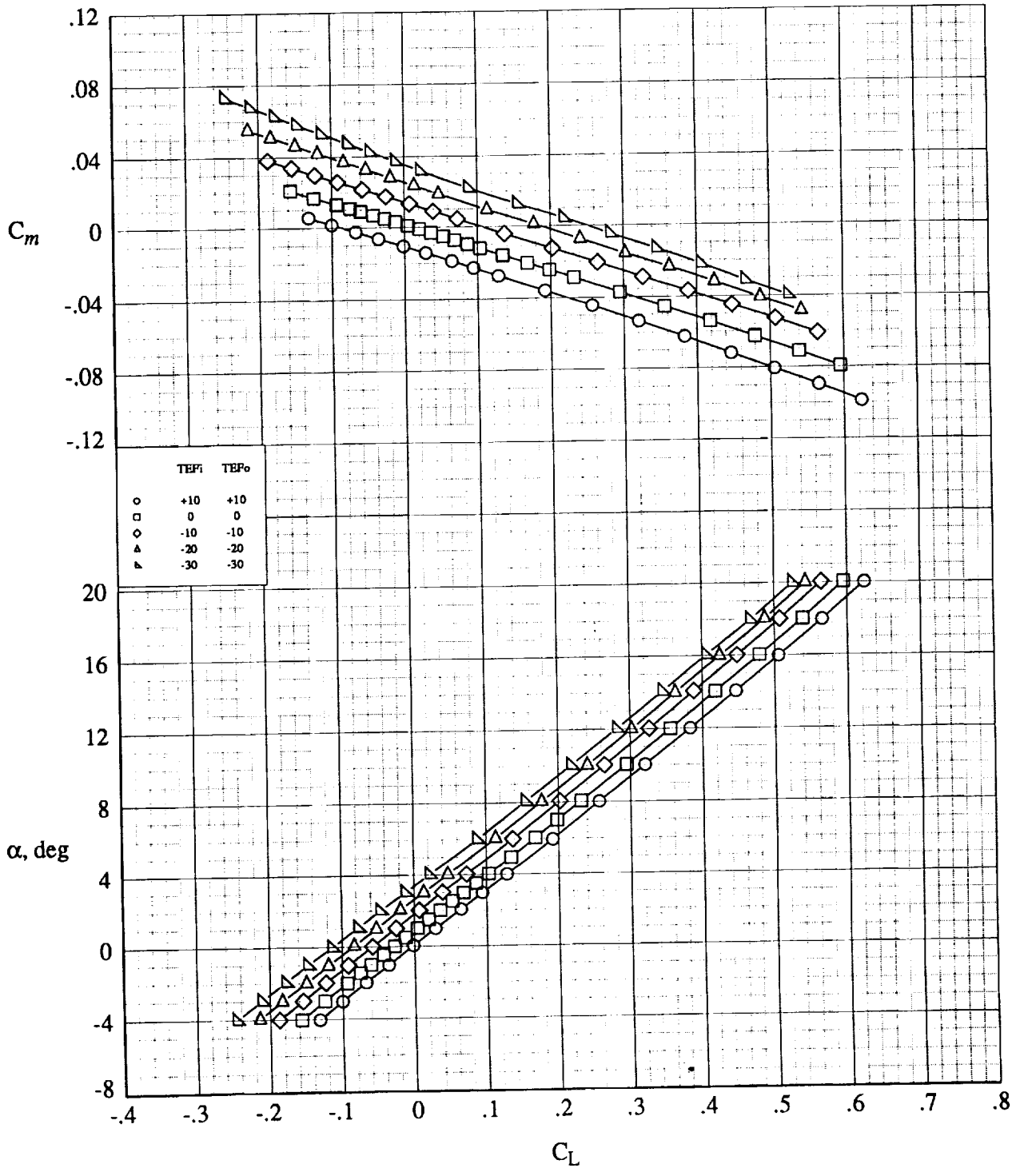

(d) $M = 2.16$.

Figure 9. Continued.

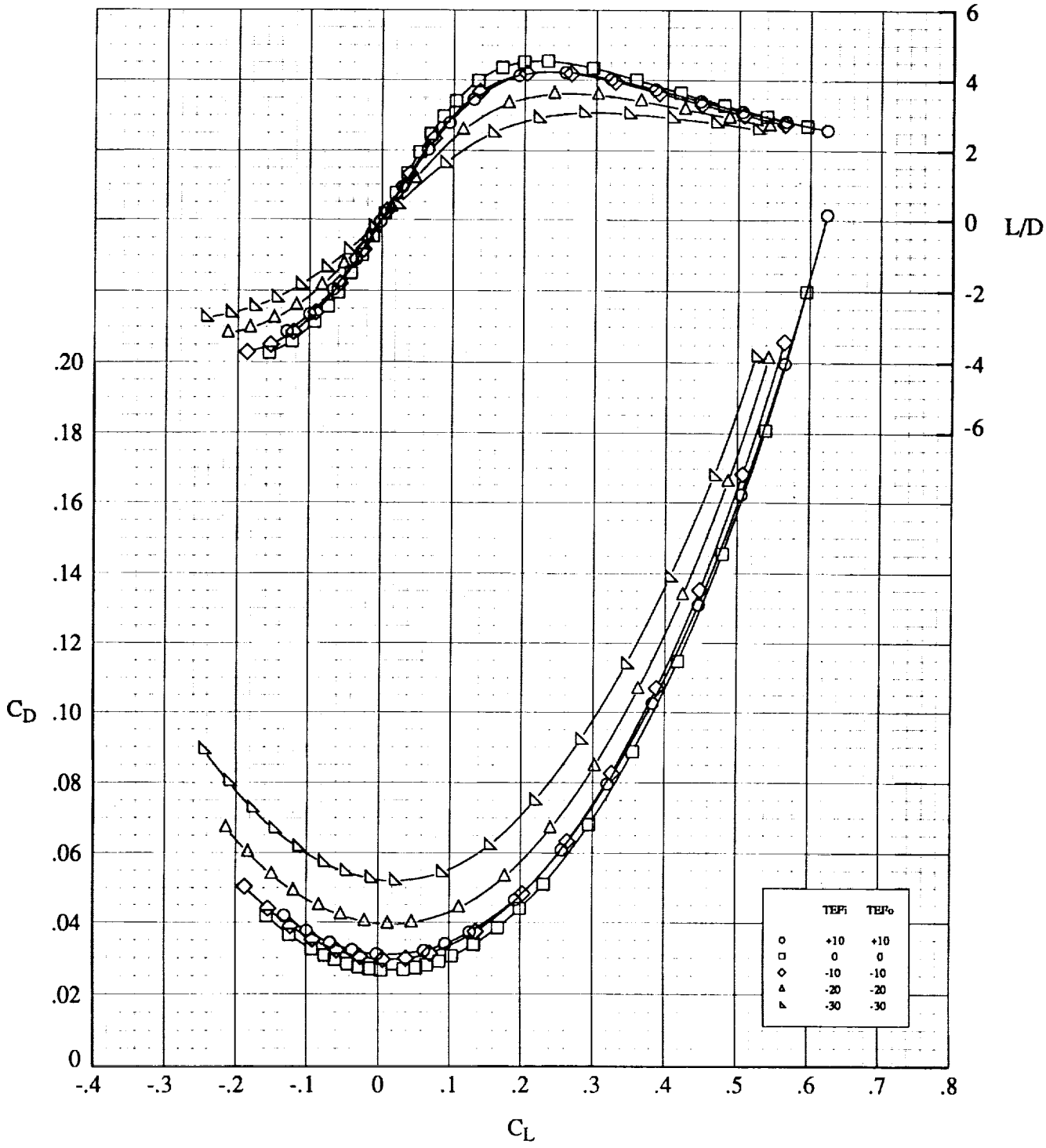

(d) Concluded.

Figure 9. Concluded.

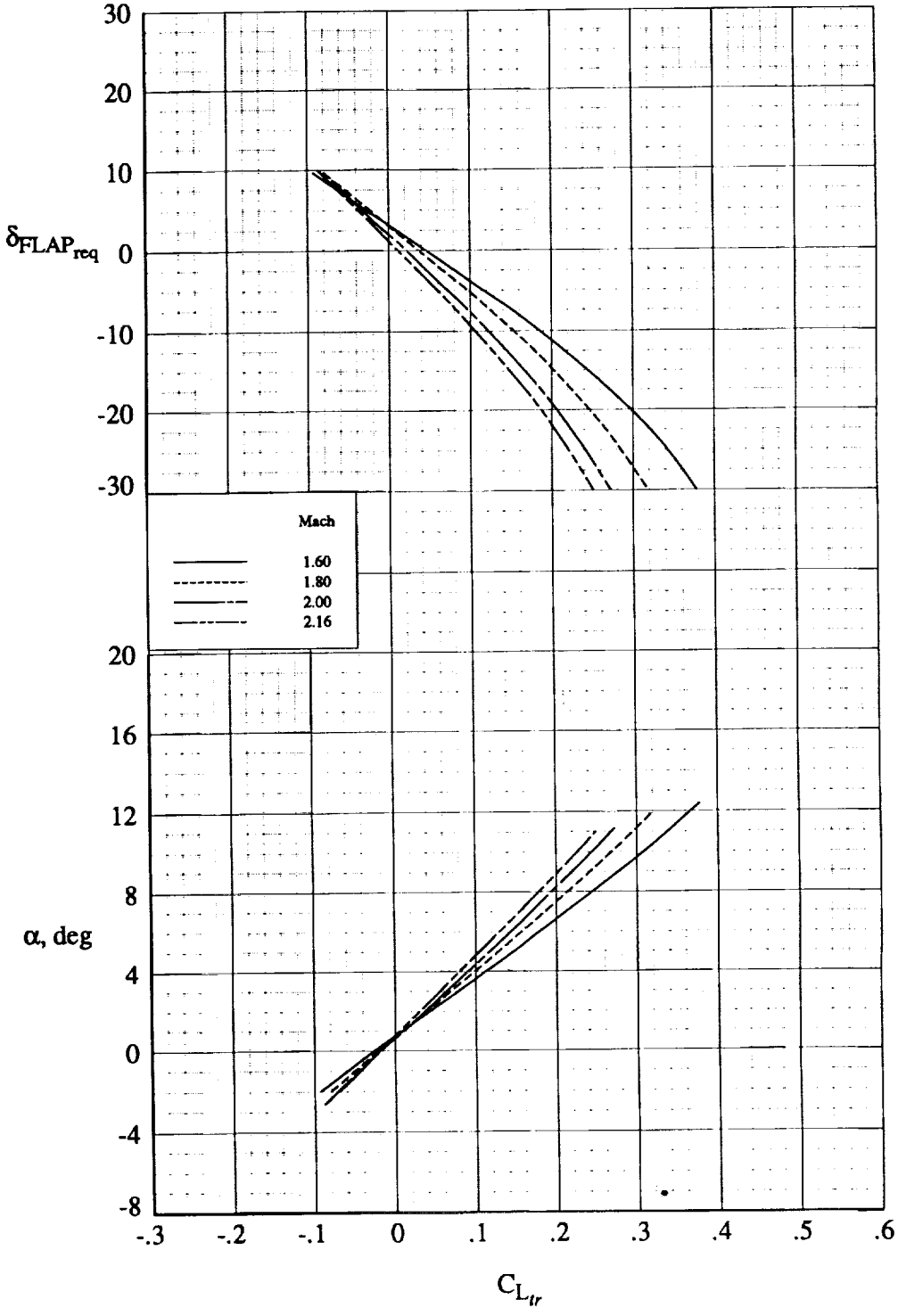

Figure 10. Longitudinal trim characteristics for baseline model. LEF = 0°; $CG_{ref} = 0.30\bar{c}$.

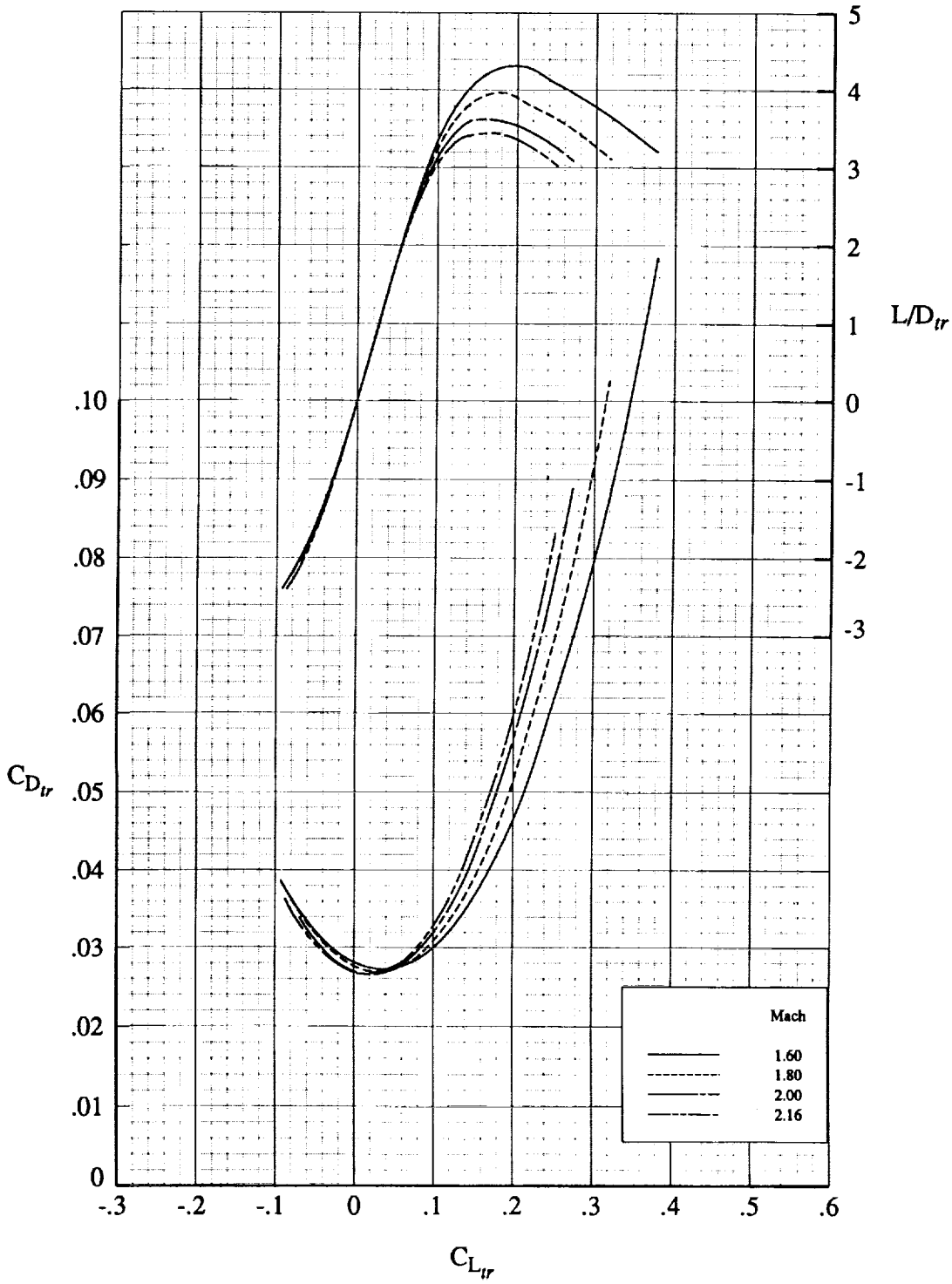

Figure 10. Concluded.

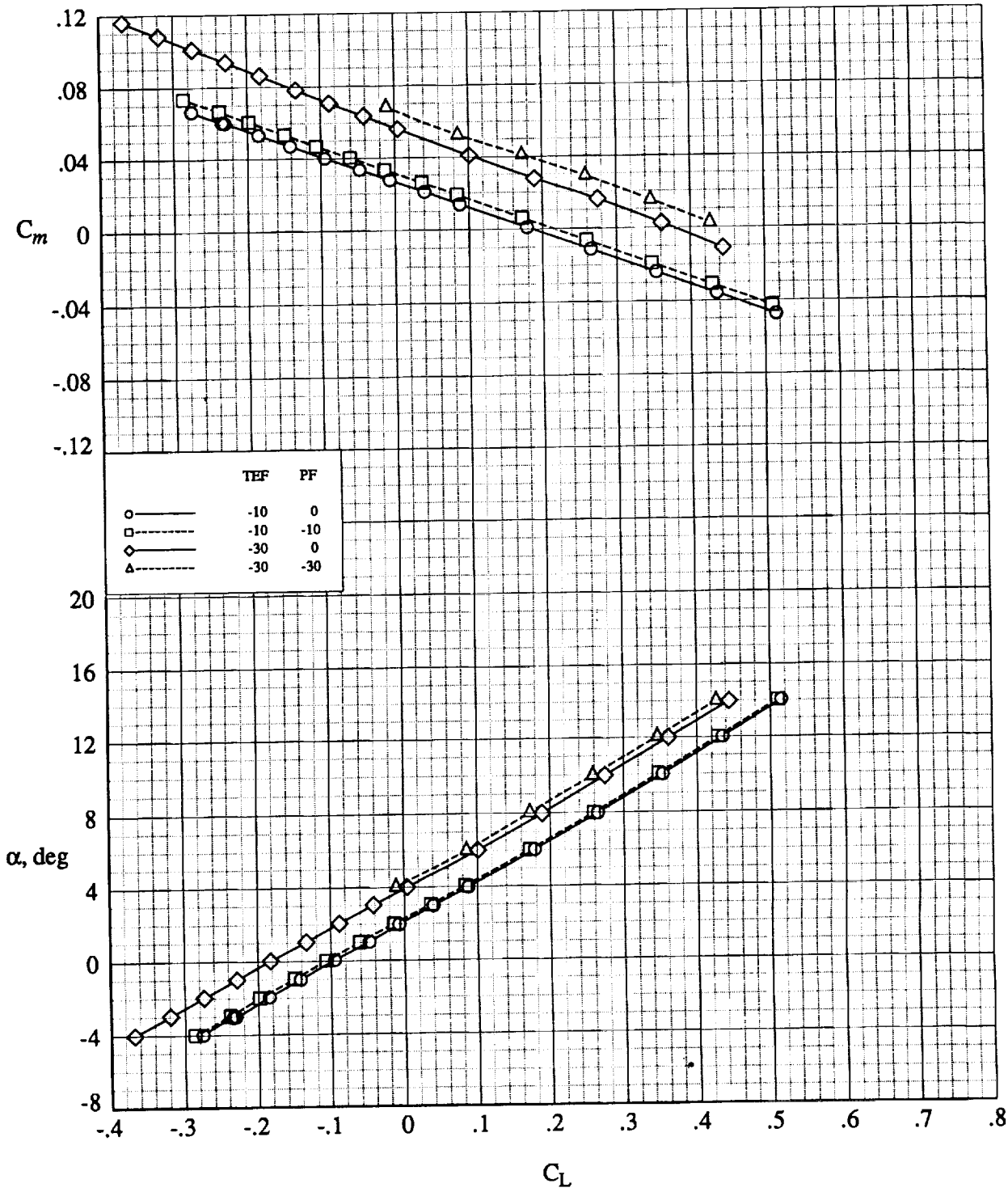

(a) $M = 1.60$.

Figure 11. Pitch flap effects on untrimmed longitudinal characteristics for baseline model. LEF = 0°; $CG_{ref} = 0.30\bar{c}$.

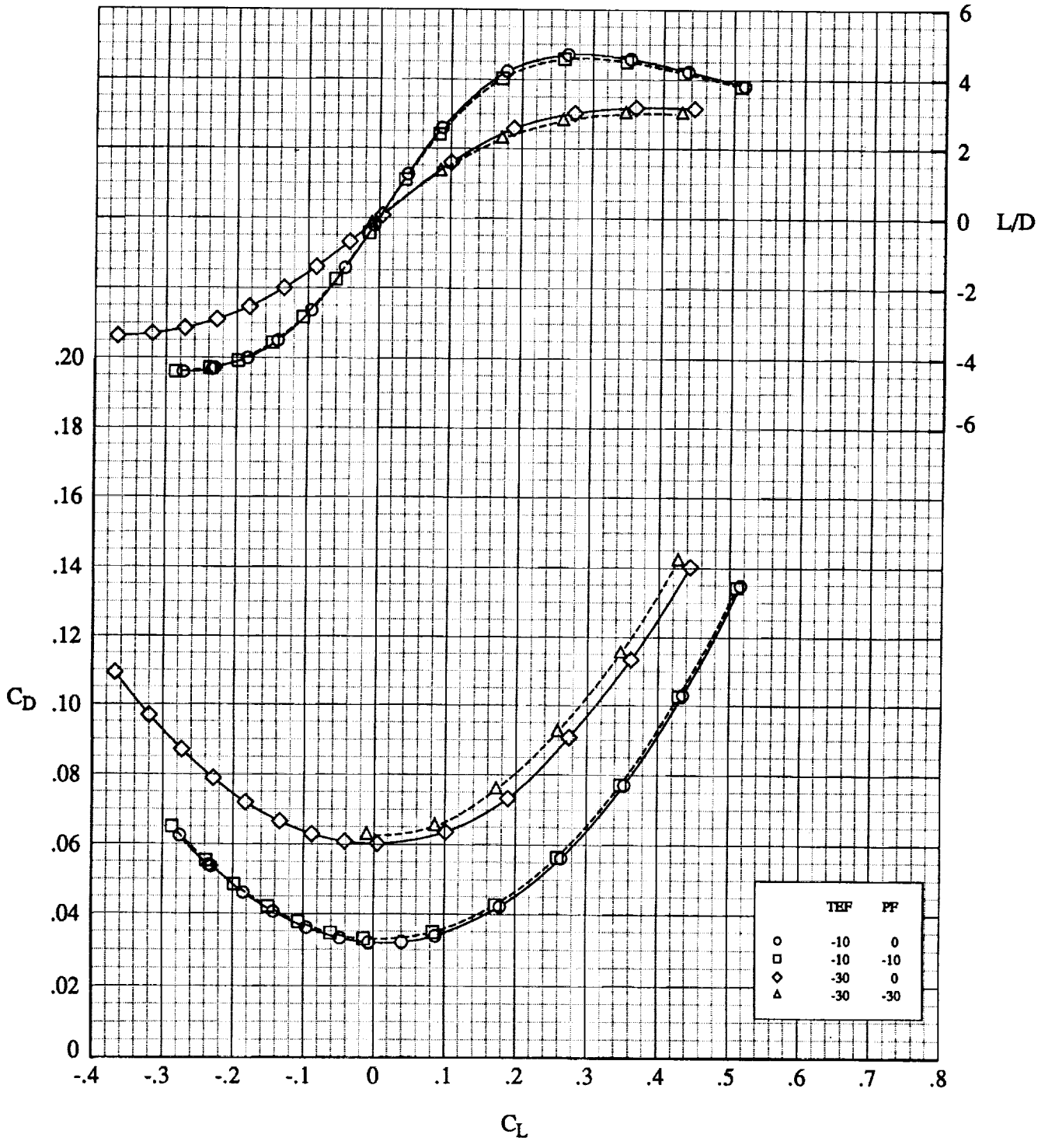

(a) Concluded.

Figure 11. Continued.

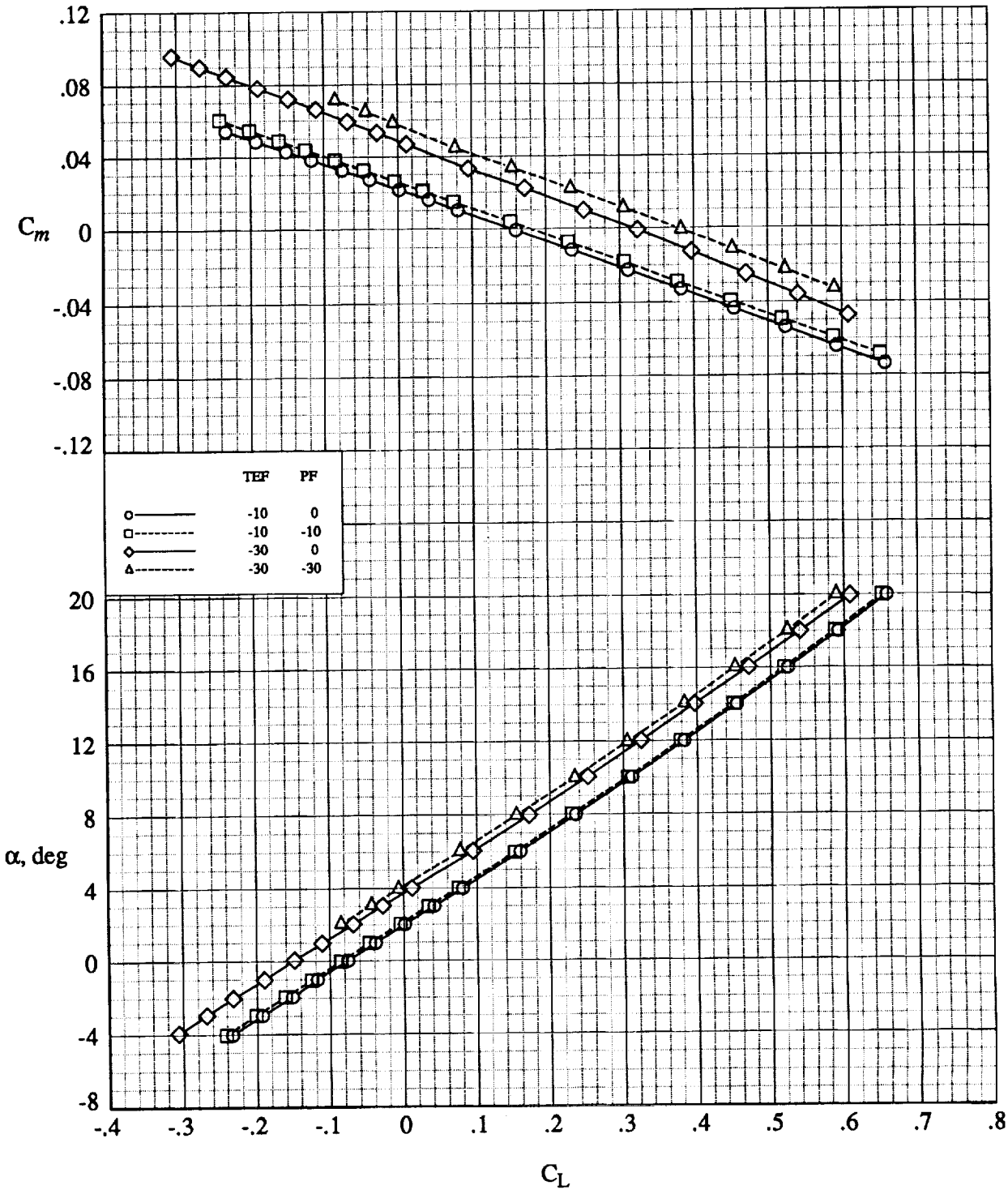

(b) $M = 1.80$.

Figure 11. Continued.

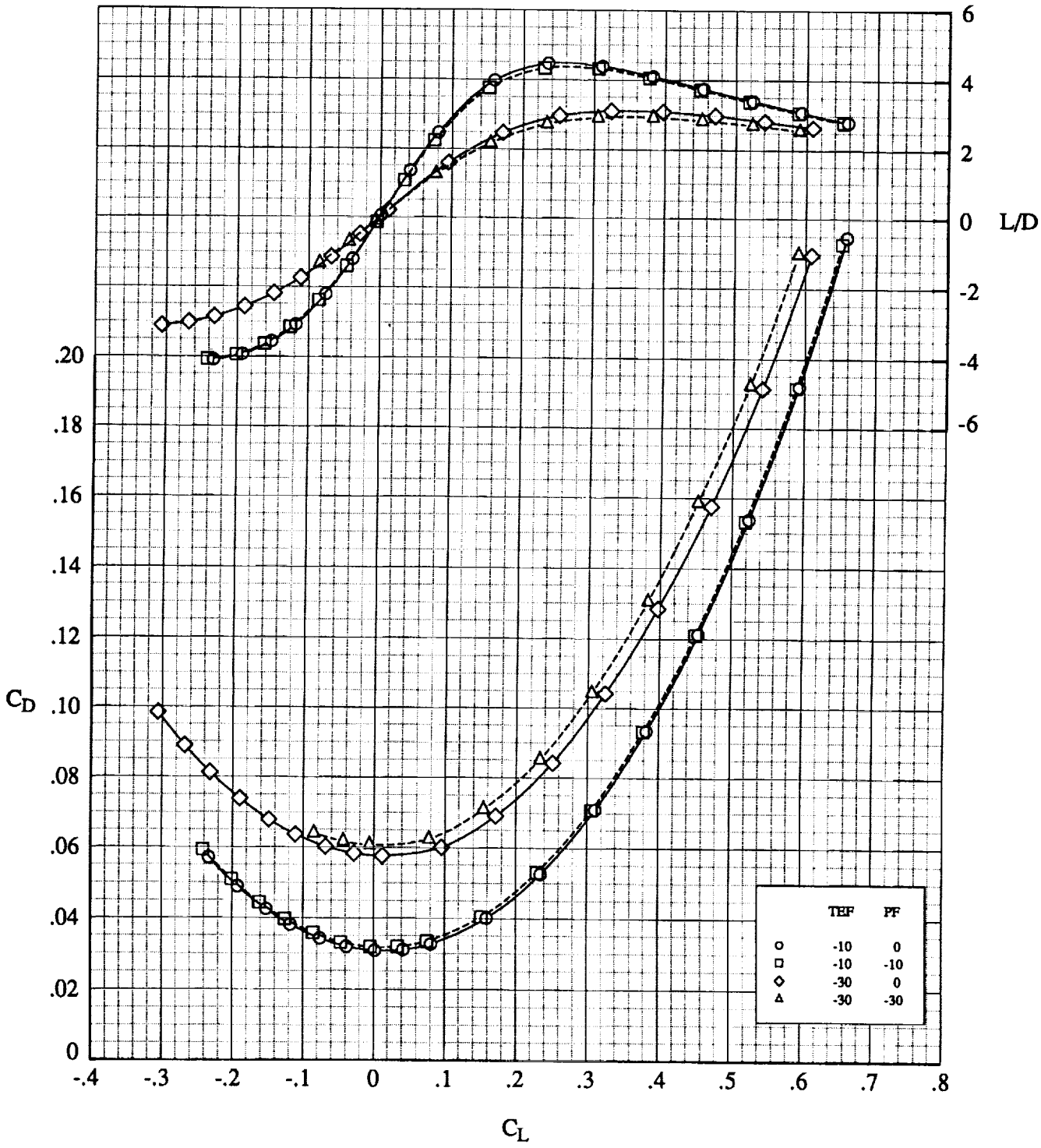

(b) Concluded.

Figure 11. Continued.

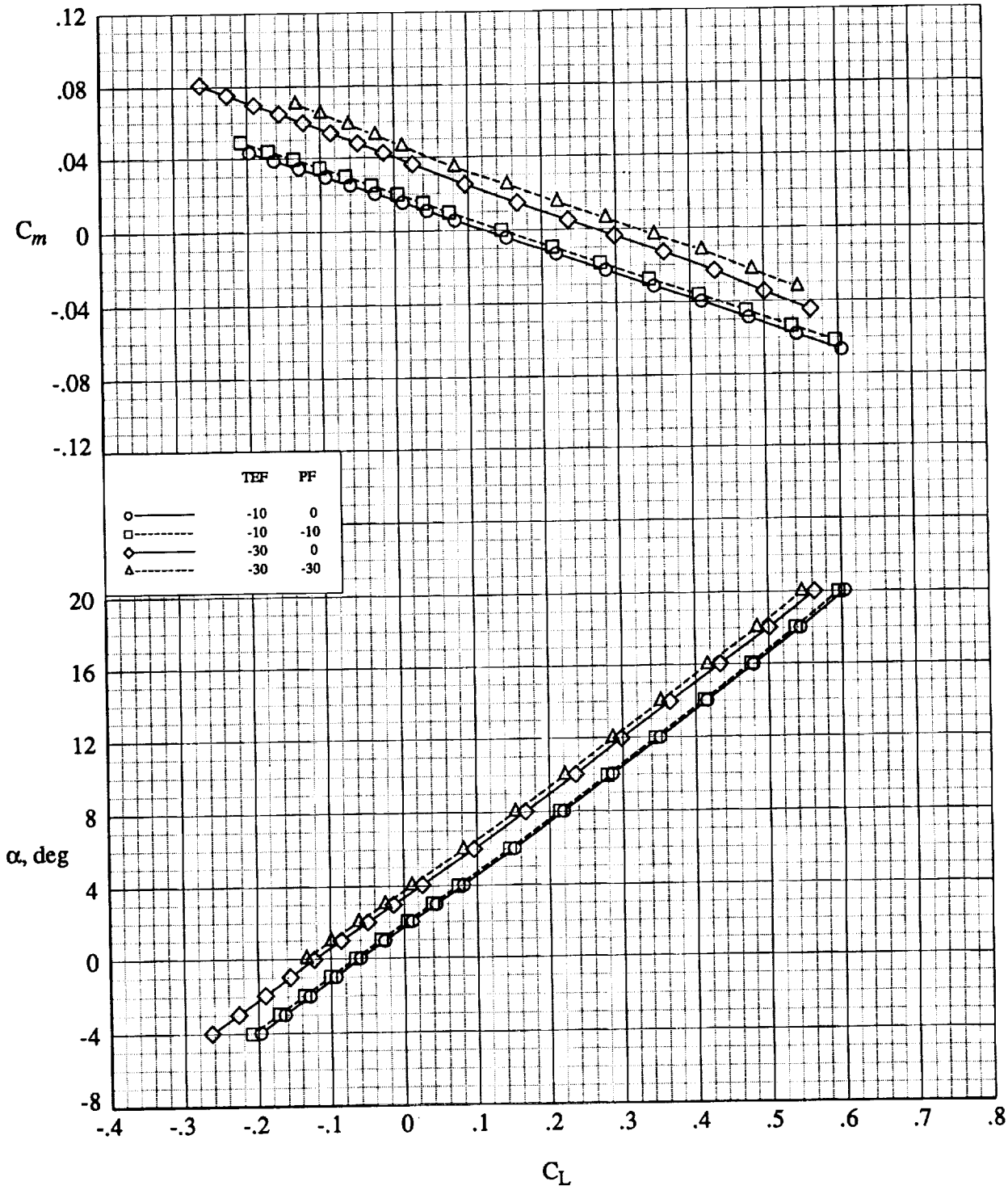

(c) $M = 2.00$.

Figure 11. Continued.

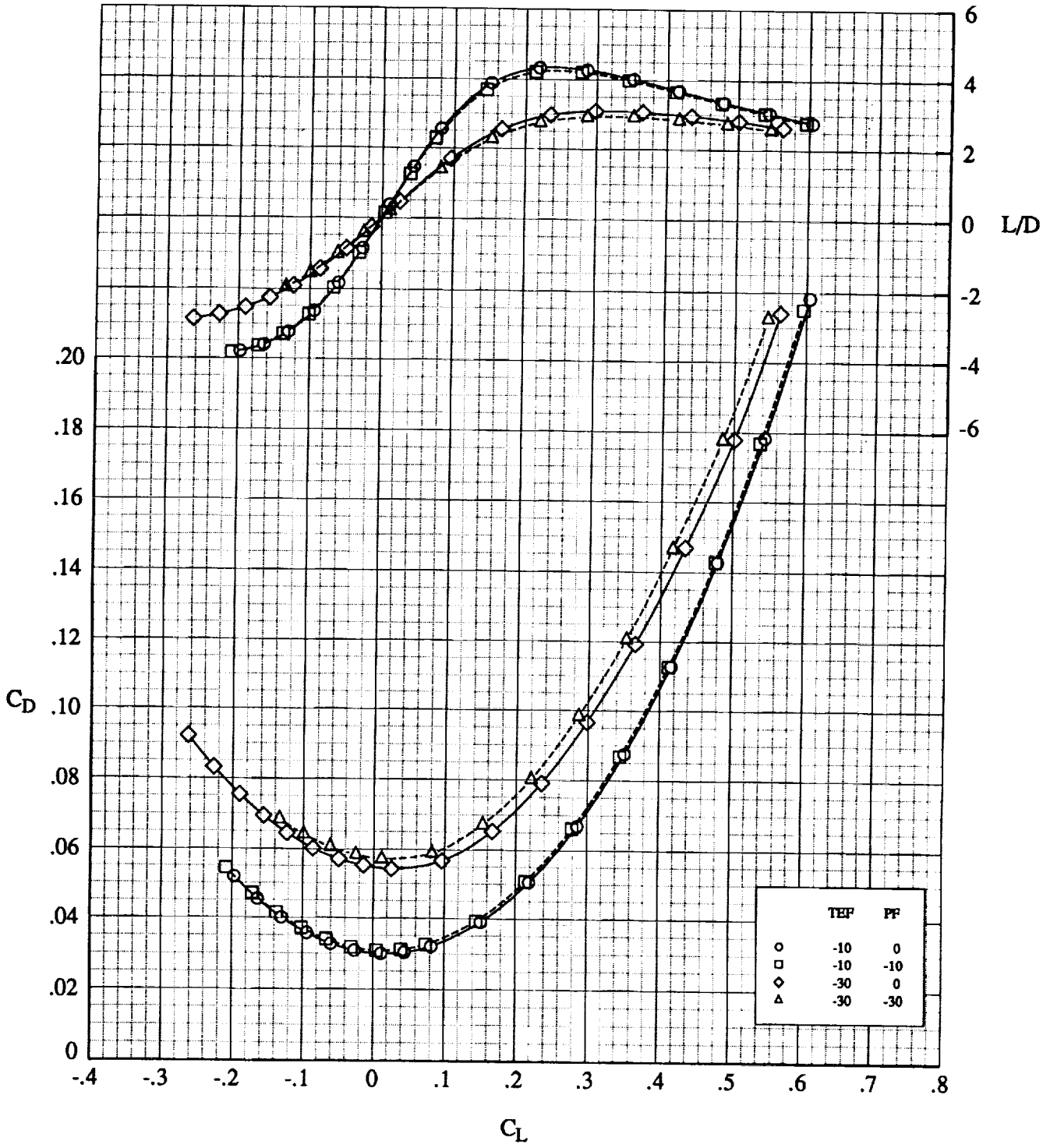

(c) Concluded.

Figure 11. Continued.

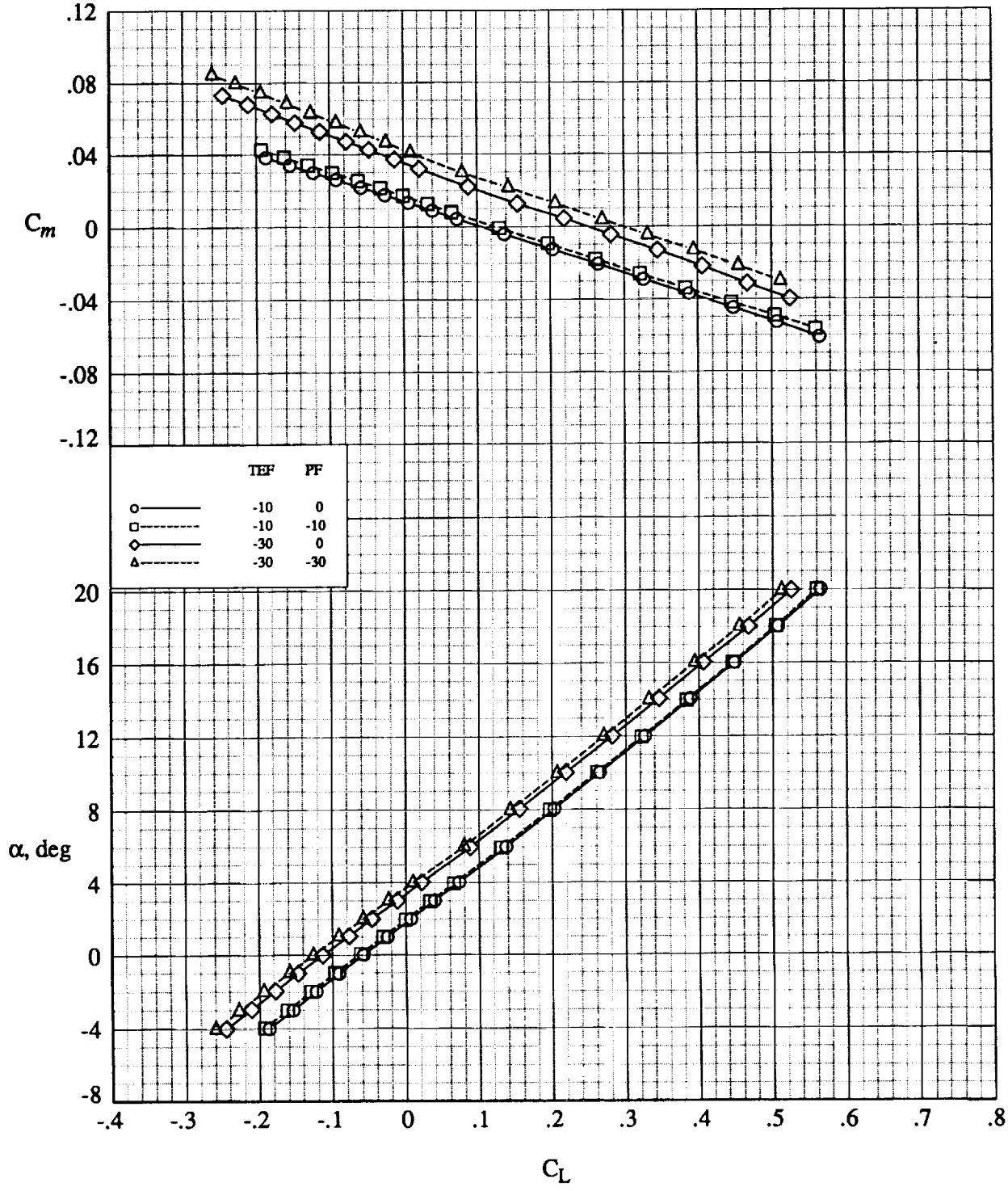

(d) $M = 2.16$.

Figure 11. Continued.

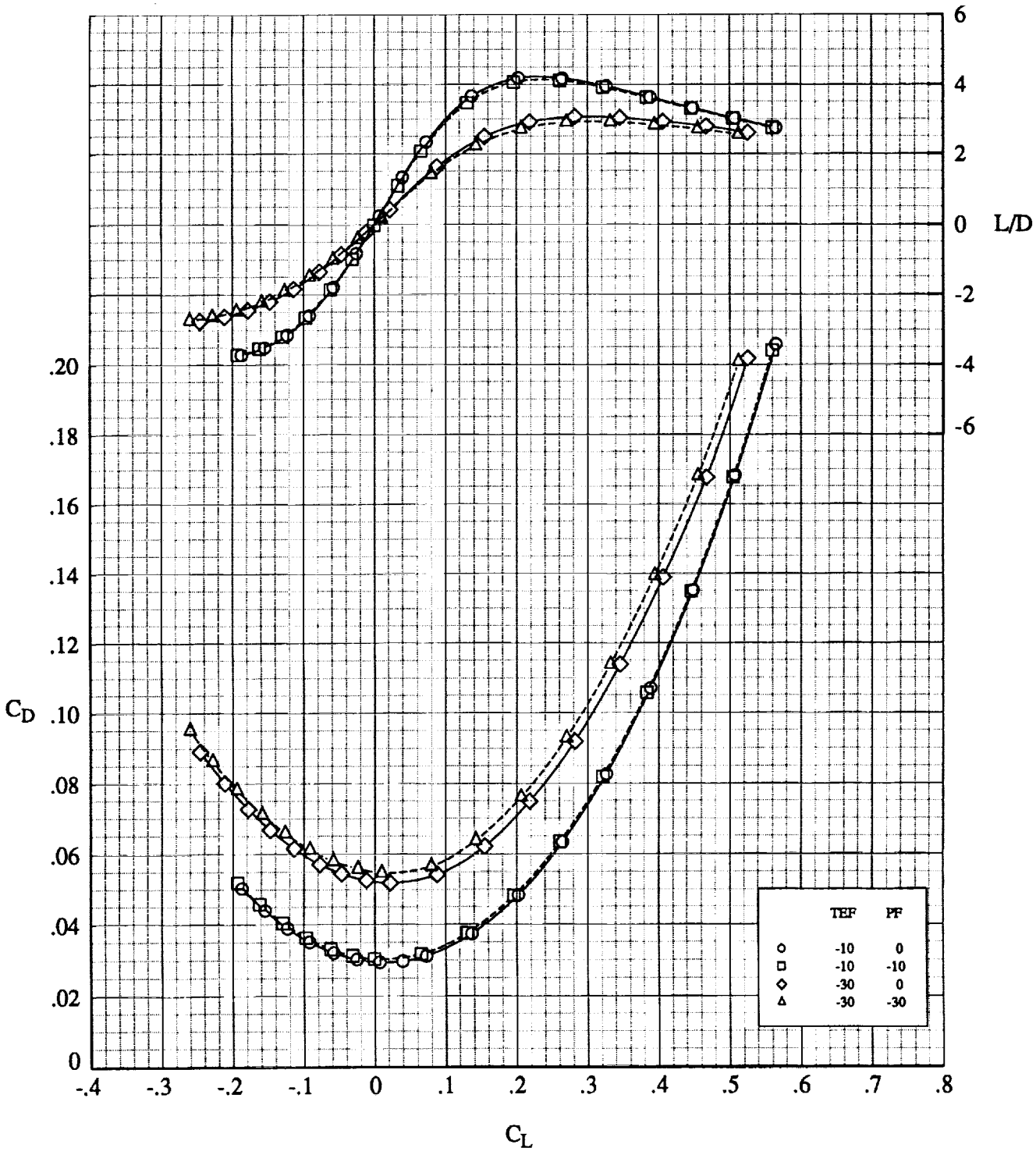

(d) Concluded.

Figure 11. Concluded.

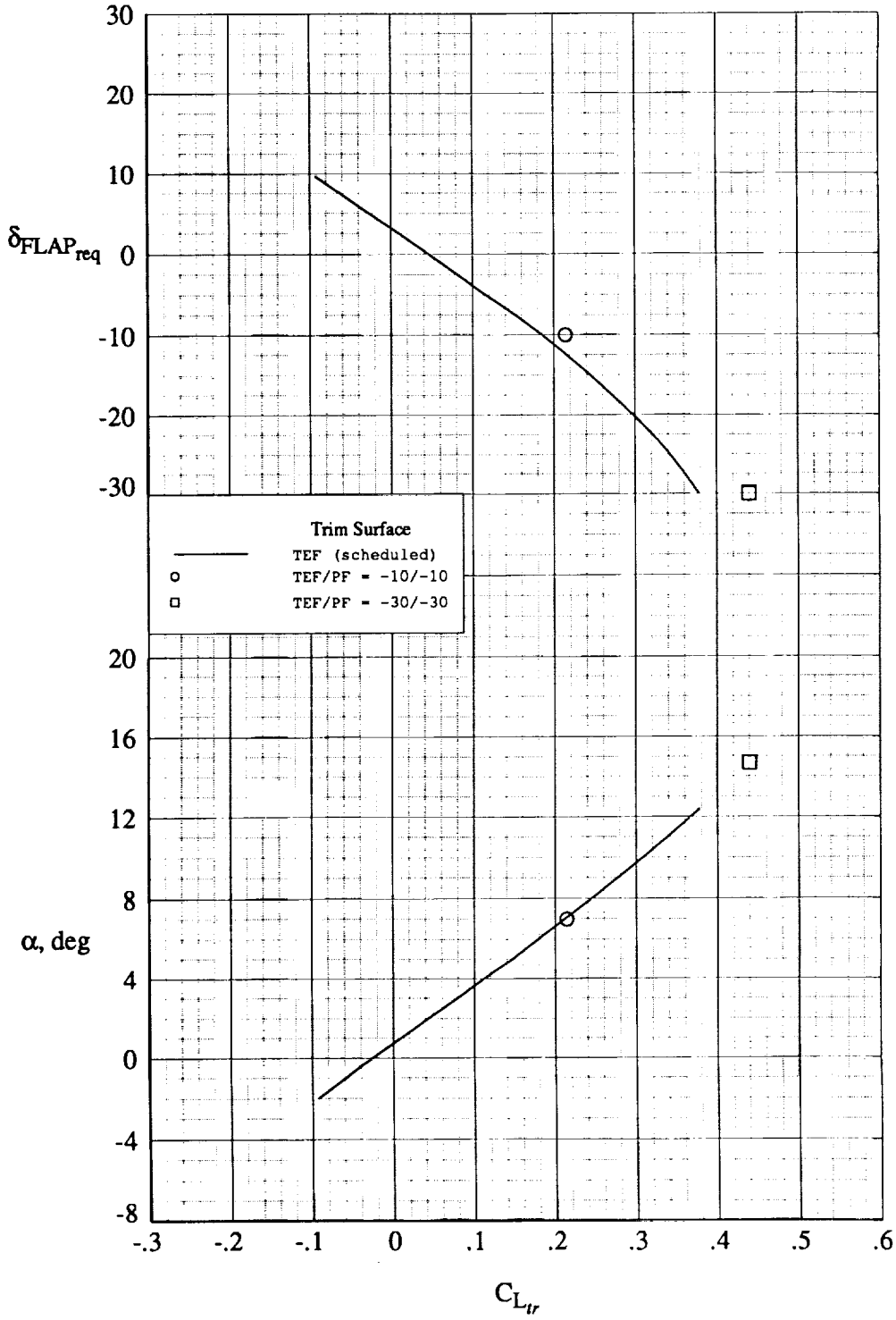

(a) $M = 1.60$.

Figure 12. Pitch flap deflection effects on longitudinal trim for baseline model. LEF = 0°; $CG_{ref} = 0.30\,\bar{c}$.

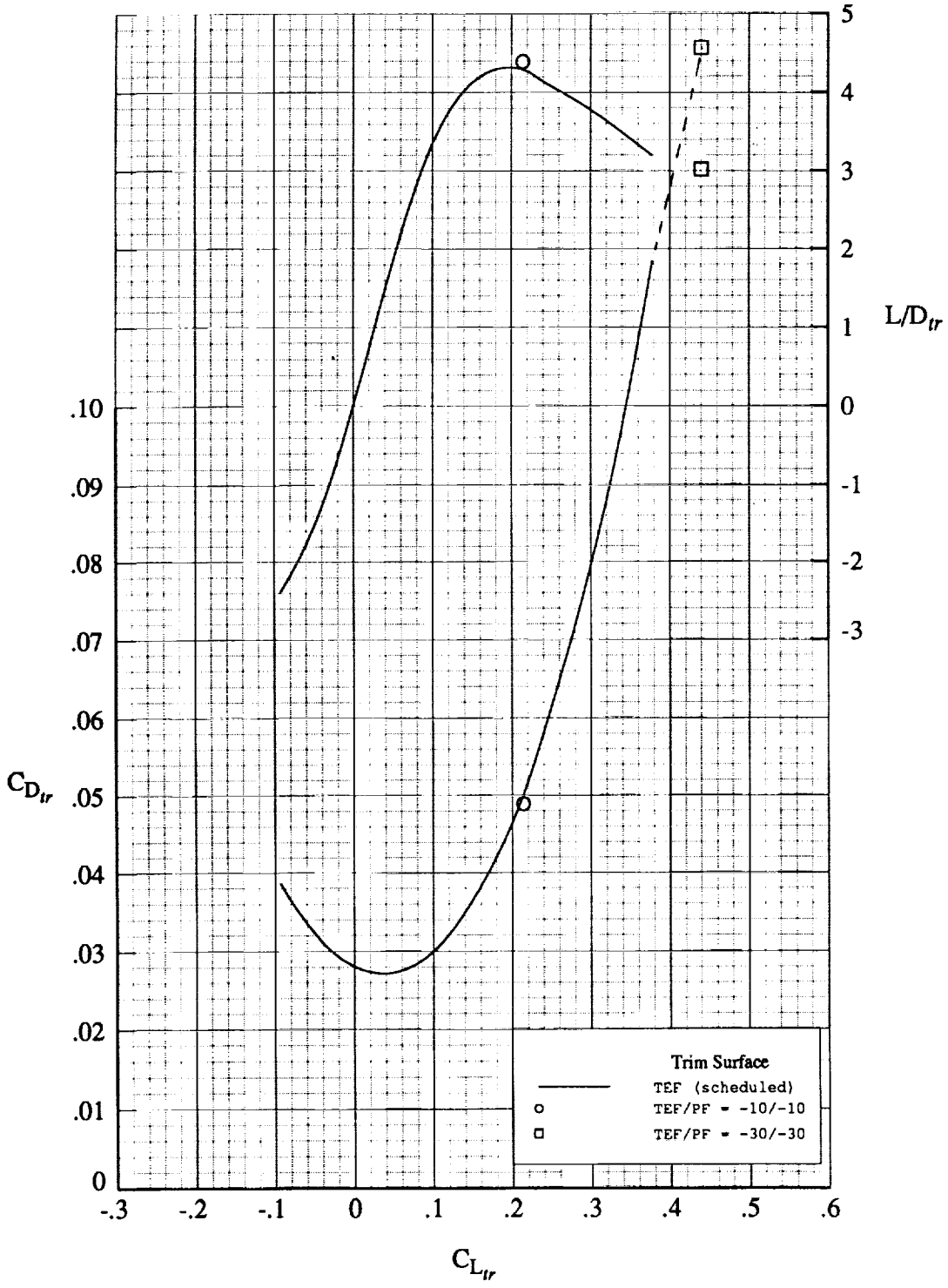

(a) Concluded.

Figure 12. Continued.

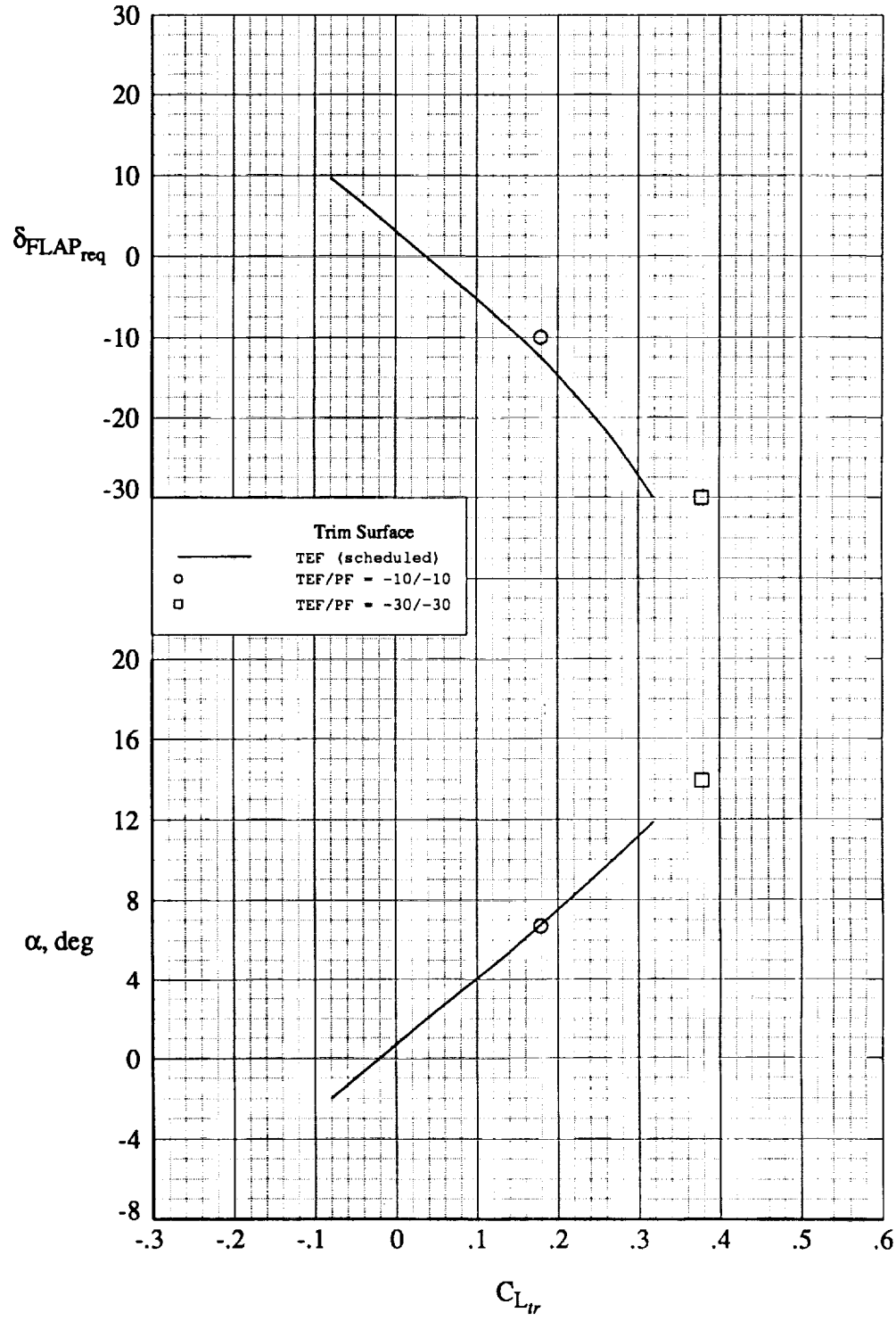

(b) $M = 1.80$.

Figure 12. Continued.

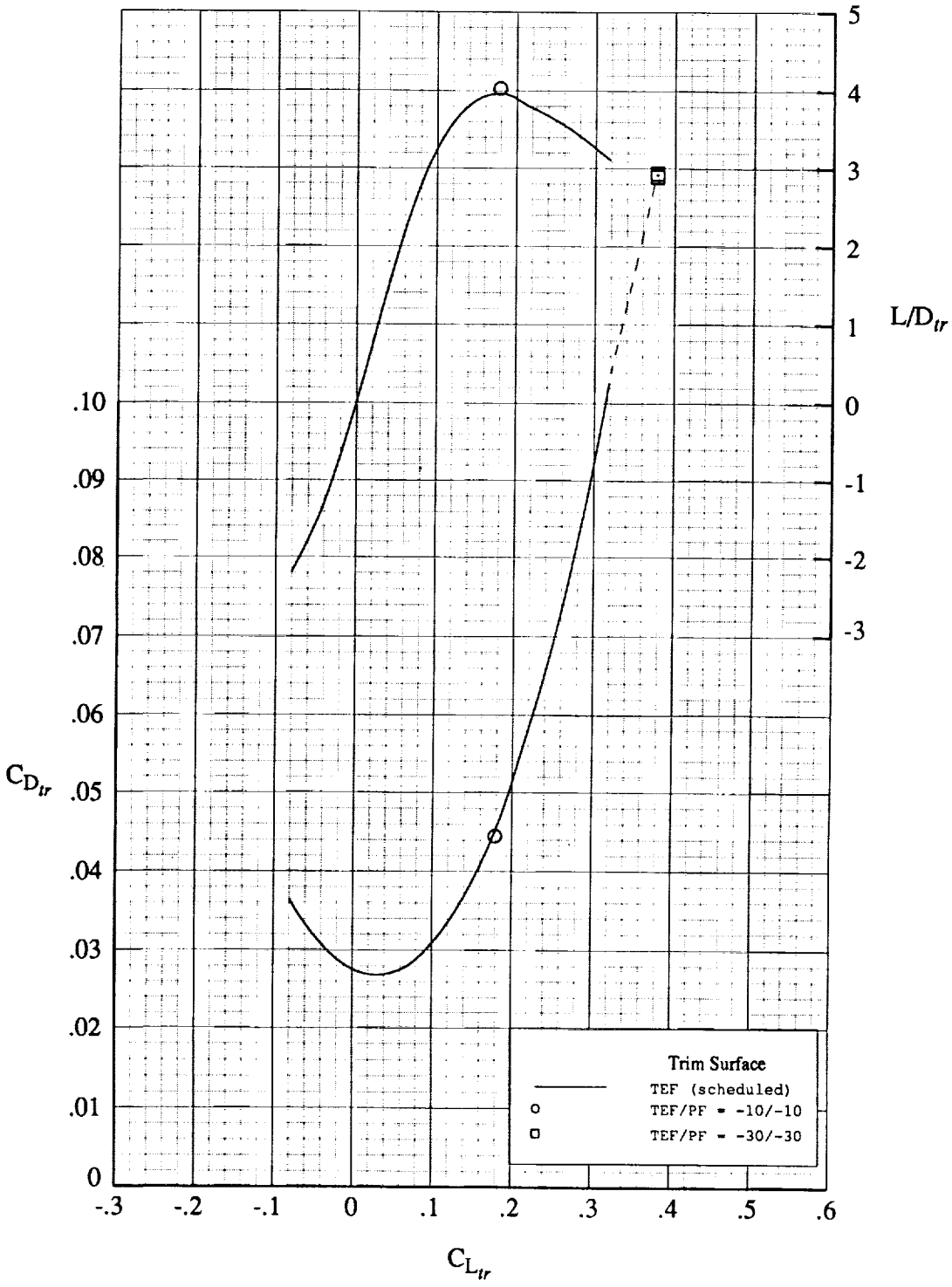

(b) Concluded.

Figure 12. Continued.

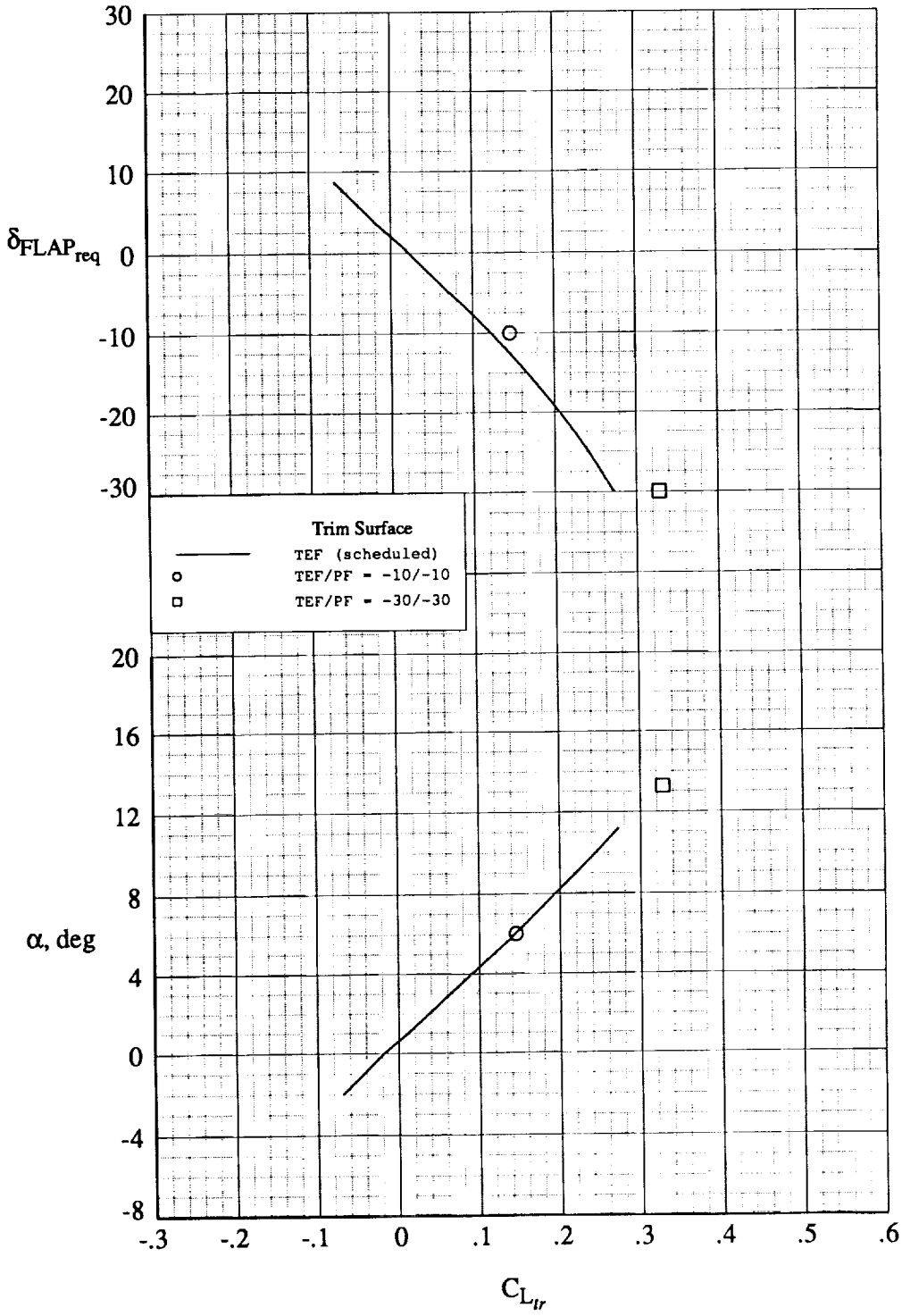

(c) $M = 2.00$.

Figure 12. Continued.

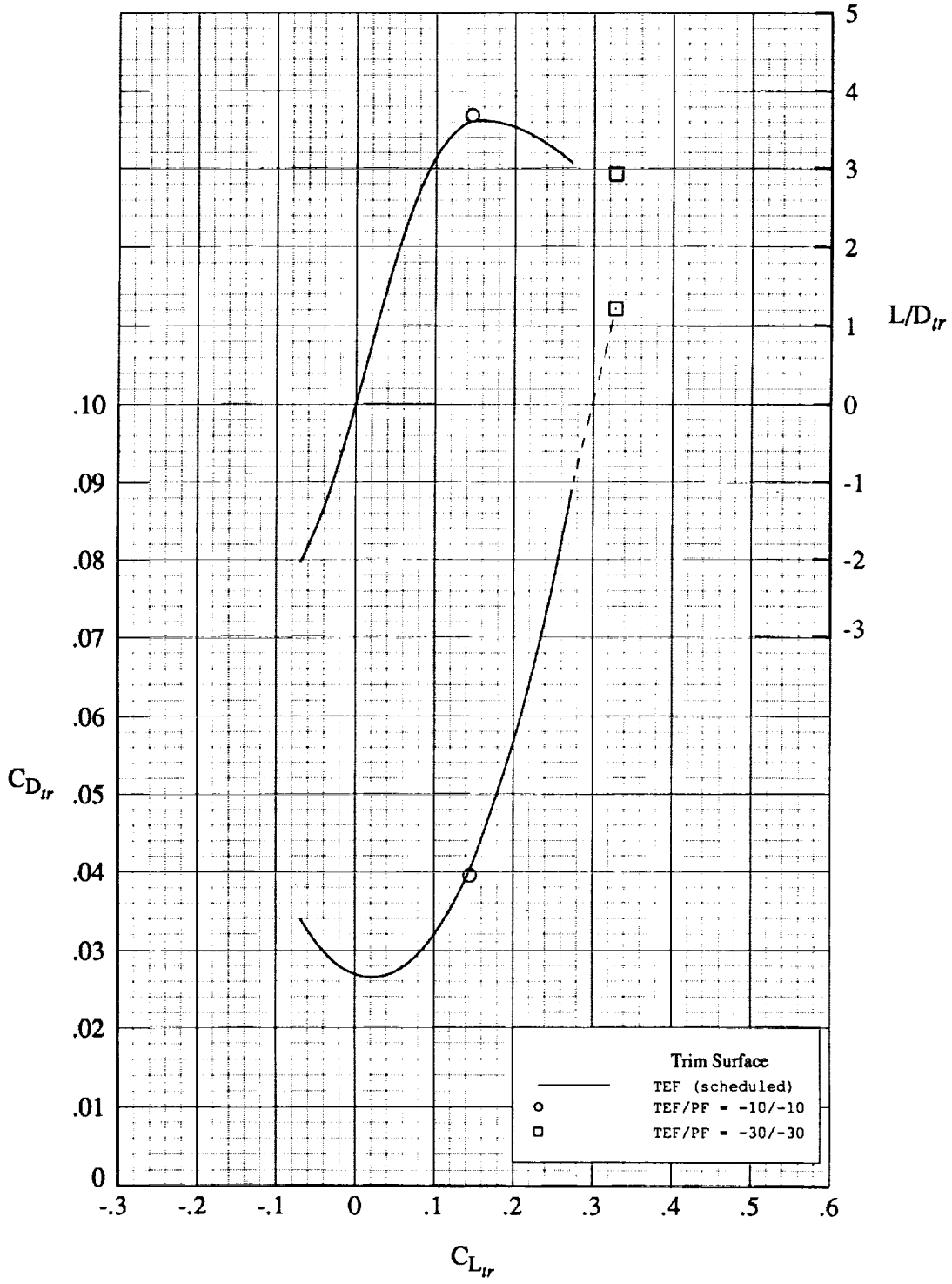

(c) Concluded.

Figure 12. Continued.

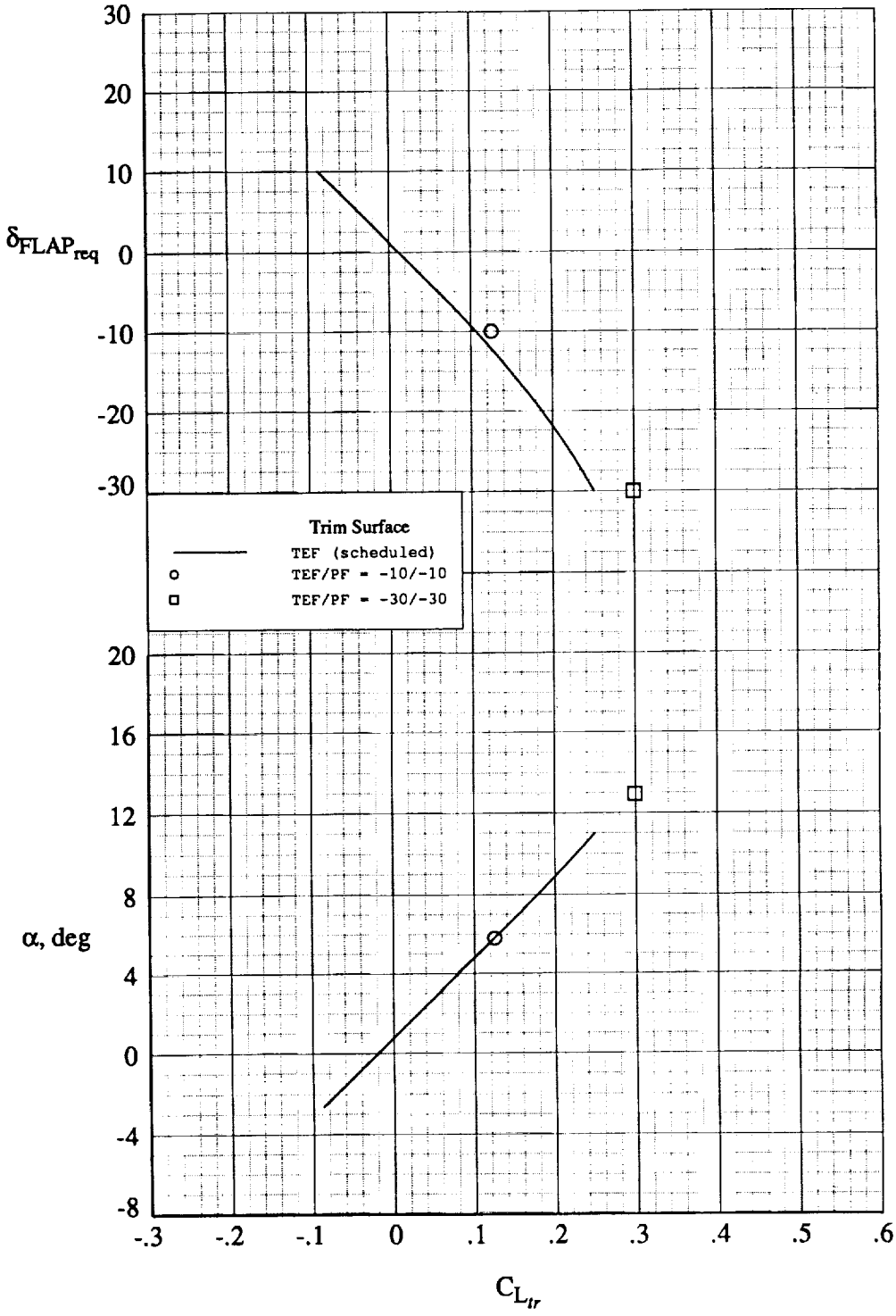

(d) $M = 2.16$.

Figure 12. Continued.

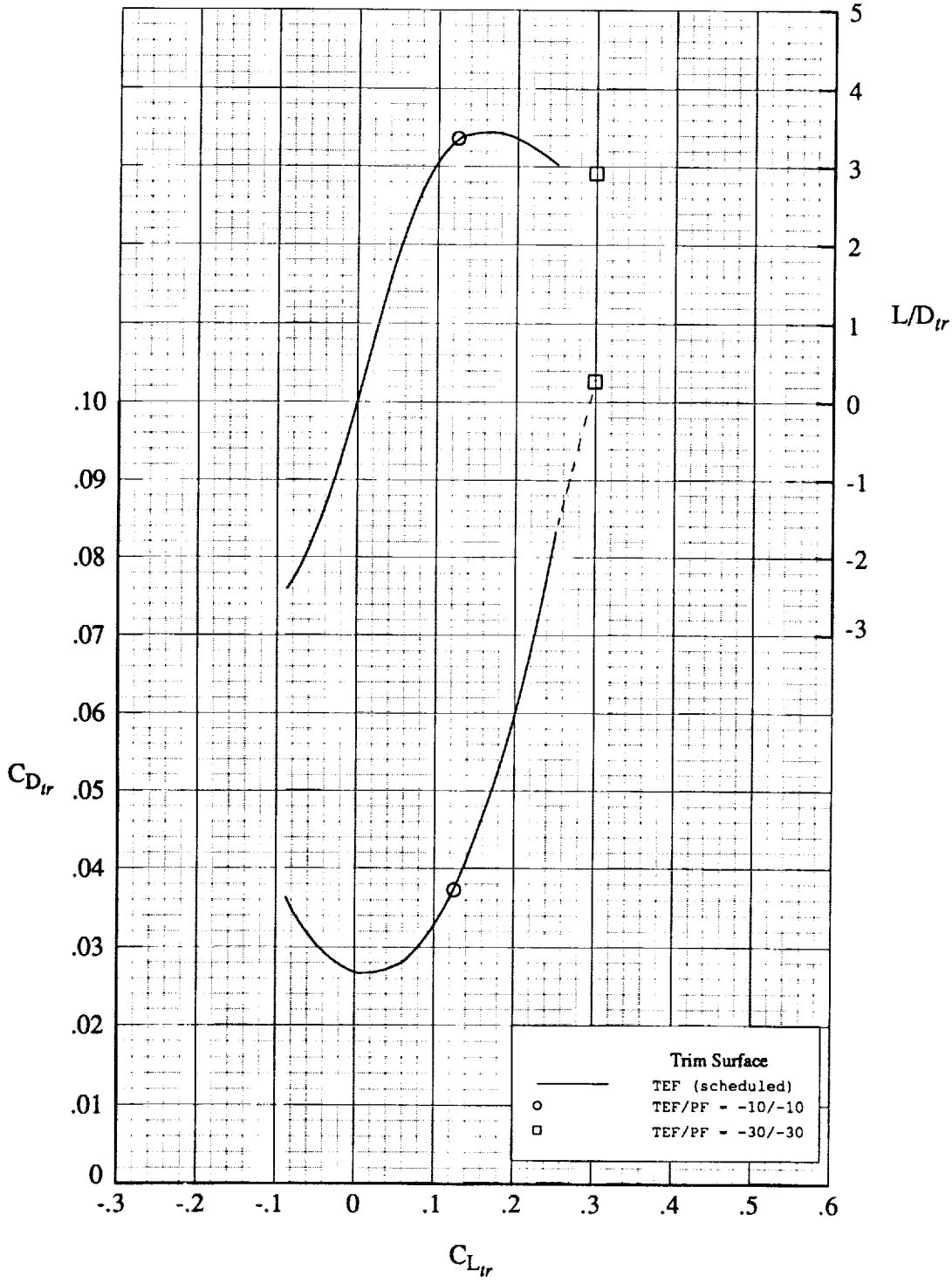

(d) Concluded.

Figure 12. Concluded.

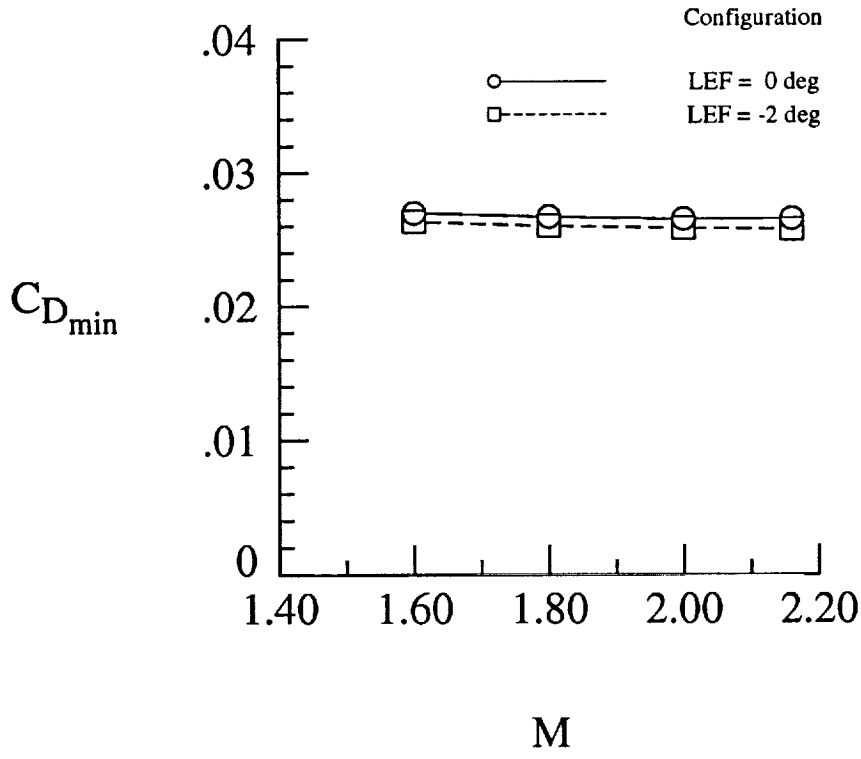

Figure 13. Uprigged leading-edge flap effect on untrimmed minimum drag for baseline model at TEF = 0°.

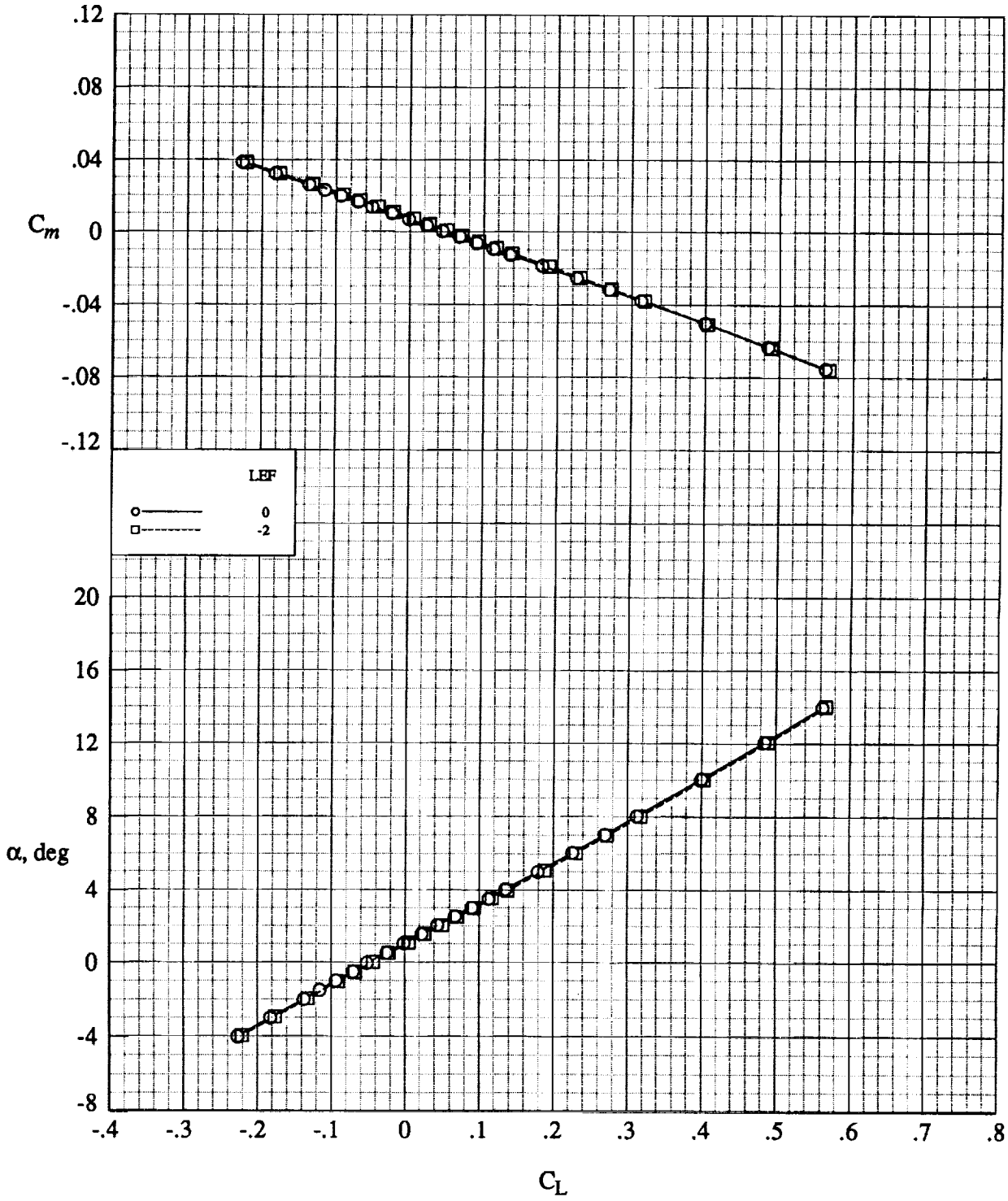

(a) $M = 1.60$.

Figure 14. Untrimmed longitudinal effect of uprigged leading-edge flaps on baseline model. TEF = 0°; $CG_{ref} = 0.30\bar{c}$.

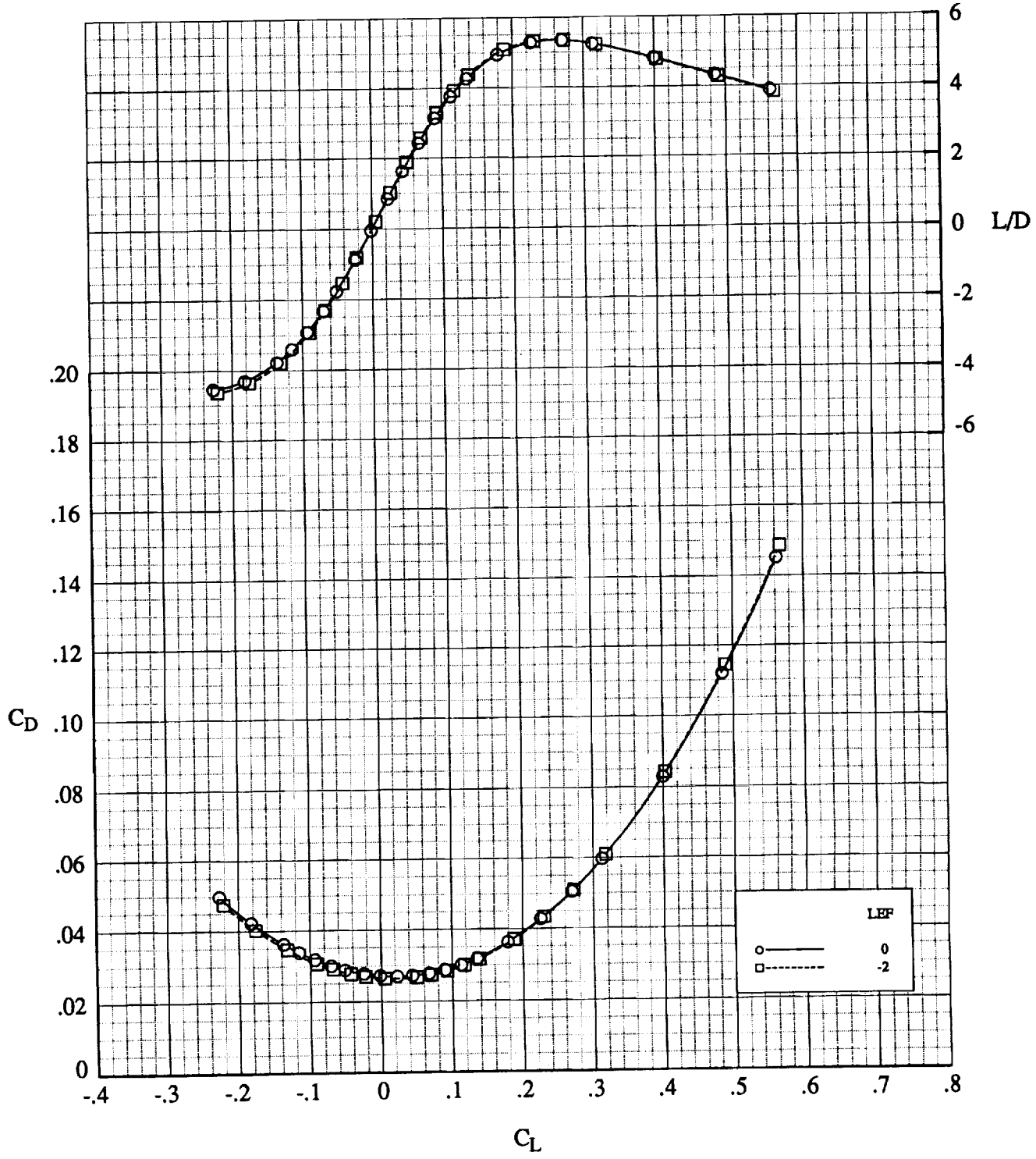

(a) Concluded.

Figure 14. Continued.

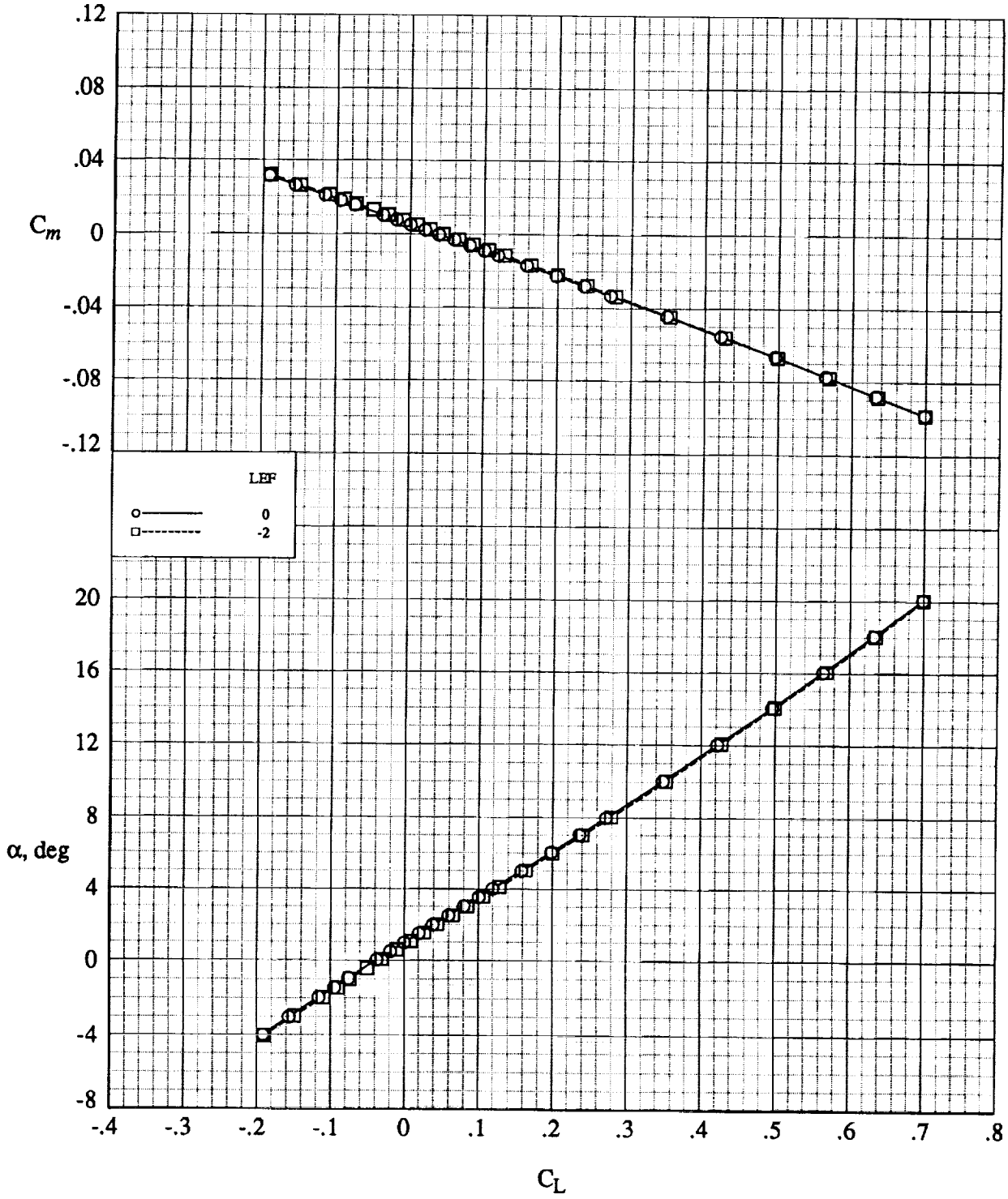

(b) $M = 1.80$.

Figure 14. Continued.

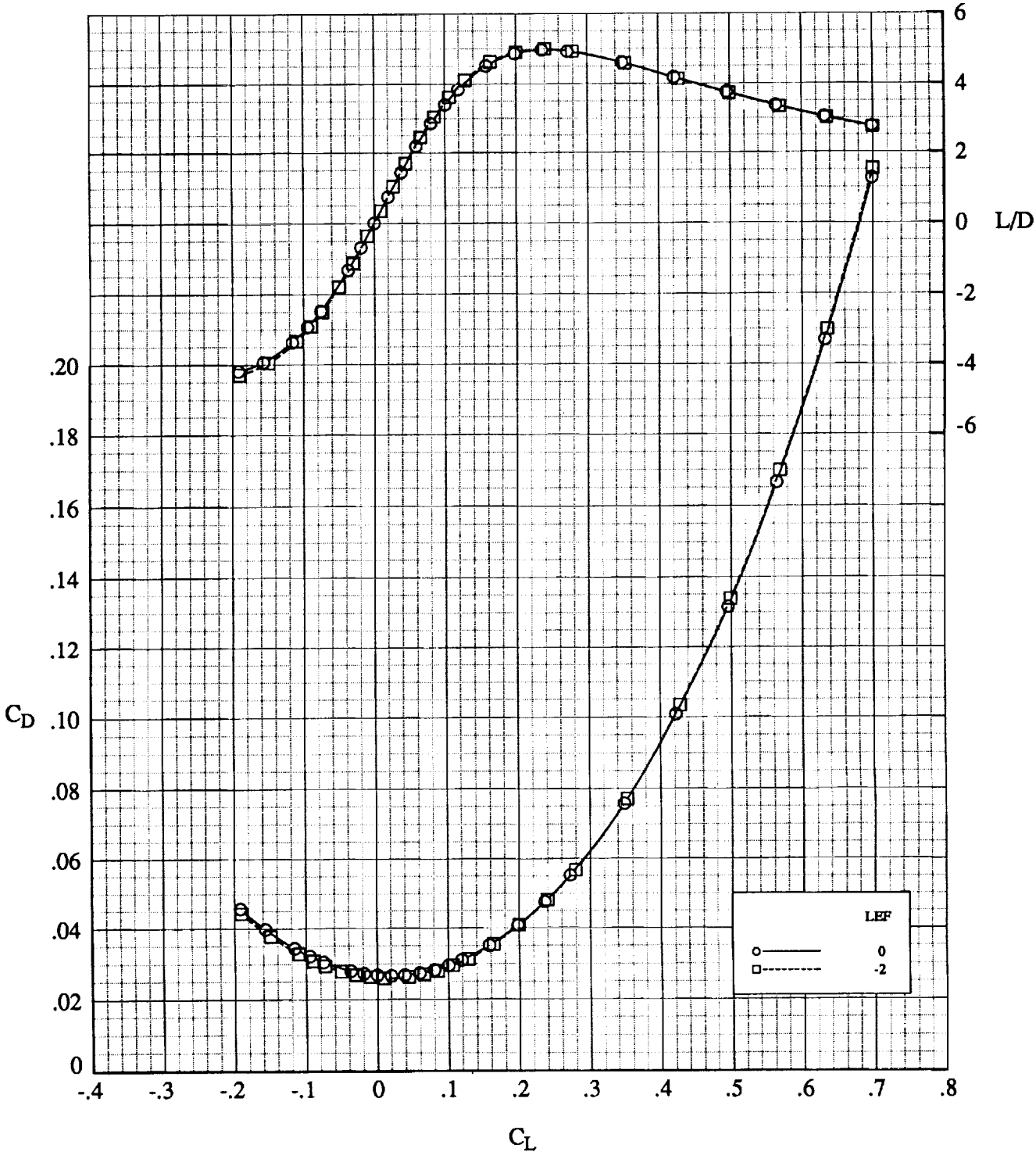

(b) Concluded.

Figure 14. Continued.

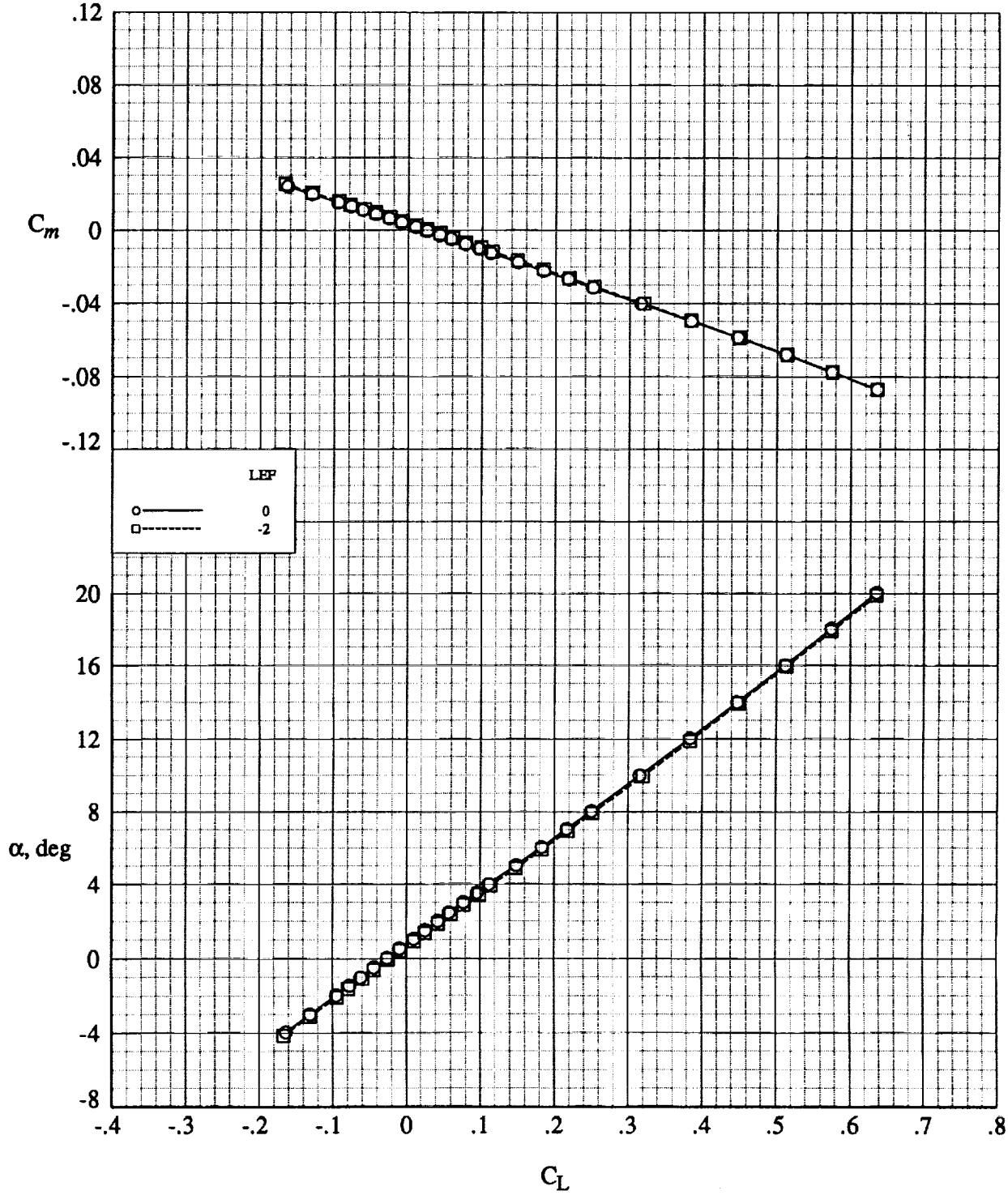

(c) $M = 2.00$.

Figure 14. Continued.

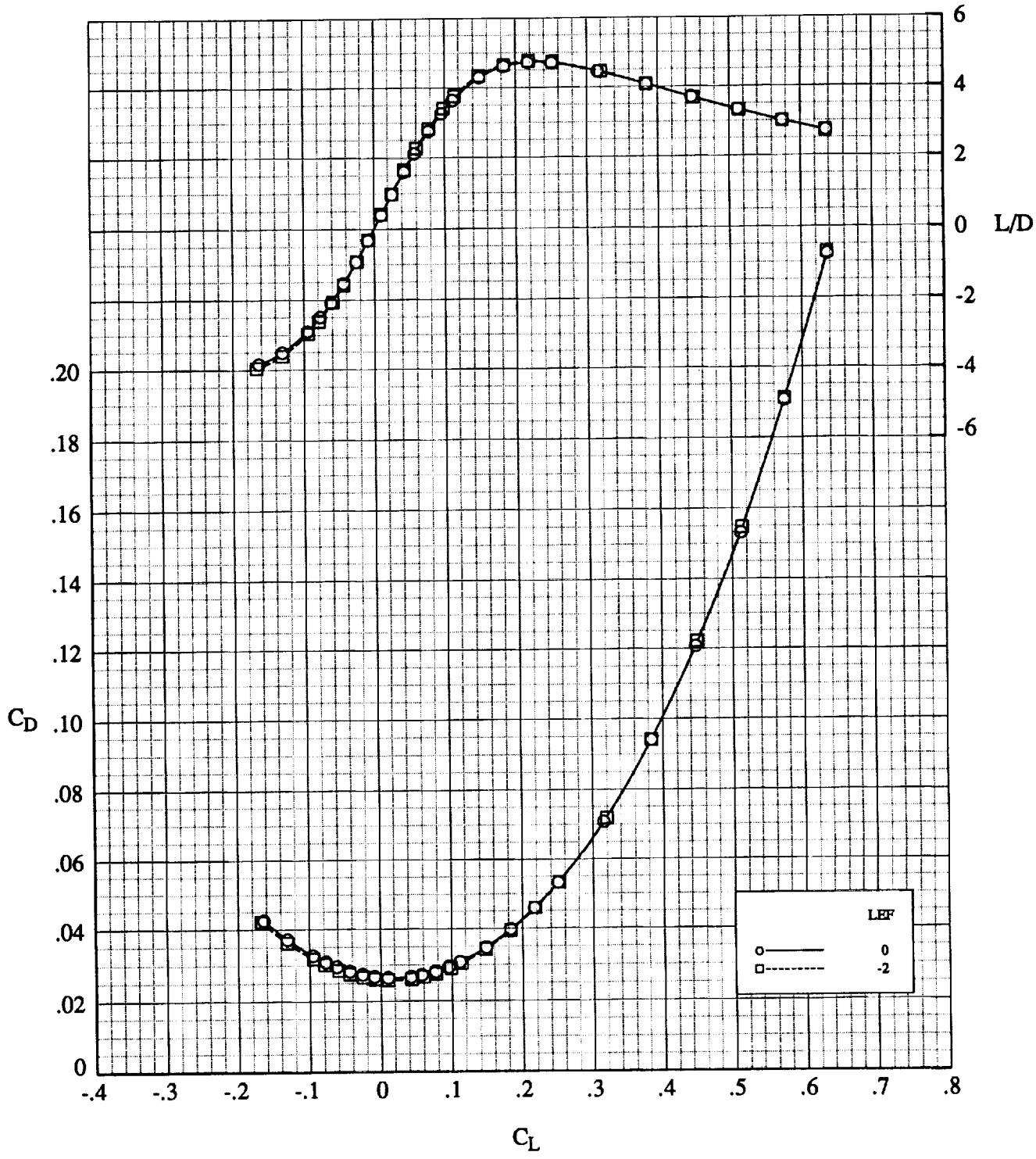

(c) Concluded.

Figure 14. Continued.

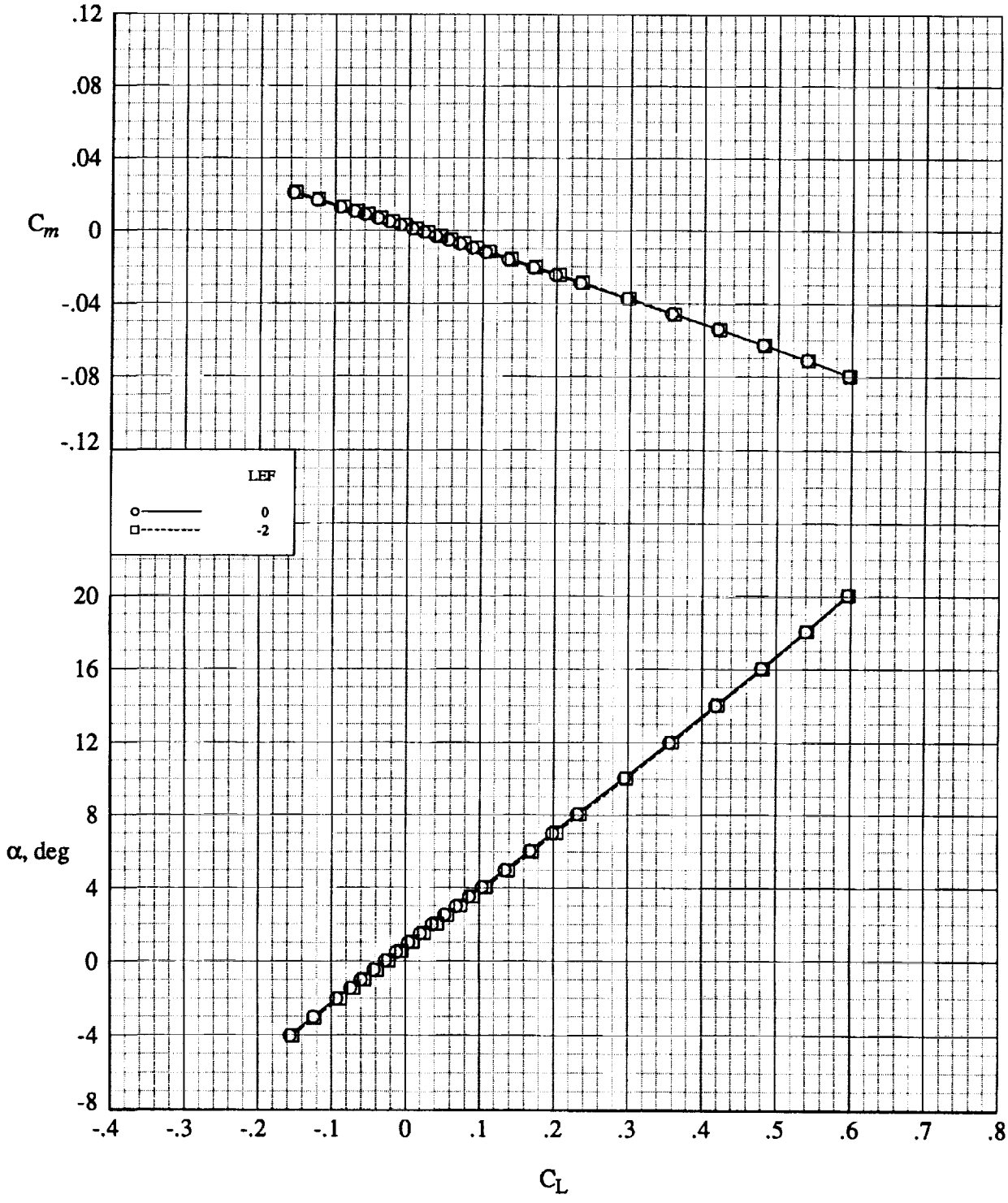

(d) $M = 2.16$.

Figure 14. Continued.

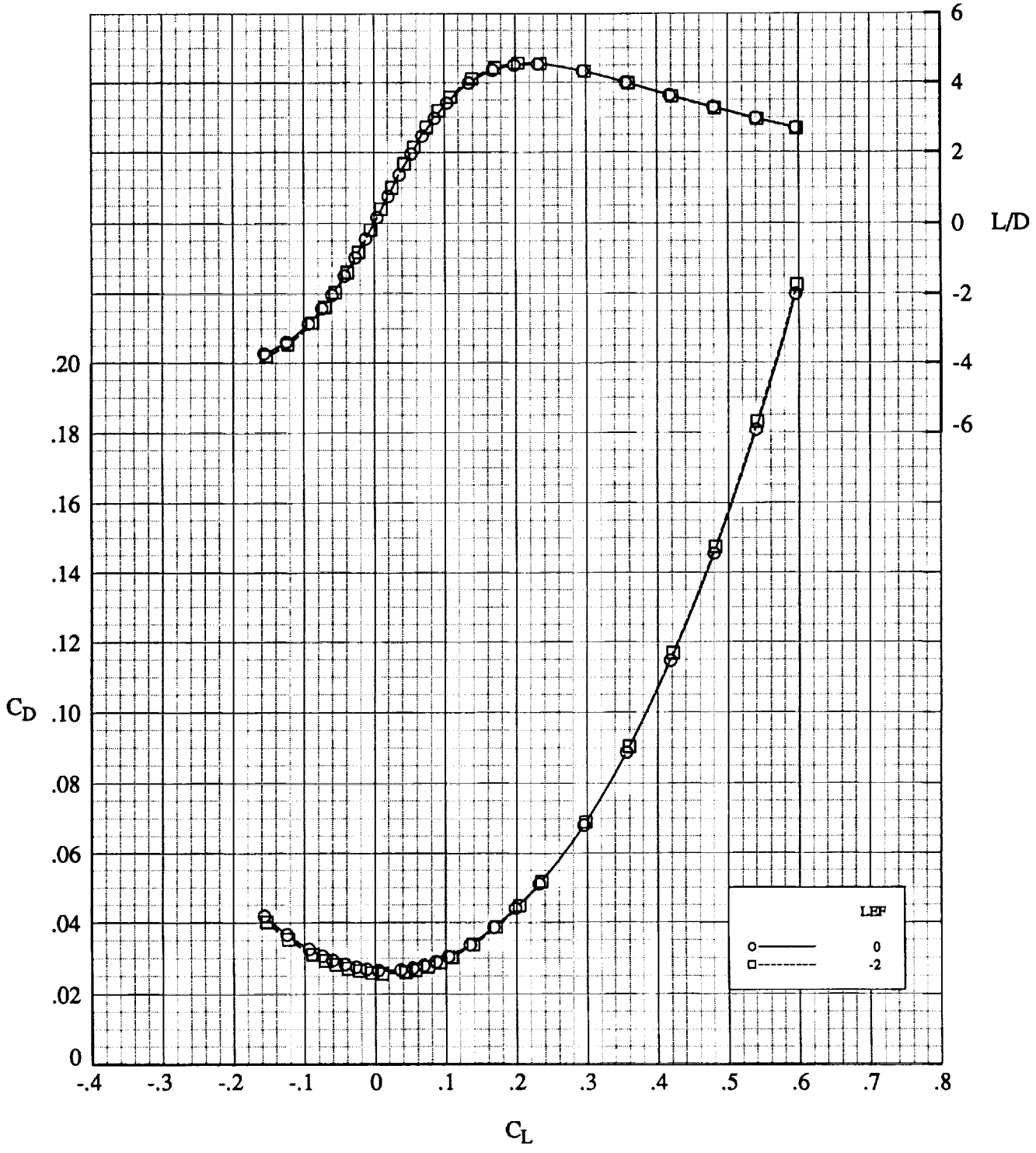

(d) Concluded.

Figure 14. Concluded.

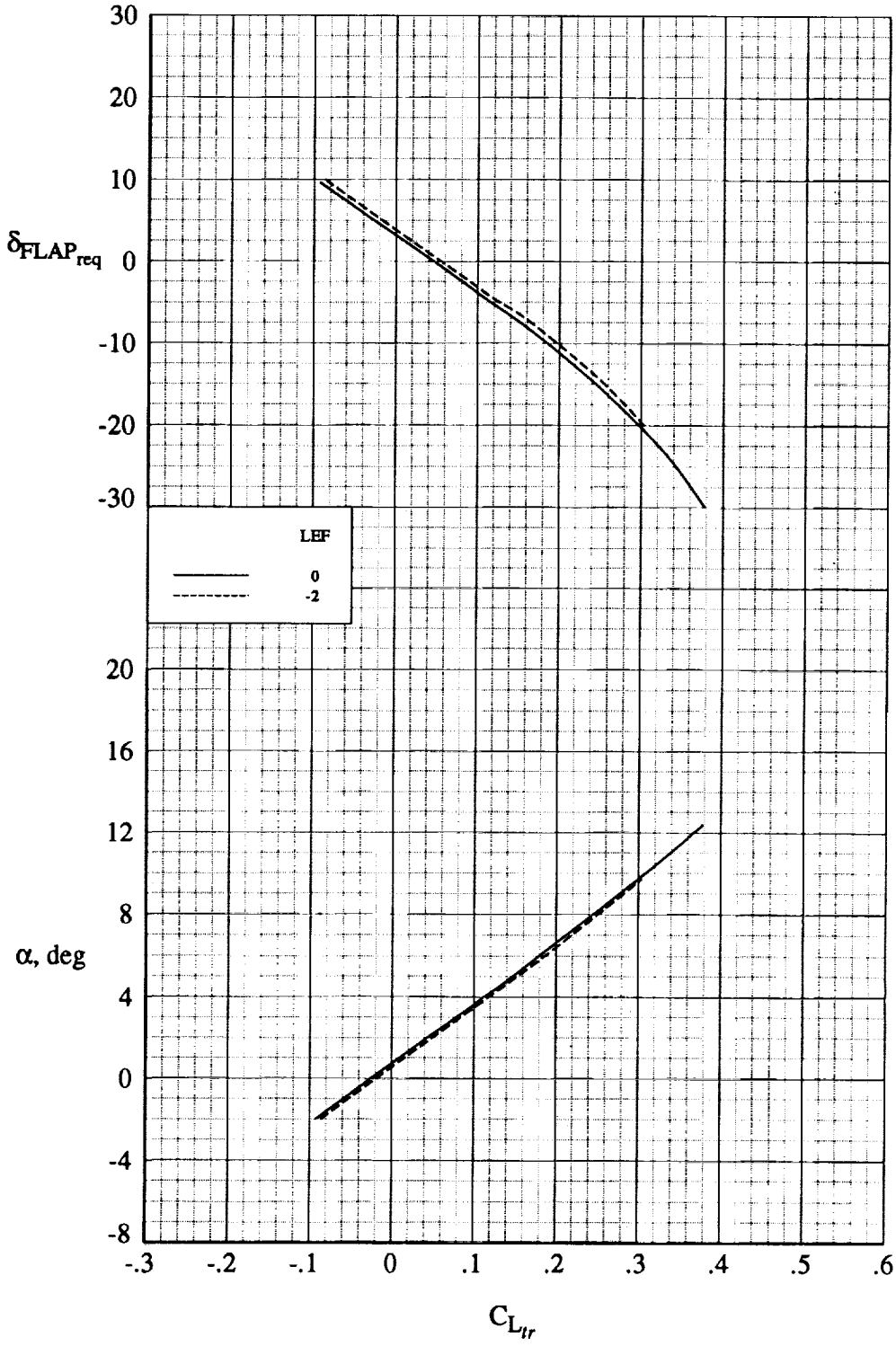

(a) $M = 1.60$.

Figure 15. Trimmed longitudinal effect of uprigged leading-edge flaps on baseline model. $CG_{ref} = 0.30\,\bar{c}$.

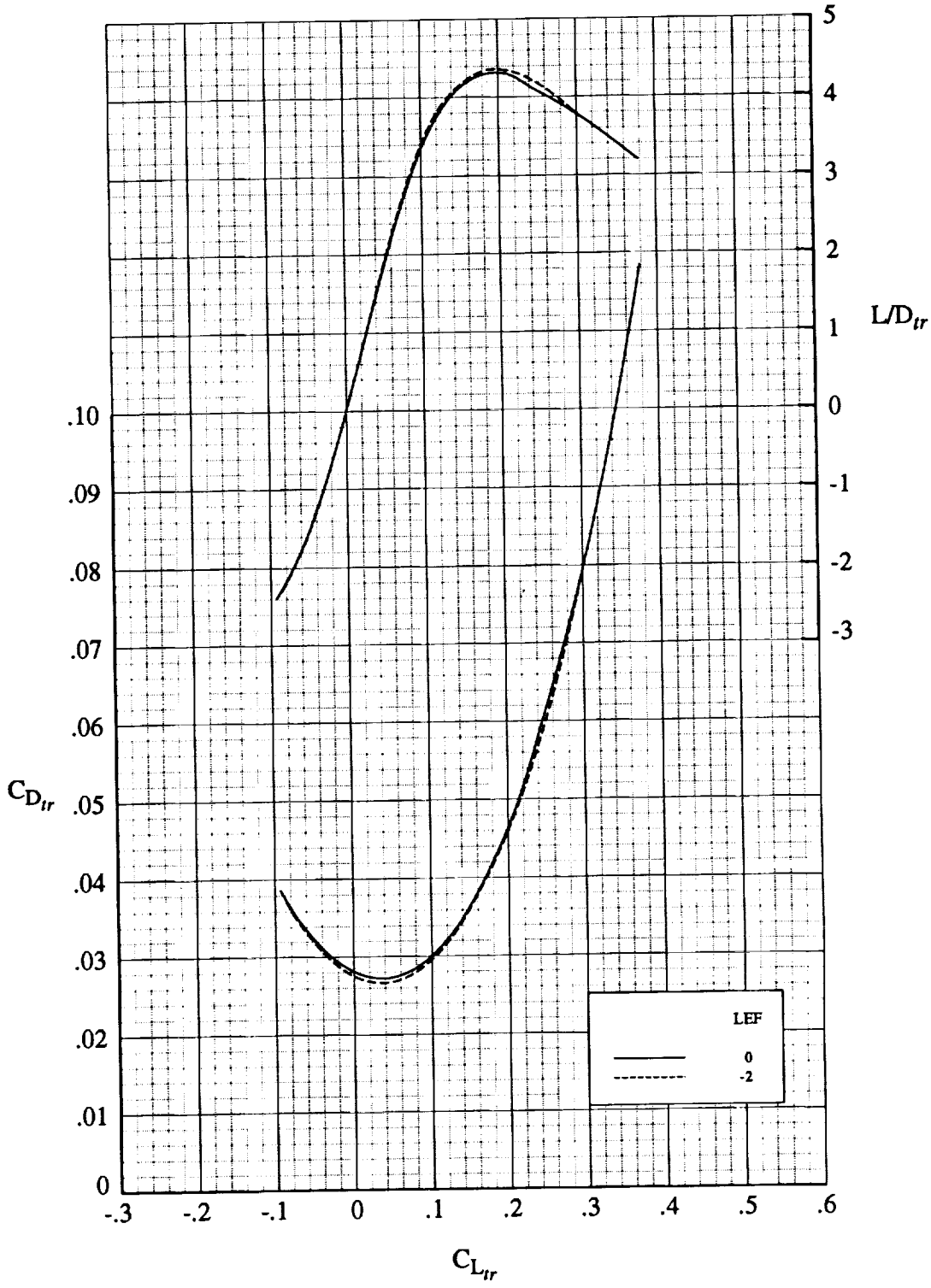

(a) Concluded.

Figure 15. Continued.

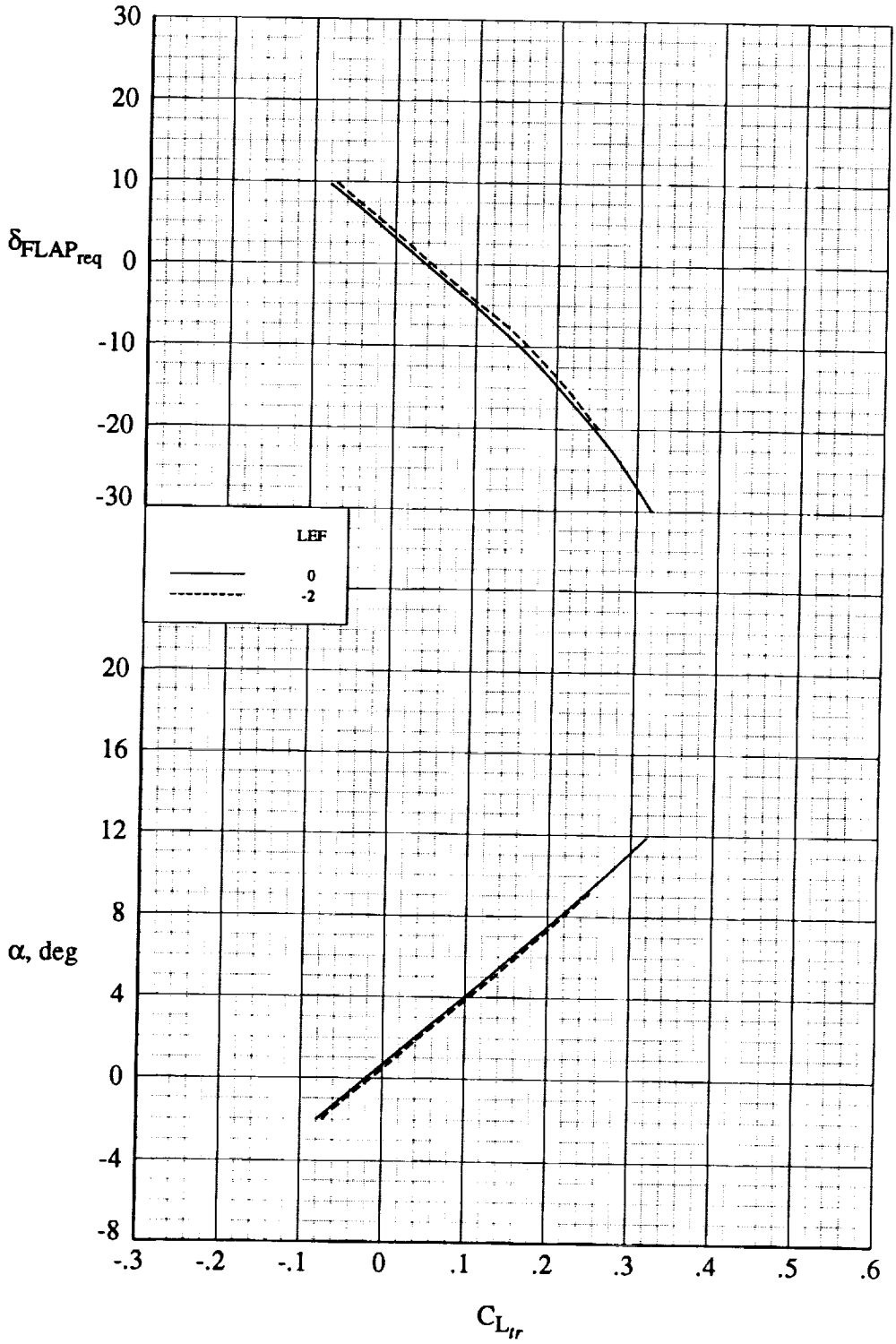

(b) $M = 1.80$.

Figure 15. Continued.

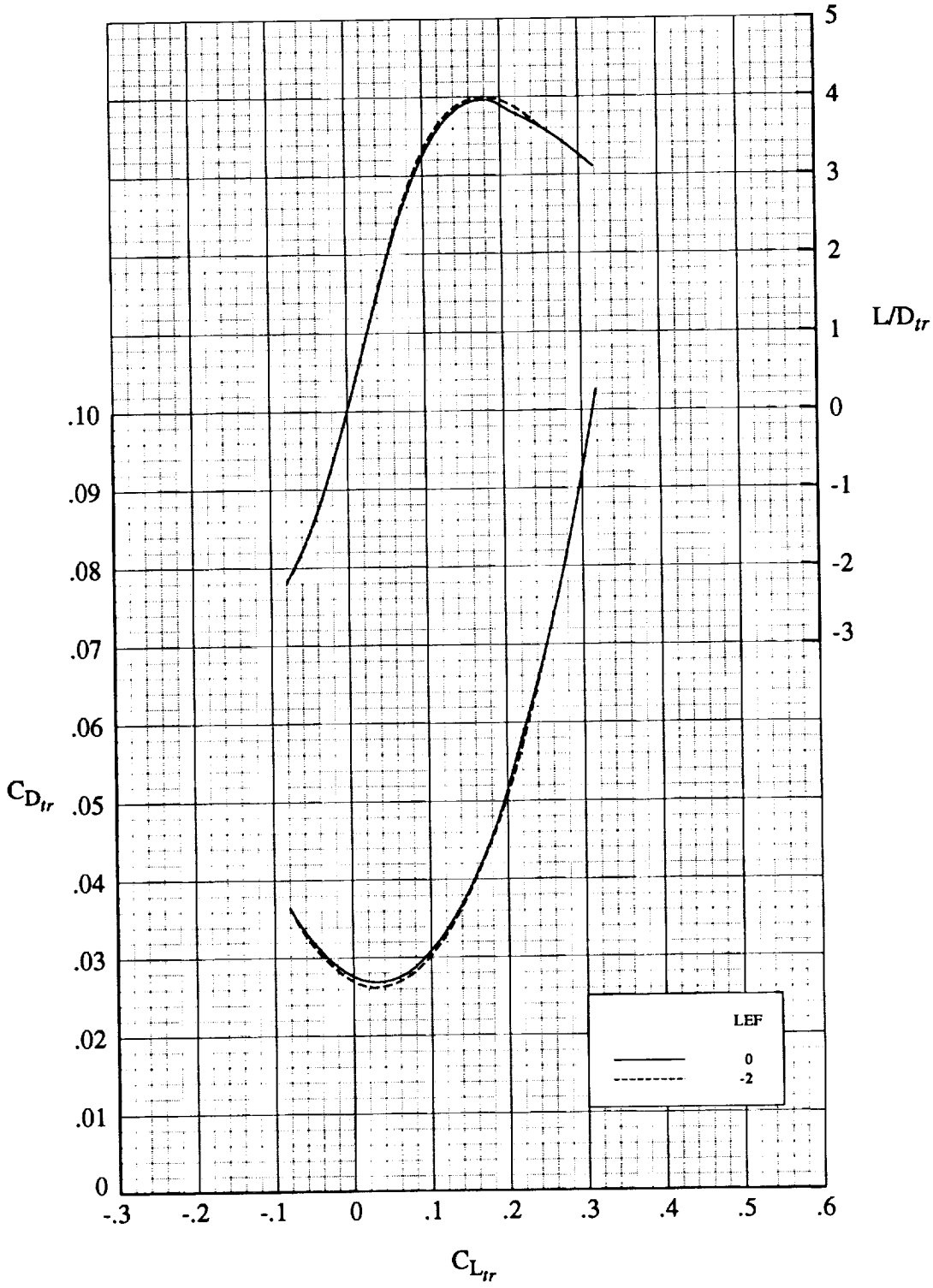

(b) Concluded.

Figure 15. Continued.

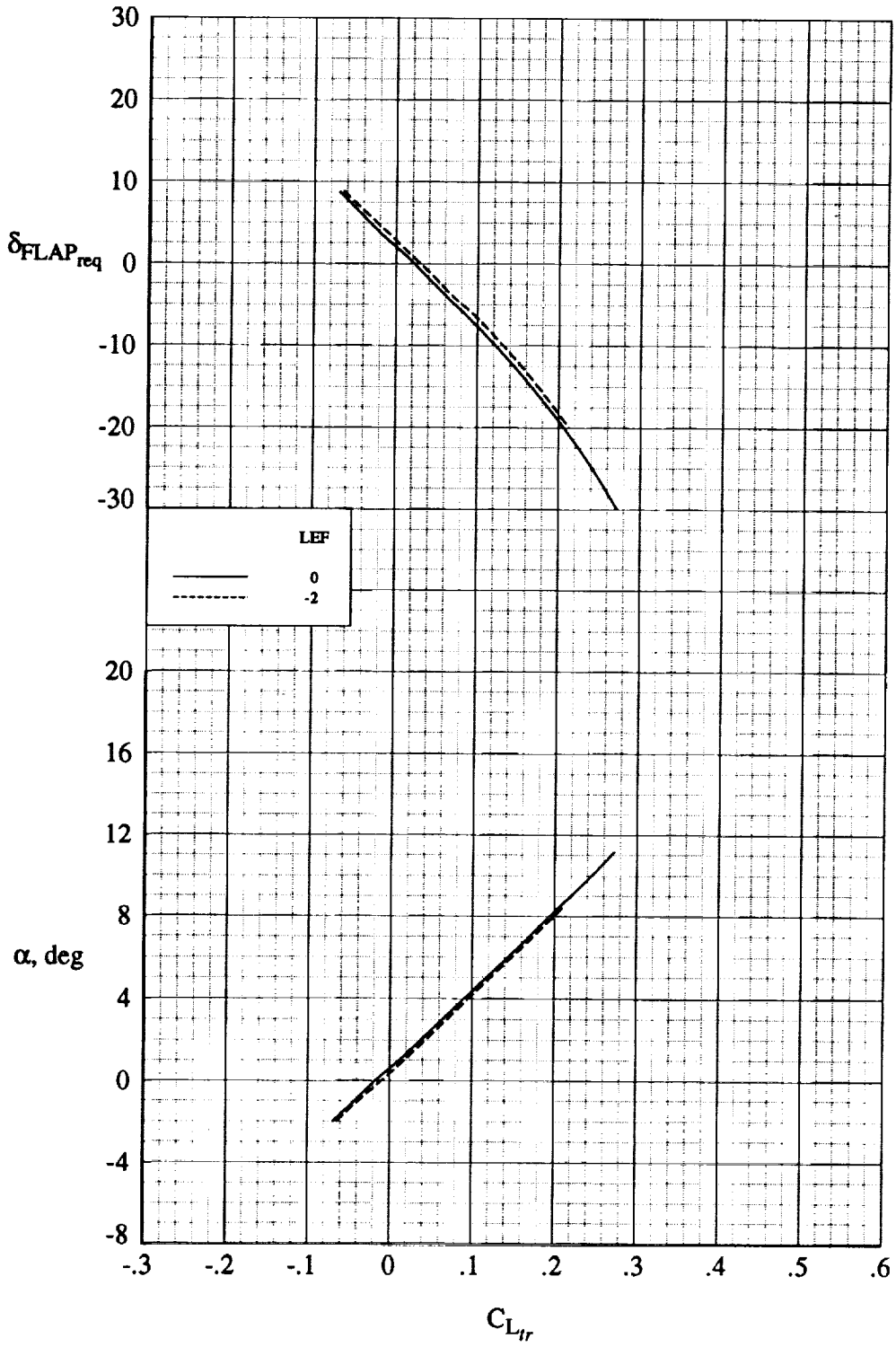

(c) $M = 2.00$.

Figure 15. Continued.

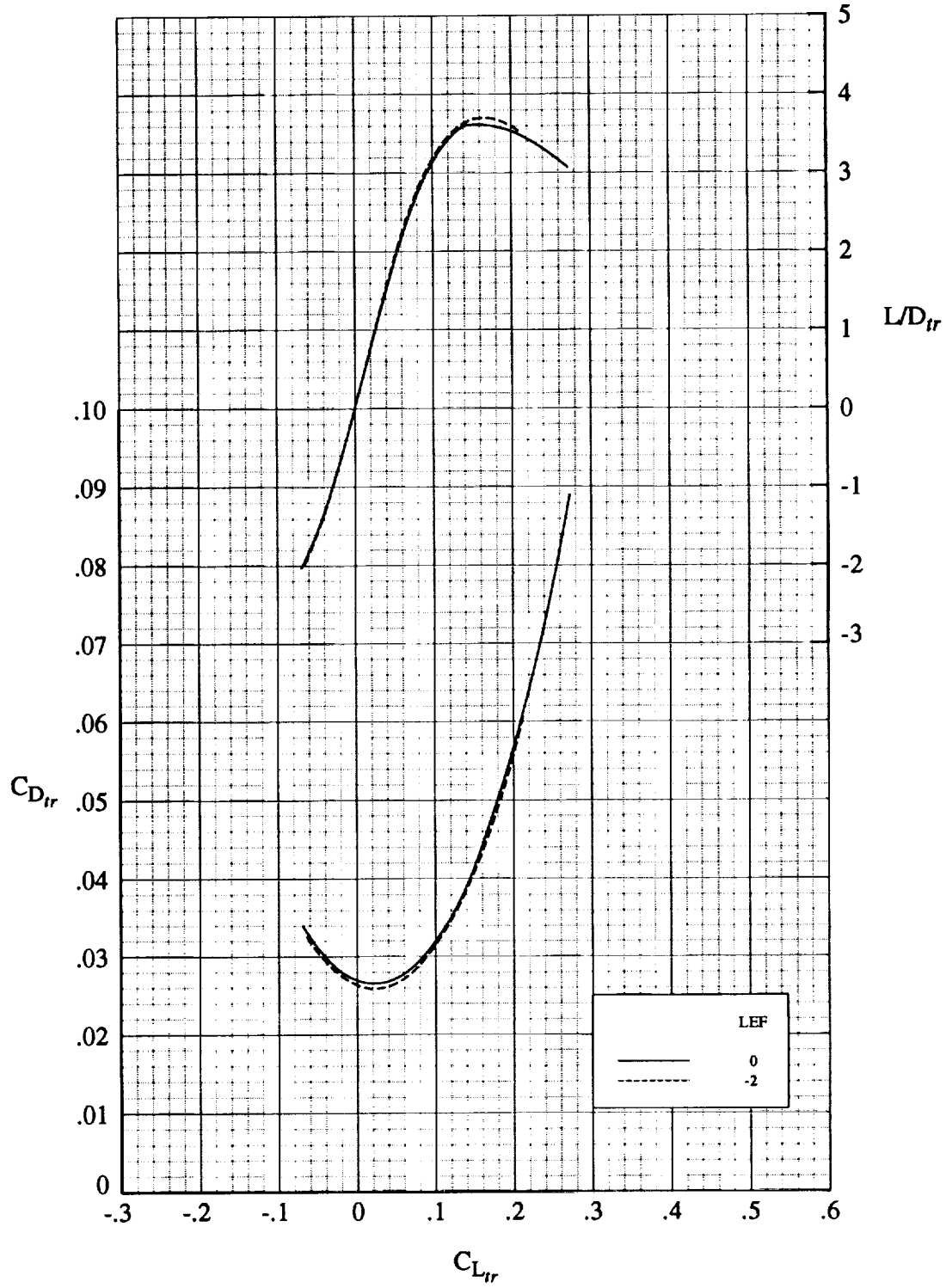

(c) Concluded.

Figure 15. Continued.

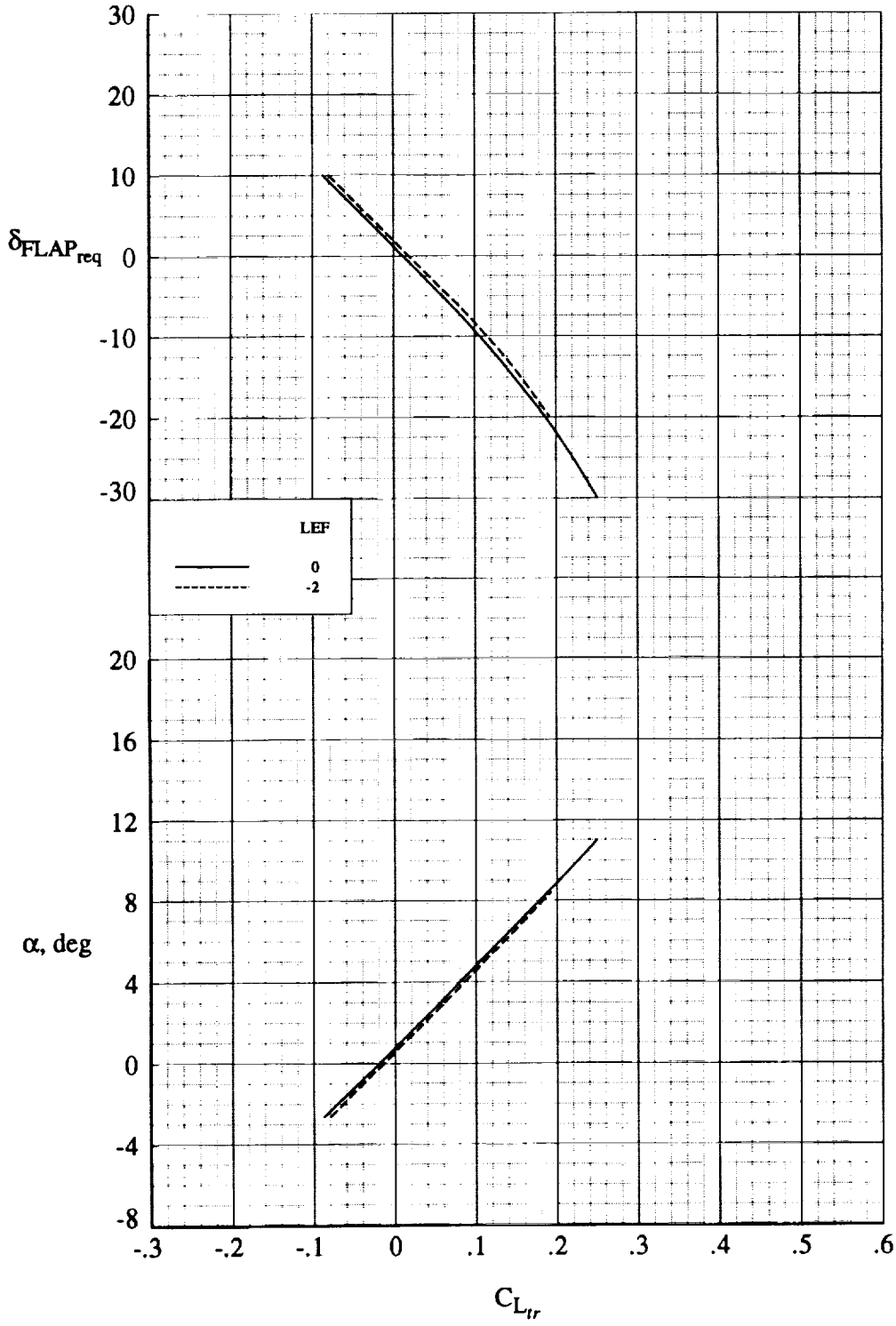

(d) $M = 2.16$.

Figure 15. Continued.

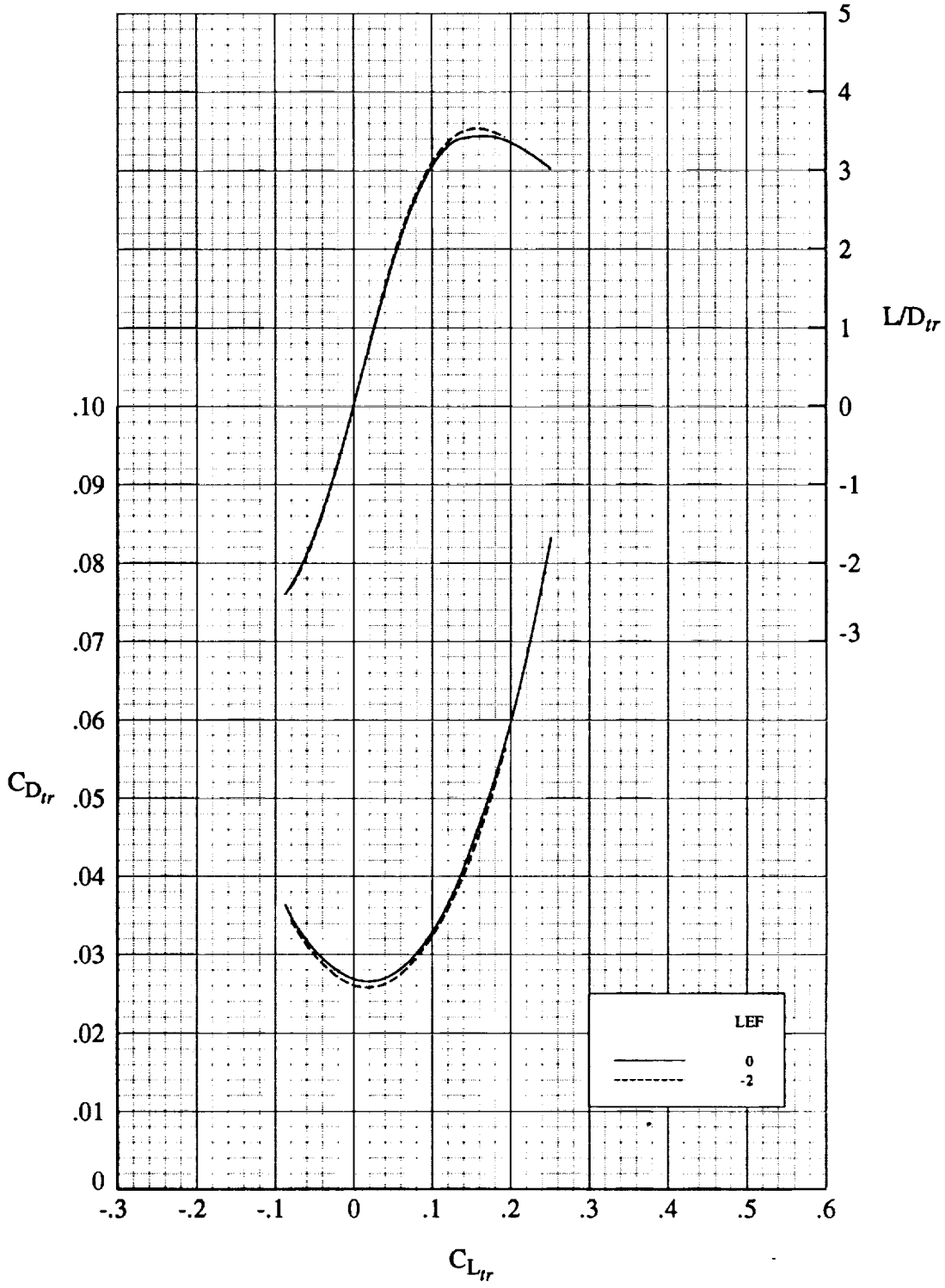

(d) Concluded.

Figure 15. Concluded.

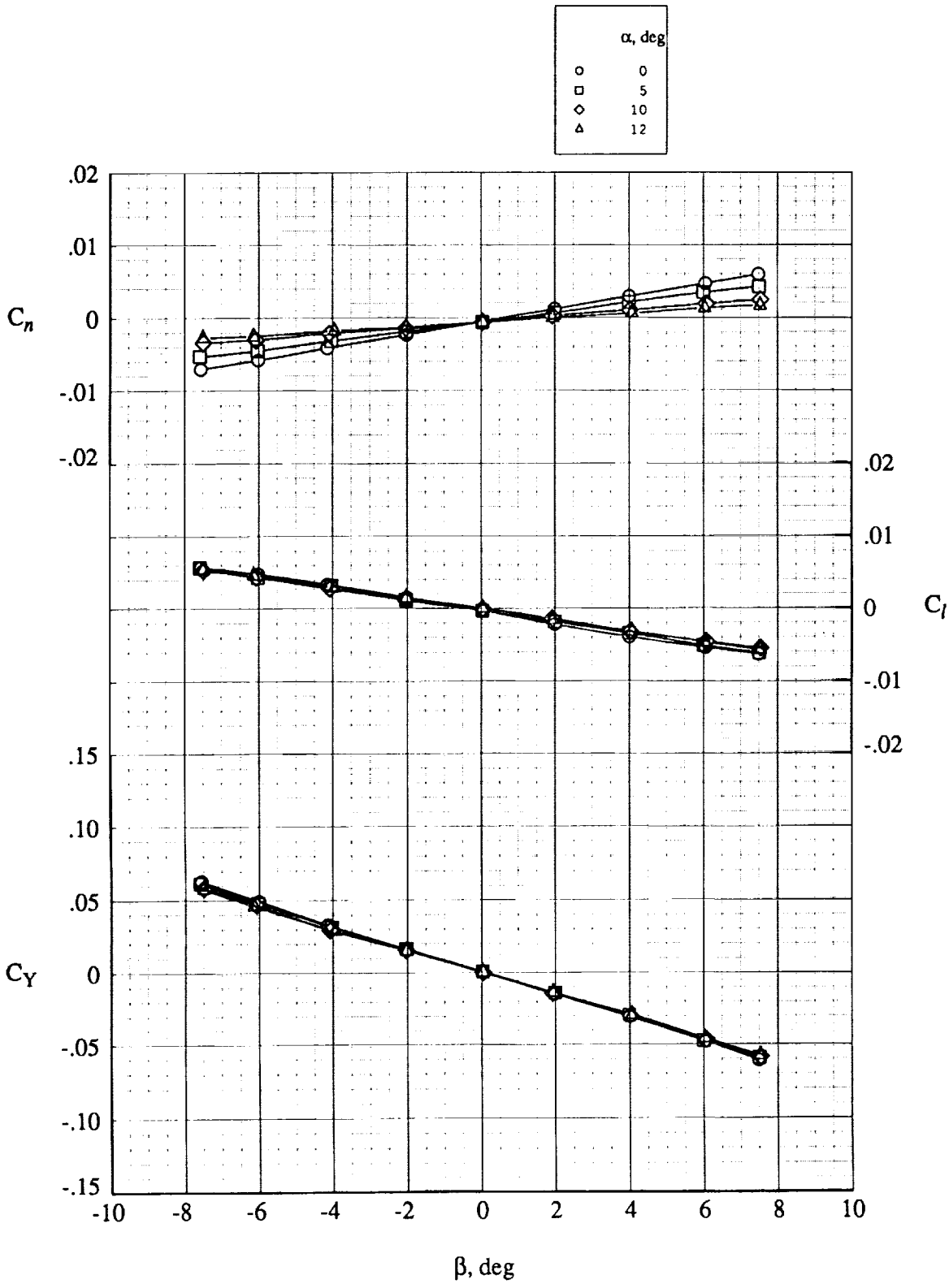

(a) $M = 1.60$.

Figure 16. Variation of yawing-moment, rolling-moment, and side-force coefficients with sideslip for baseline configuration.

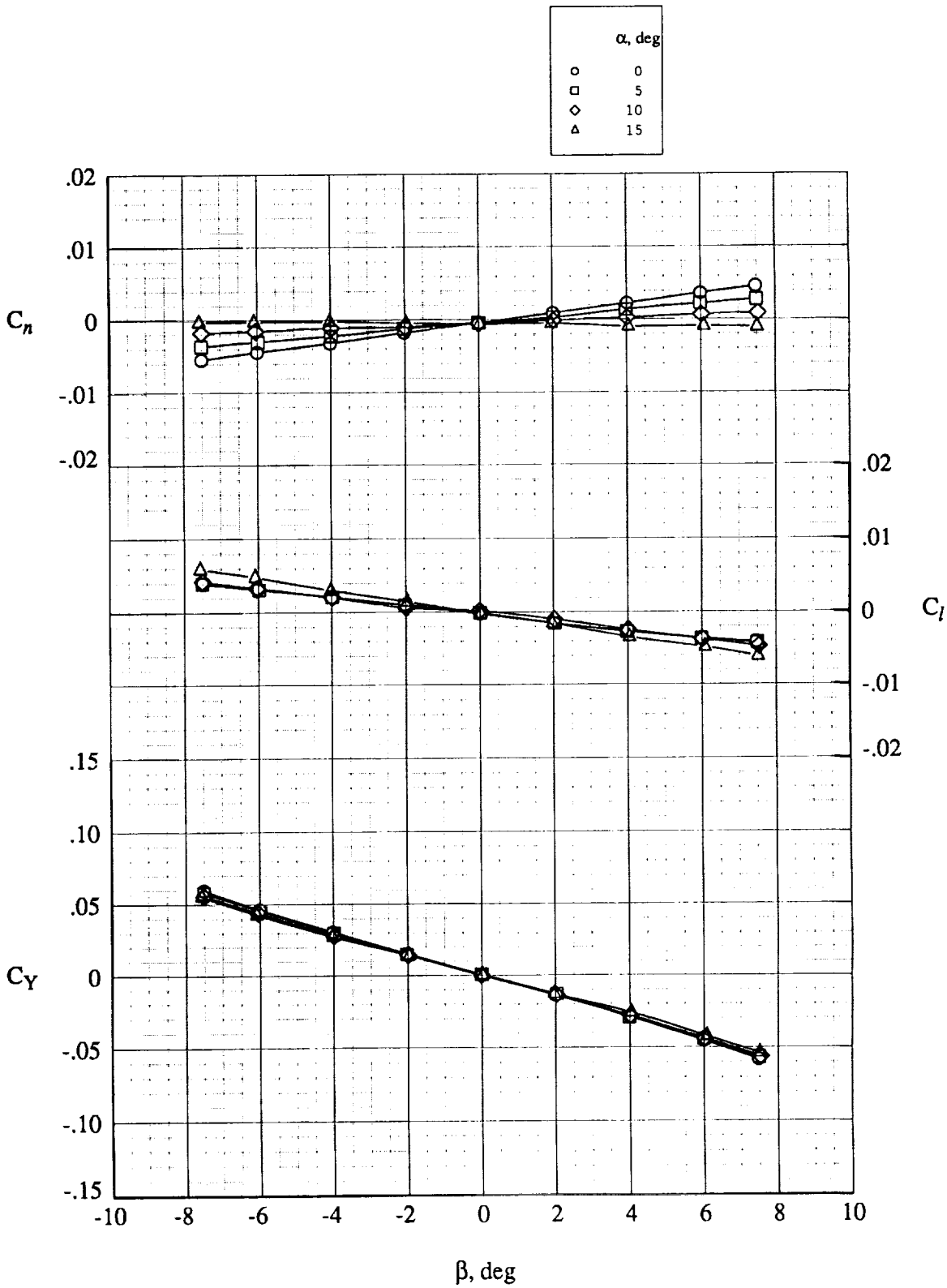

(b) $M = 1.80$.

Figure 16. Continued.

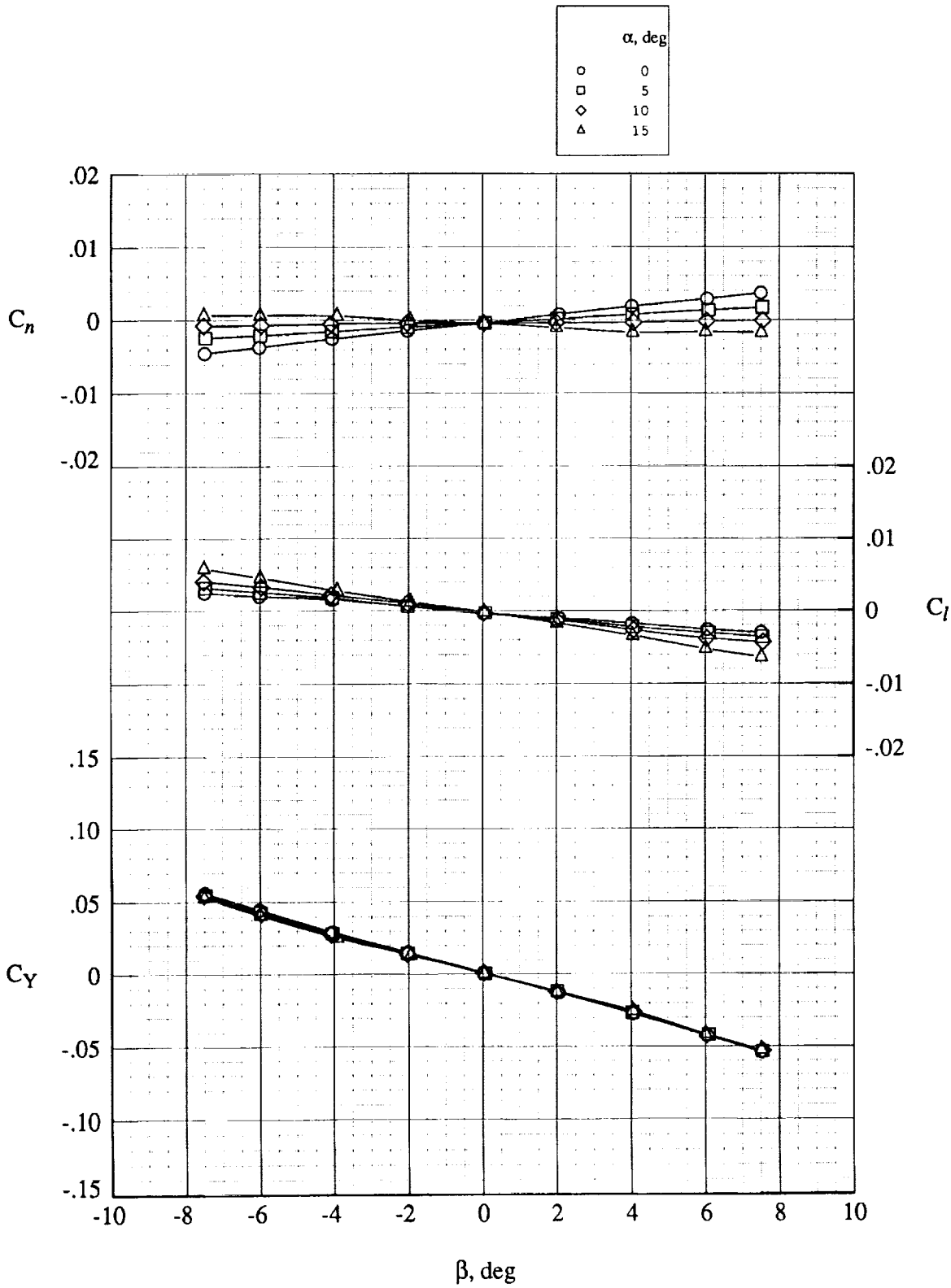

(c) $M = 2.00$.

Figure 16. Concluded.

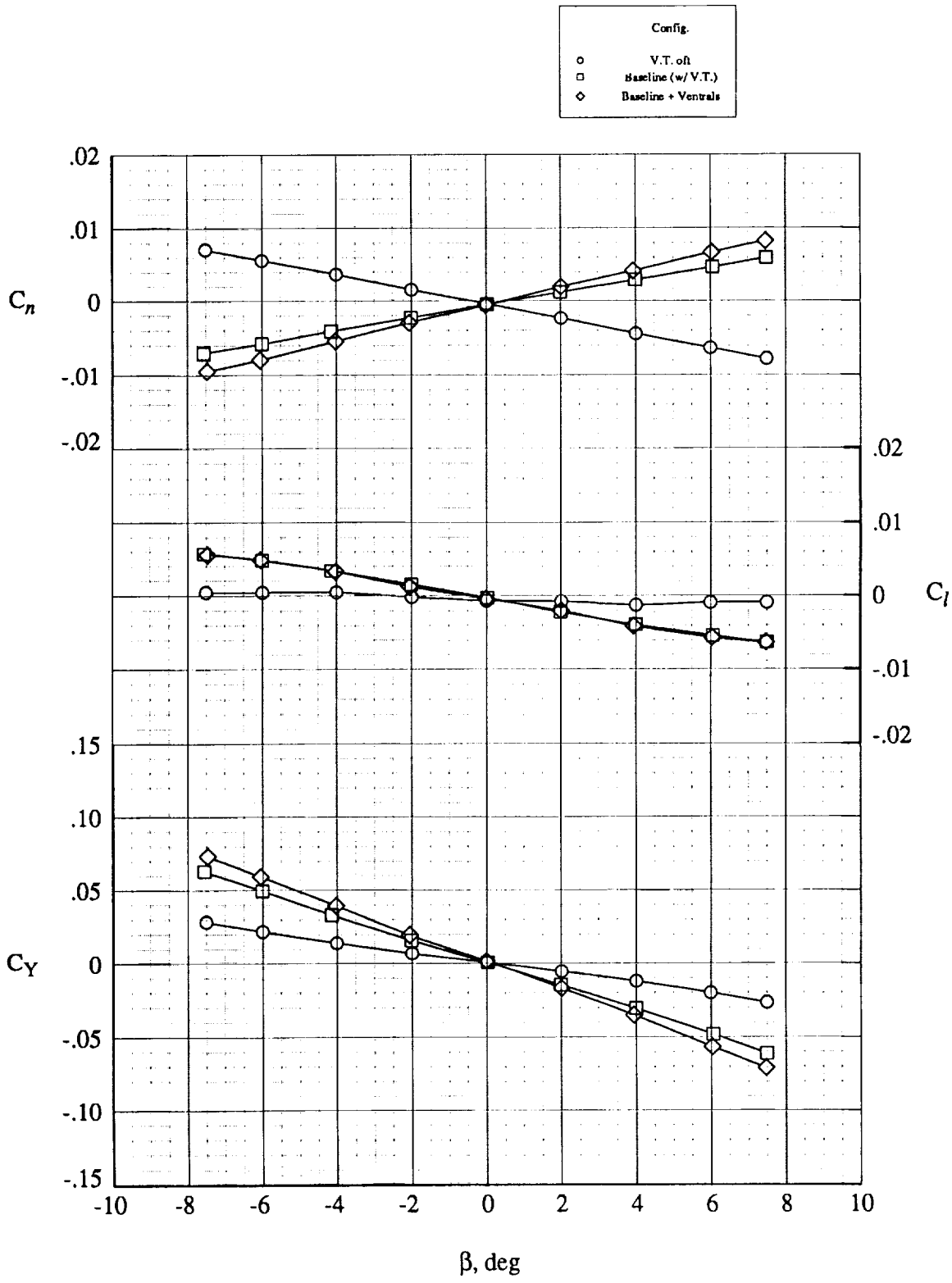

(a) $M = 1.60$.

Figure 17. Comparison of yawing-moment, rolling-moment, and side-force coefficients with selected vertical control surfaces for baseline model at $\alpha = 0°$.

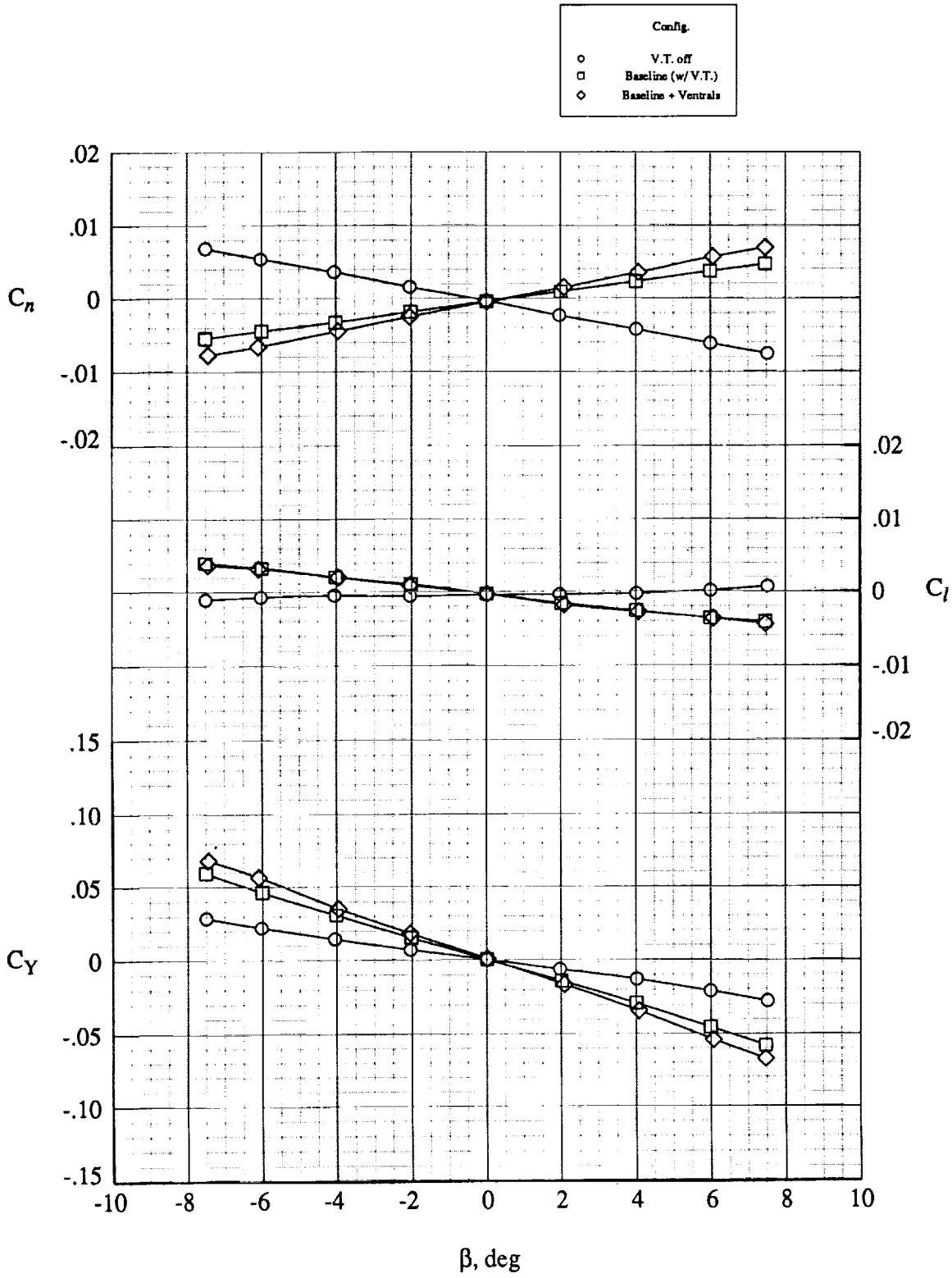

(b) $M = 1.80$.

Figure 17. Continued.

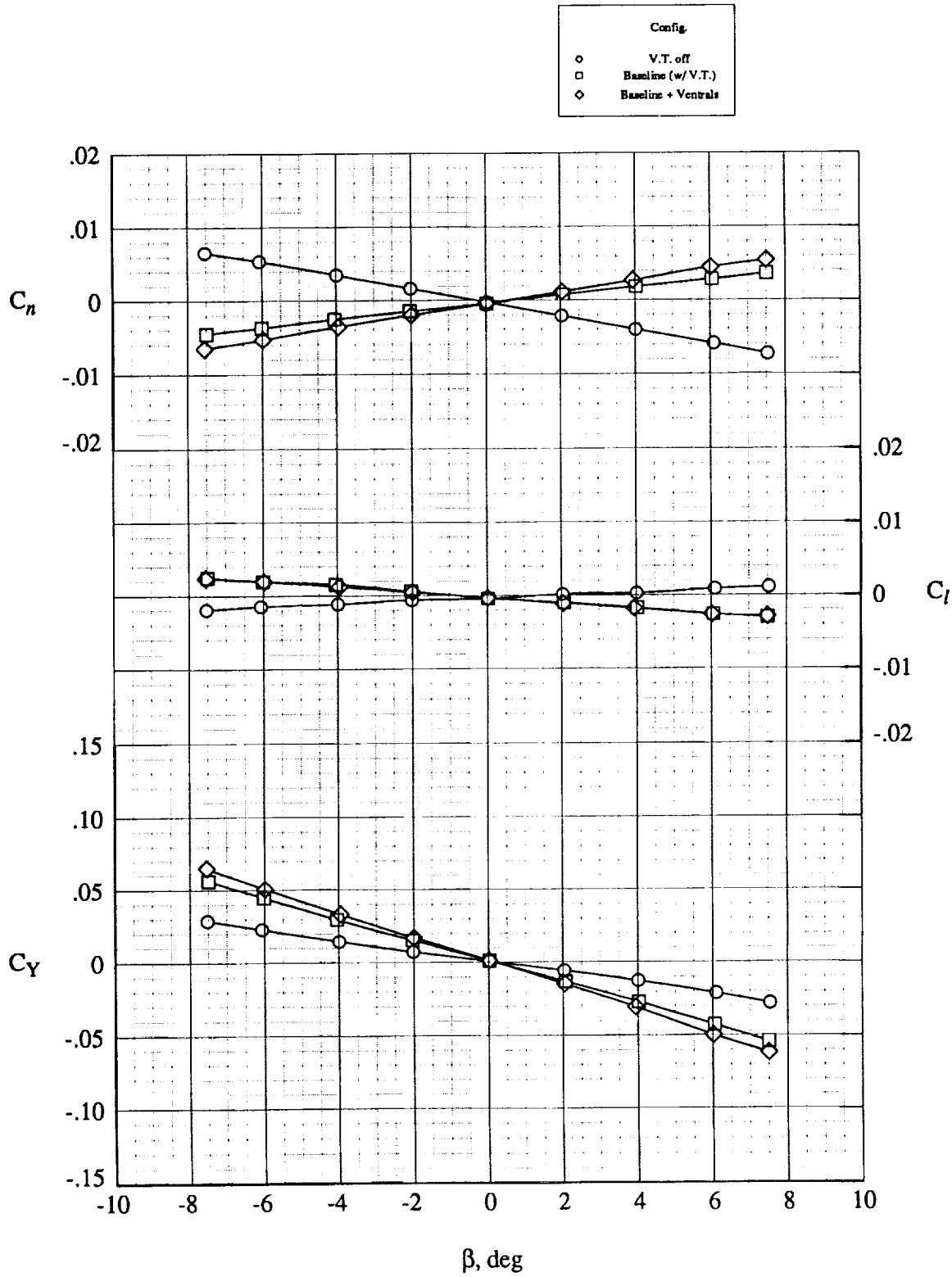

(c) $M = 2.00$.

Figure 17. Concluded.

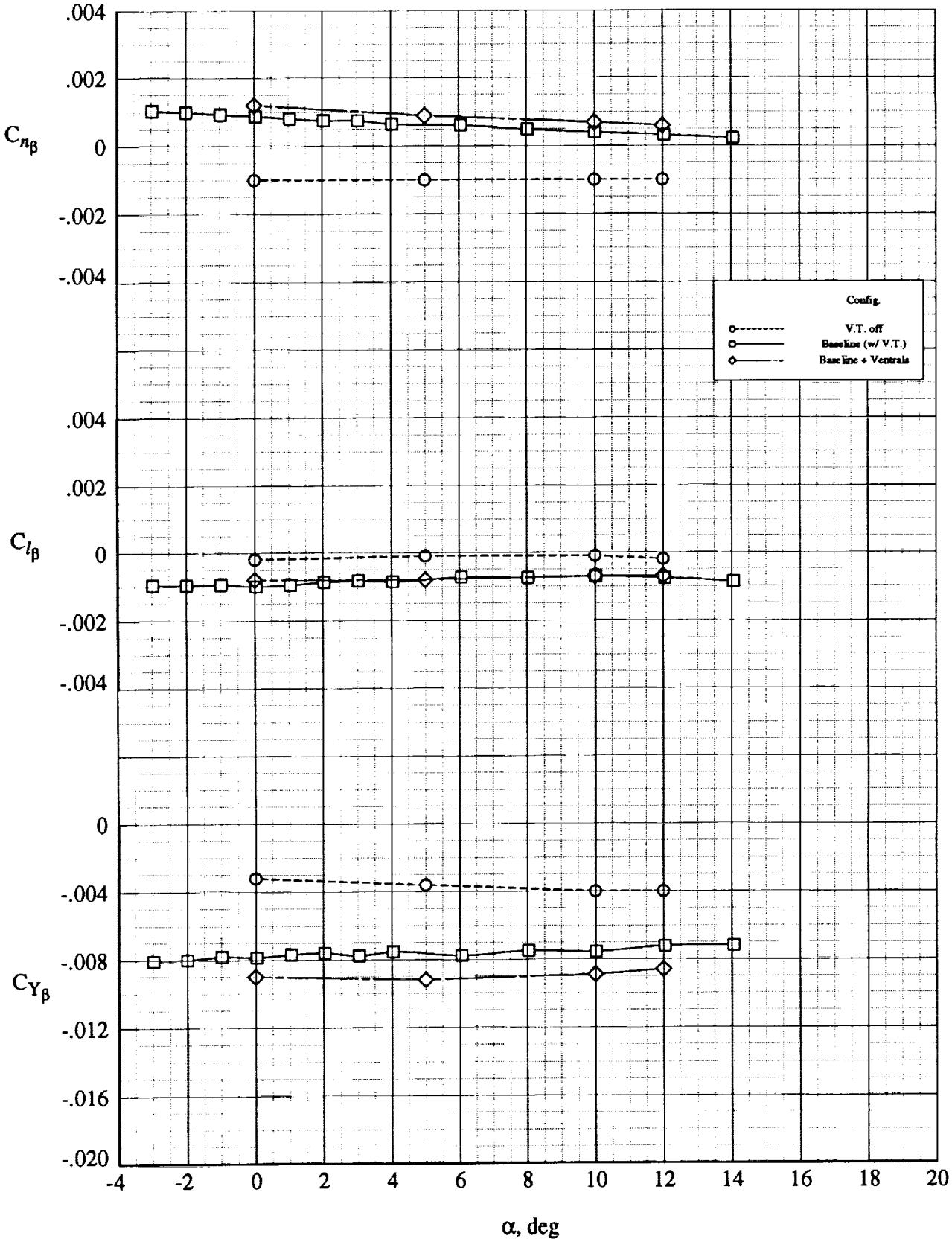

(a) $M = 1.60$.

Figure 18. Lateral-directional stability effect of centerline vertical tail and ventral fins on baseline model.

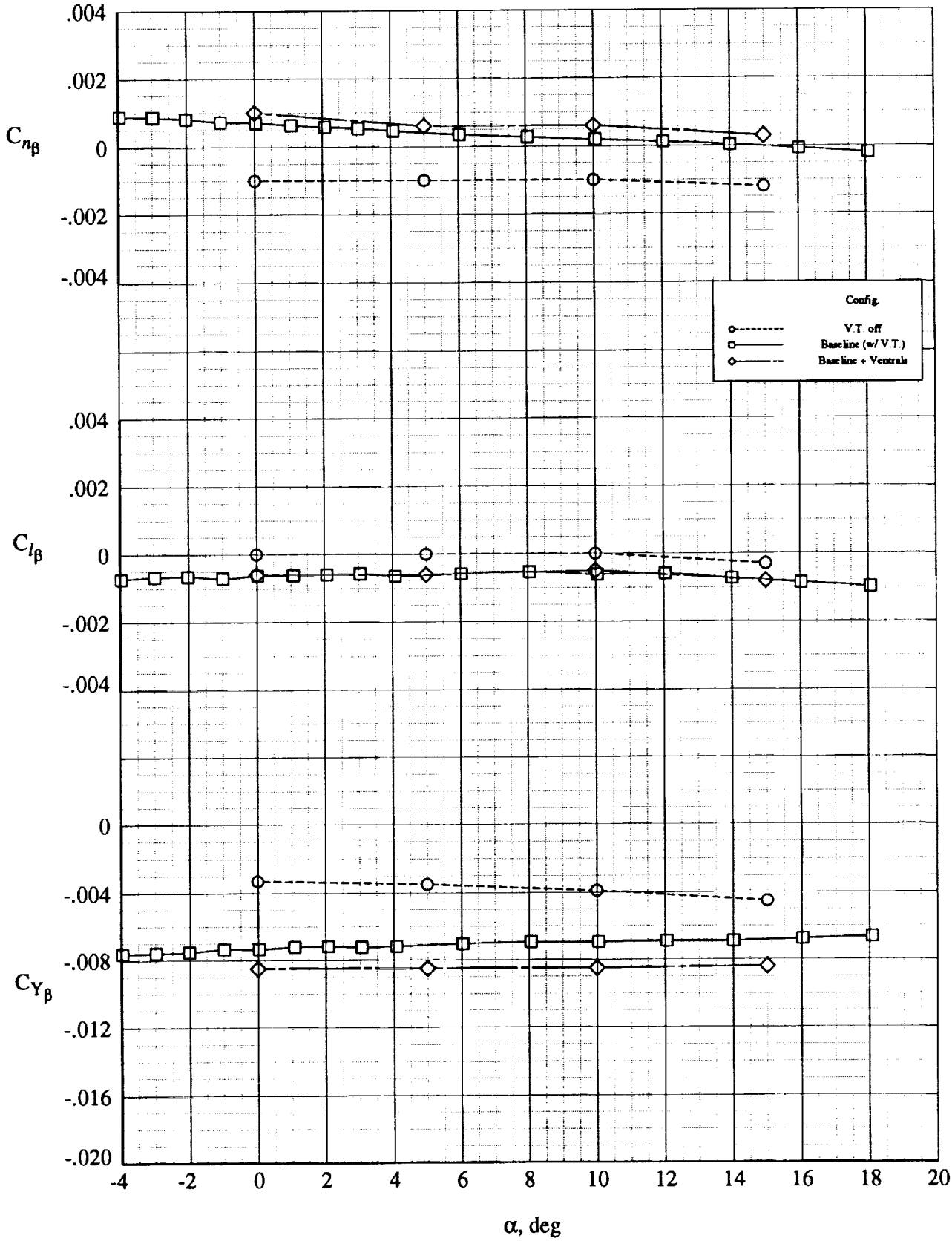

(b) $M = 1.80$.

Figure 18. Continued.

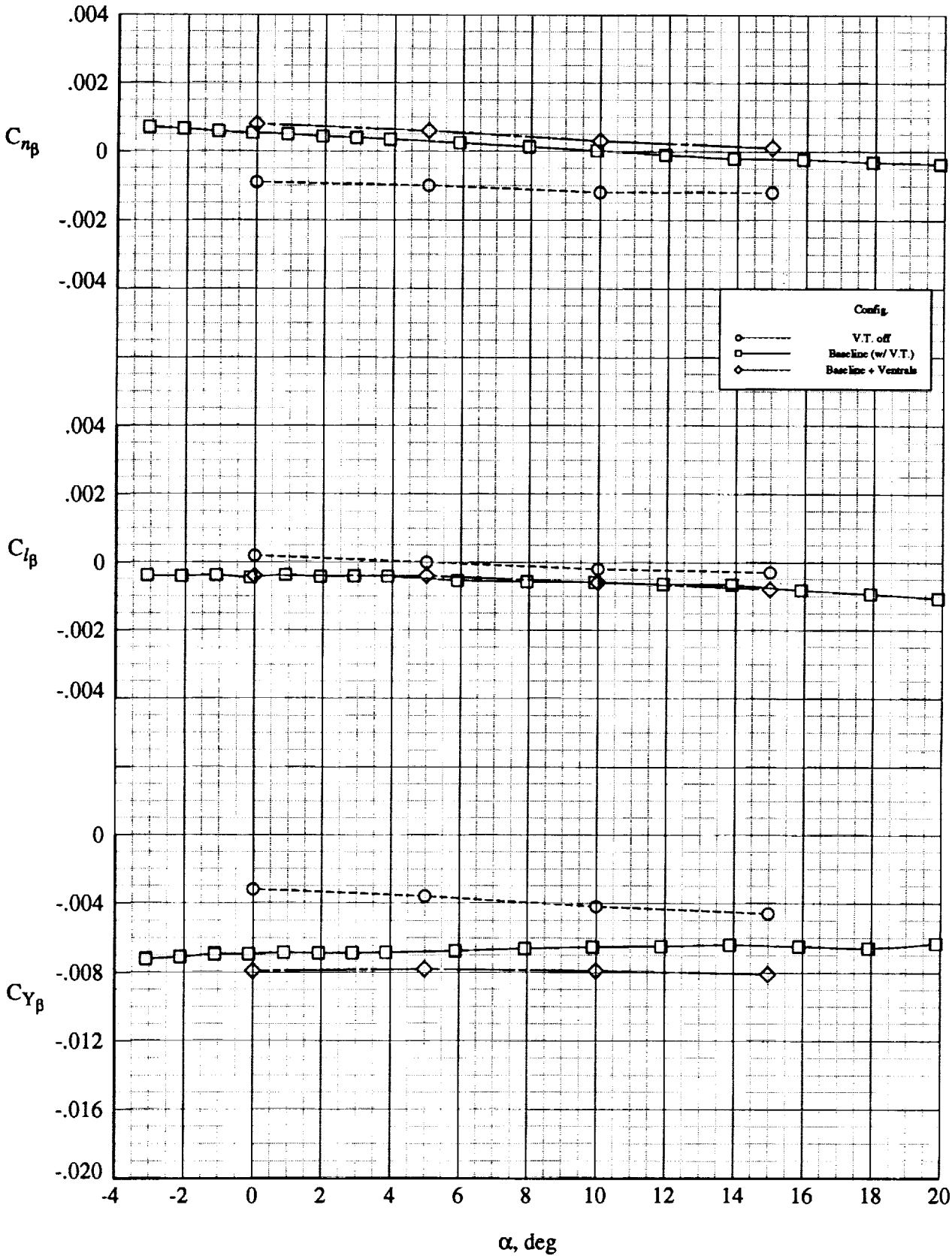

(c) $M = 2.00$.

Figure 18. Concluded.

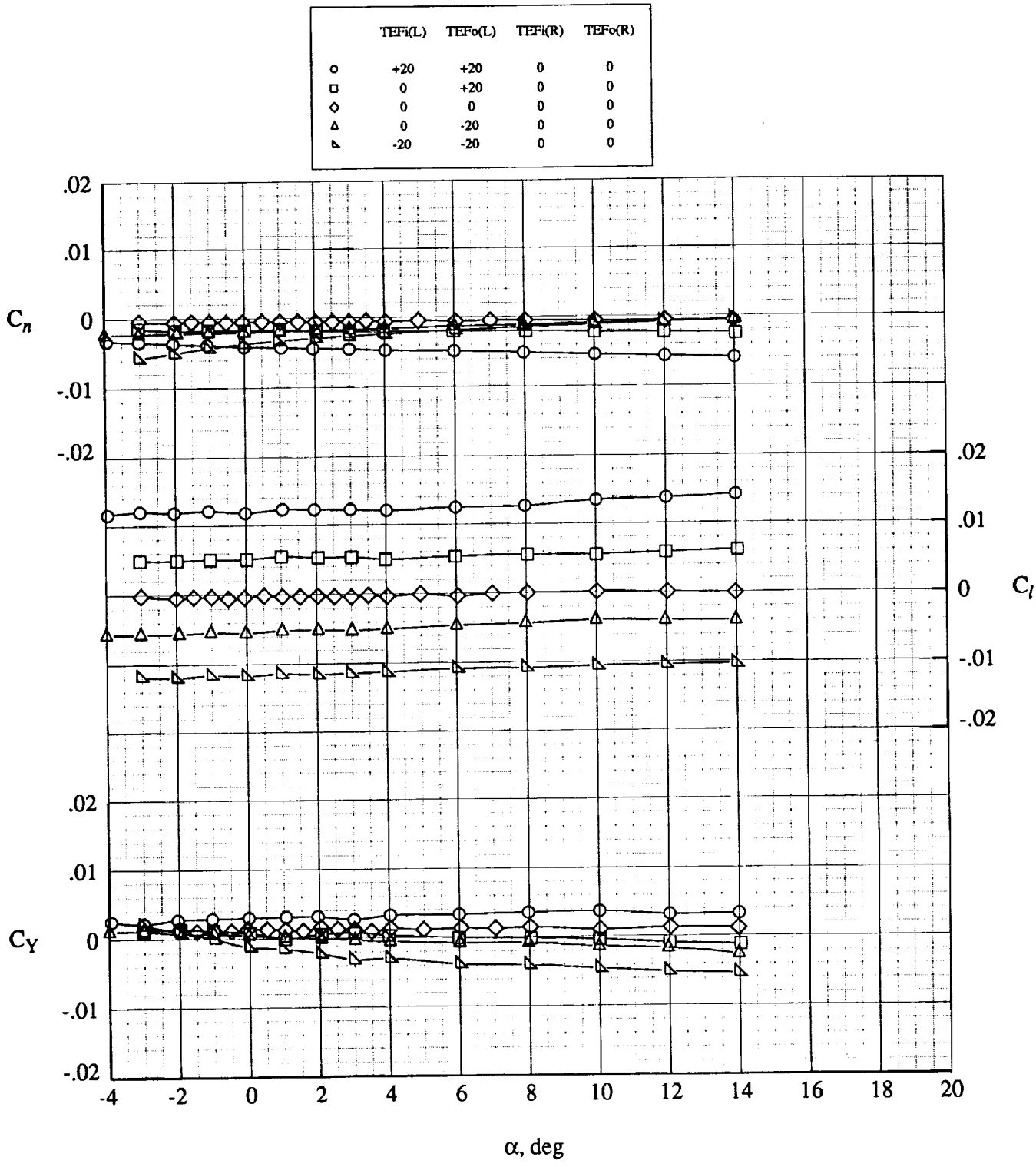

(a) $M = 1.60$.

Figure 19. Variation of yawing-moment, rolling-moment, and side-force coefficients with angle of attack for trailing-edge flap deflection combinations (baseline model).

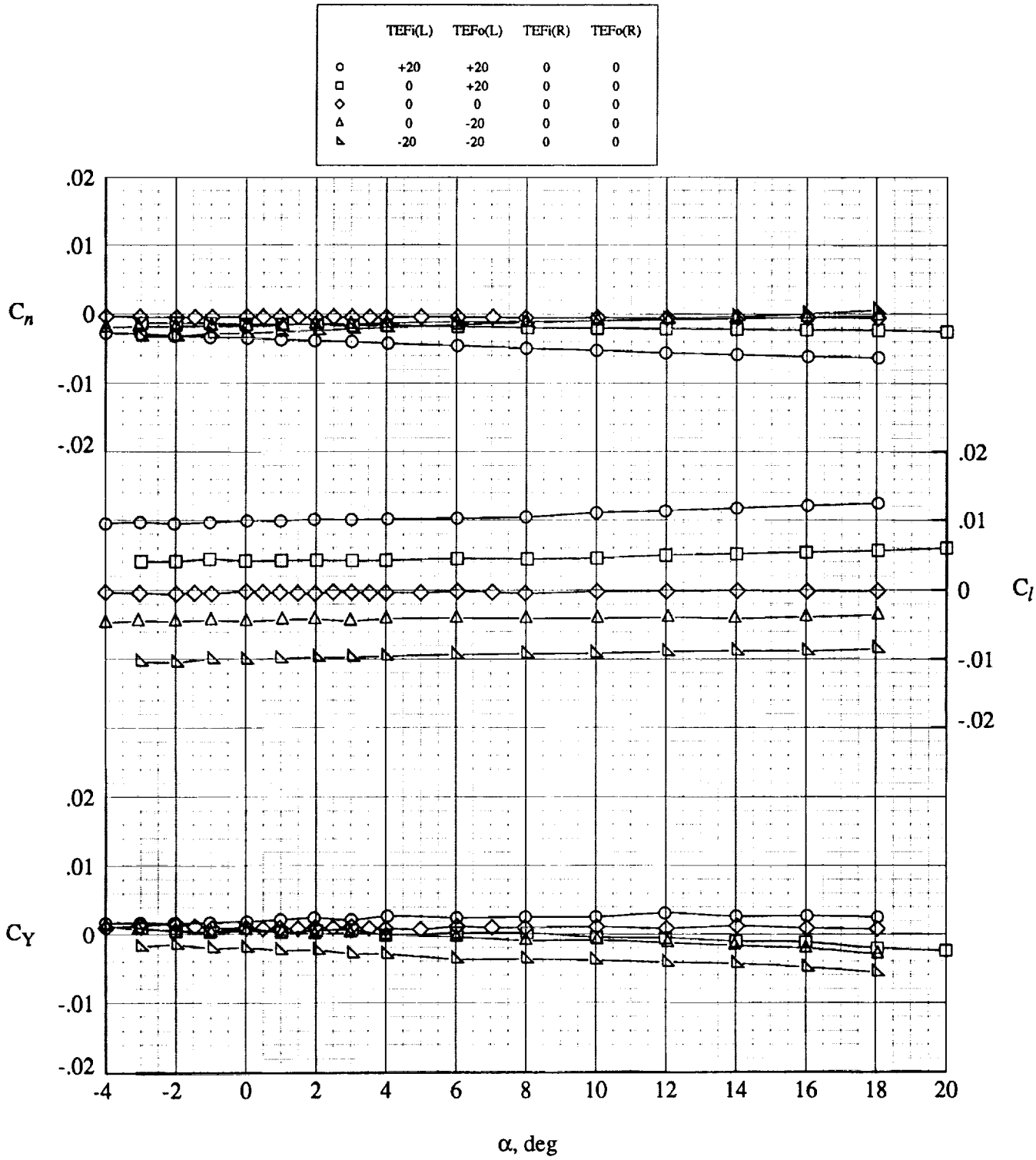

(b) $M = 1.80$.

Figure 19. Continued.

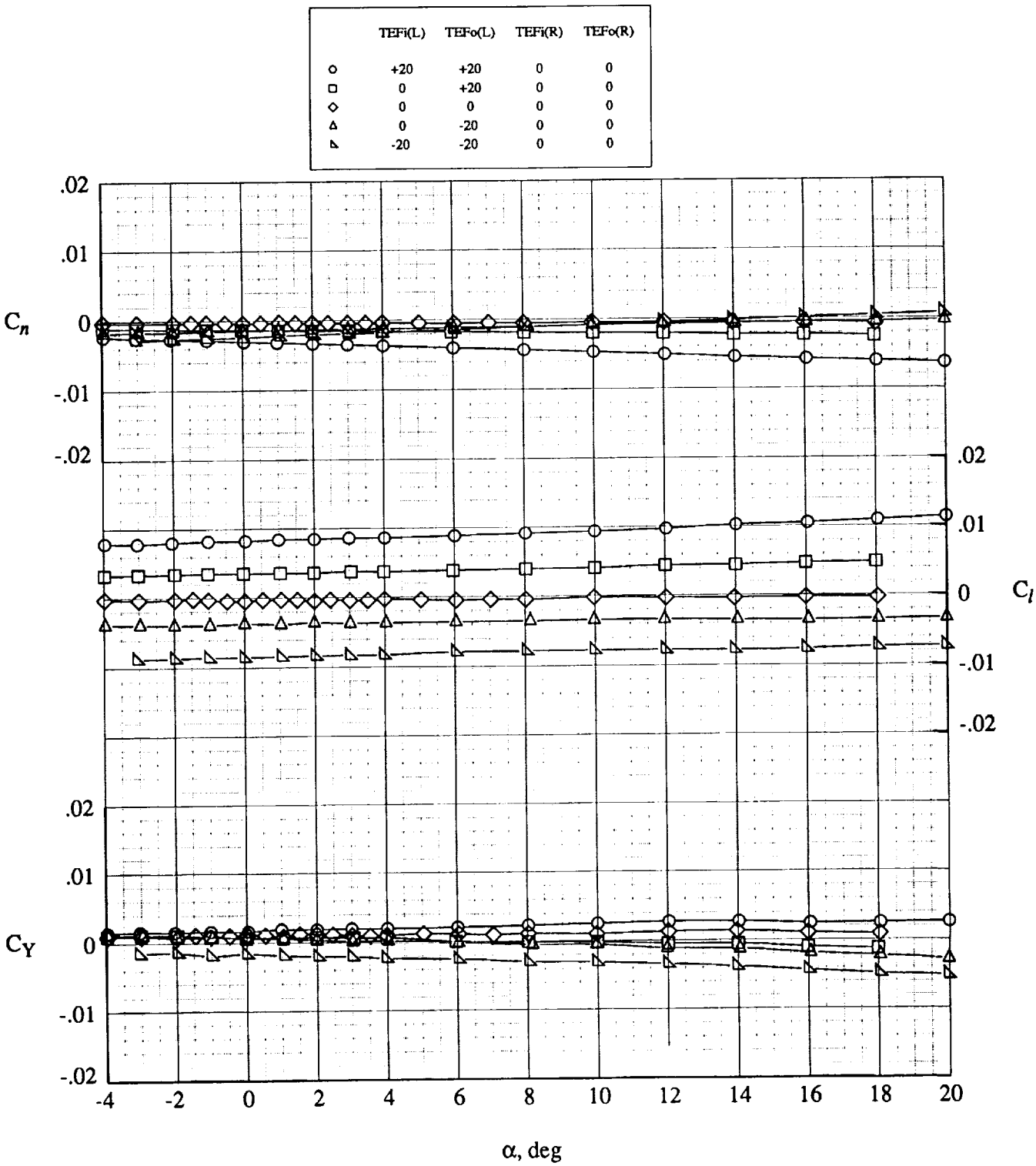

(c) $M = 2.00$.

Figure 19. Concluded.

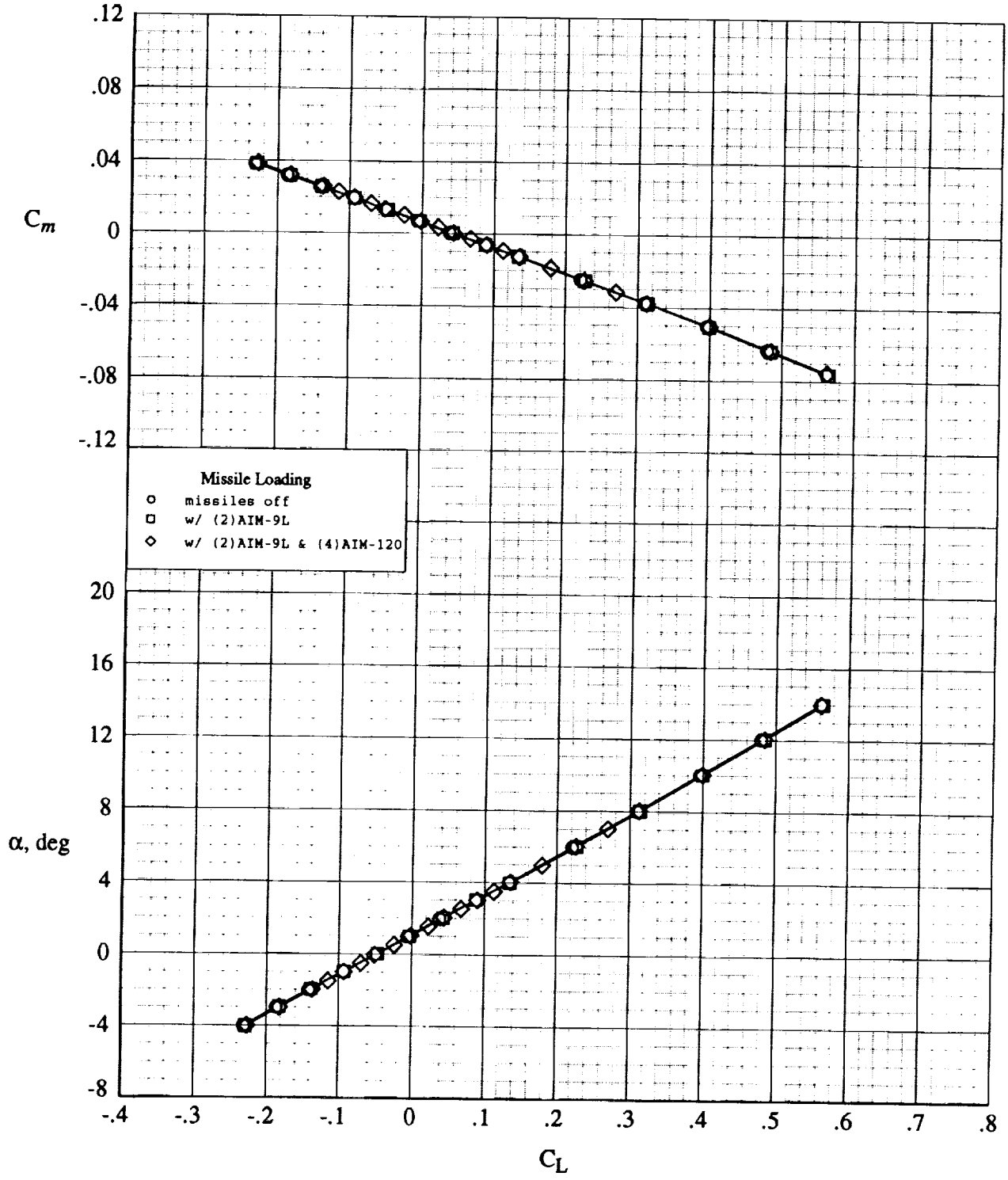

(a) $M = 1.60$.

Figure 20. Longitudinal aerodynamic characteristics with air-to-air missiles (baseline model).

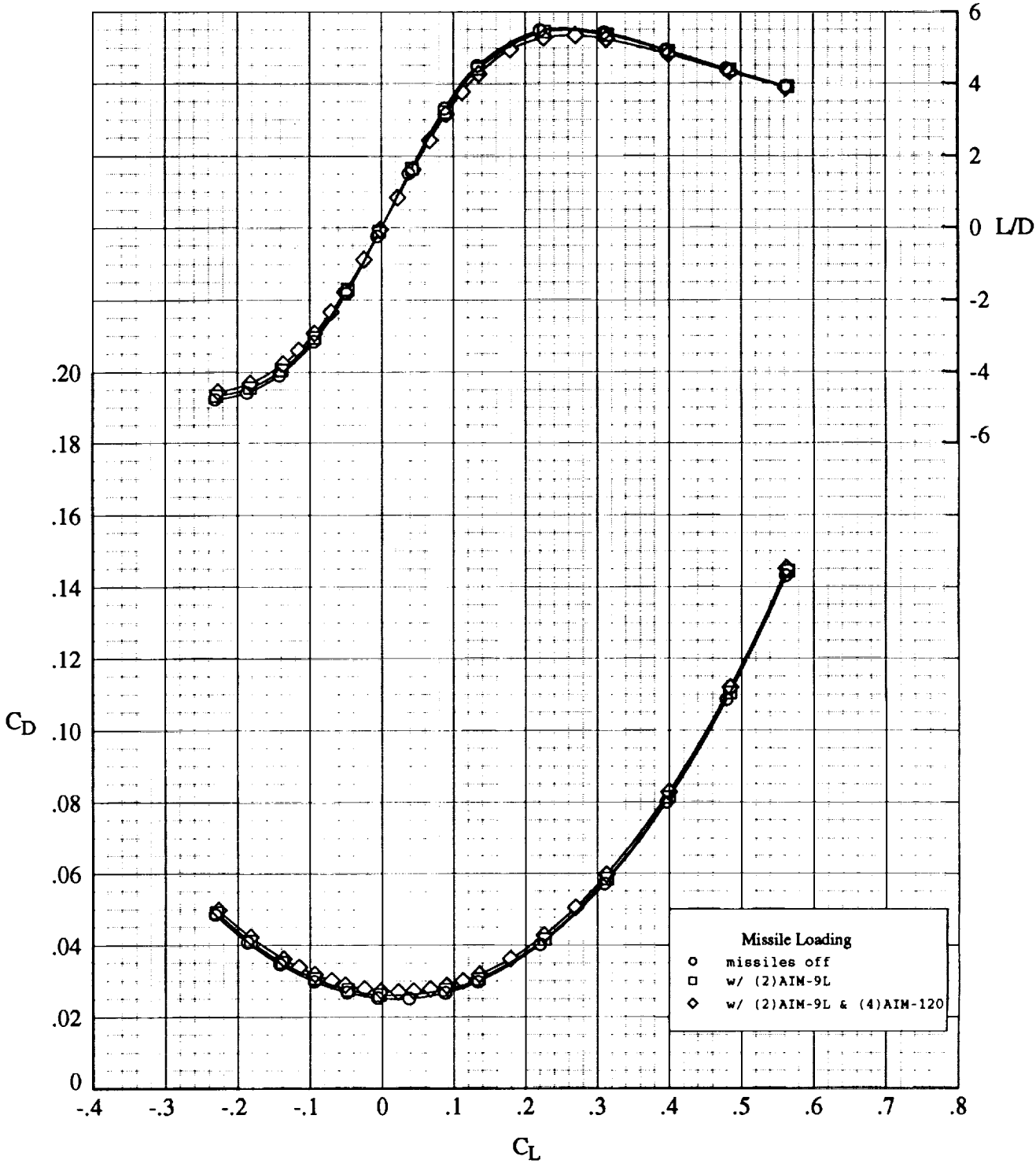

(a) Concluded.

Figure 20. Continued.

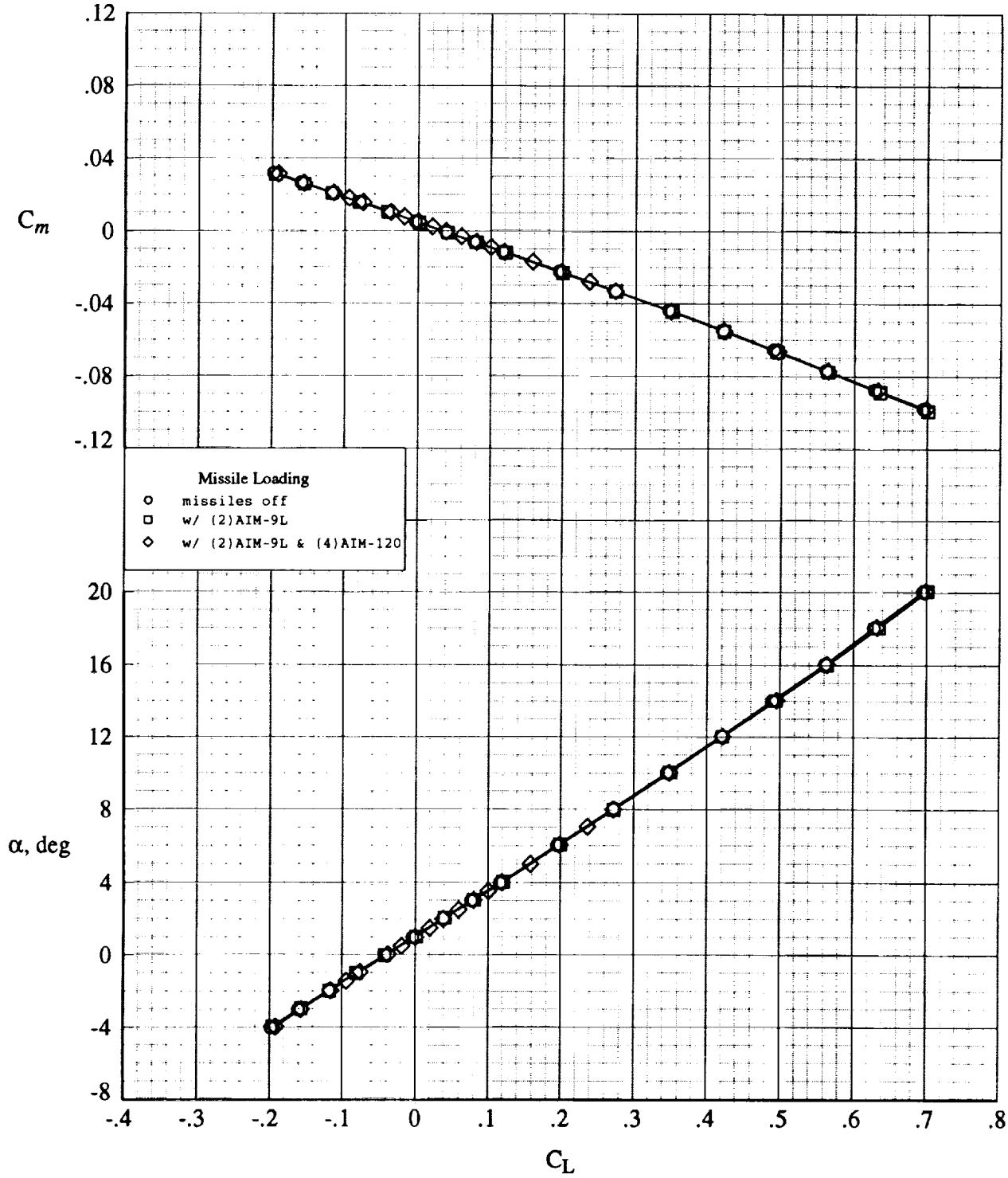

(b) $M = 1.80$.

Figure 20. Continued.

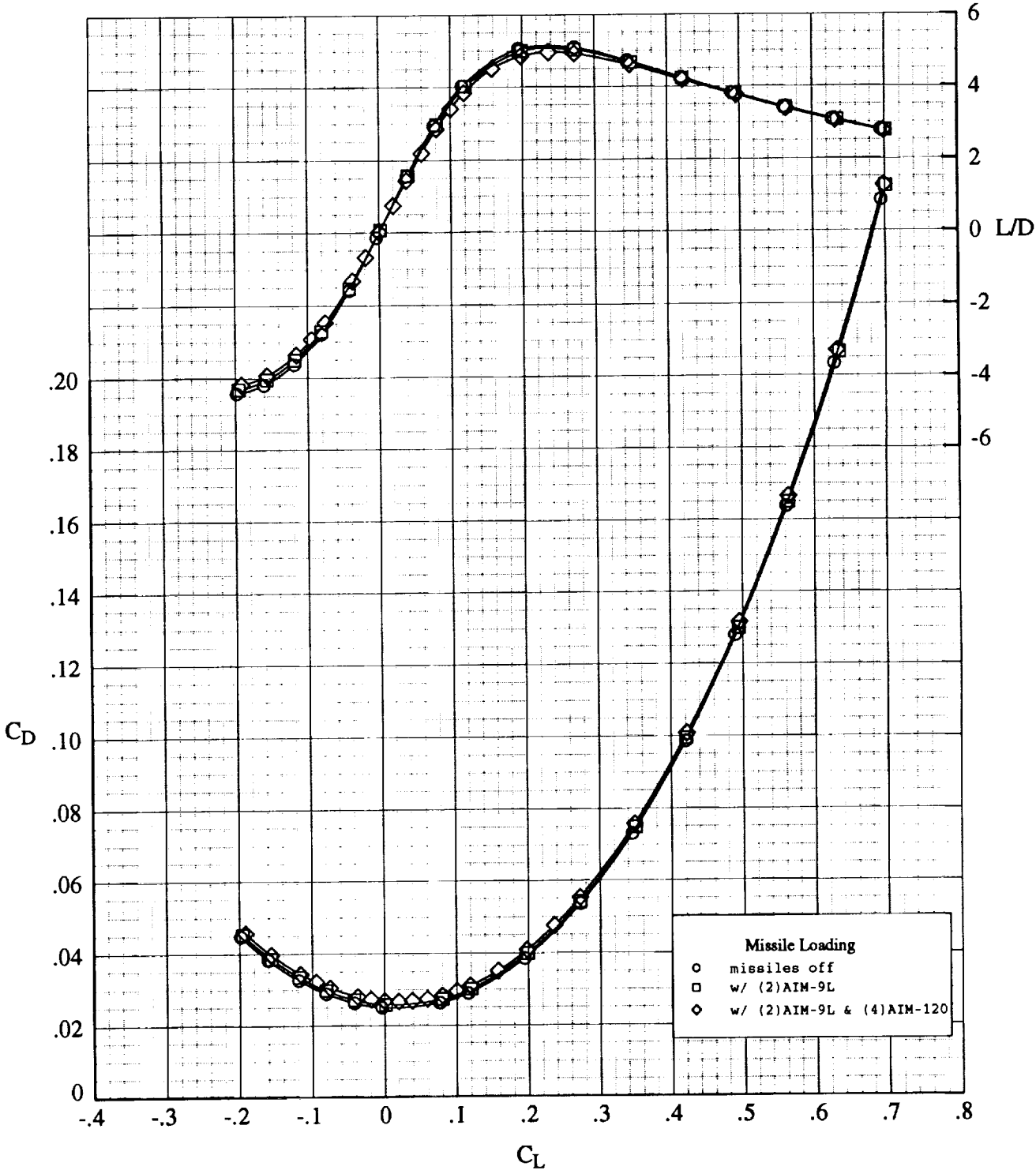

(b) Concluded.

Figure 20. Continued.

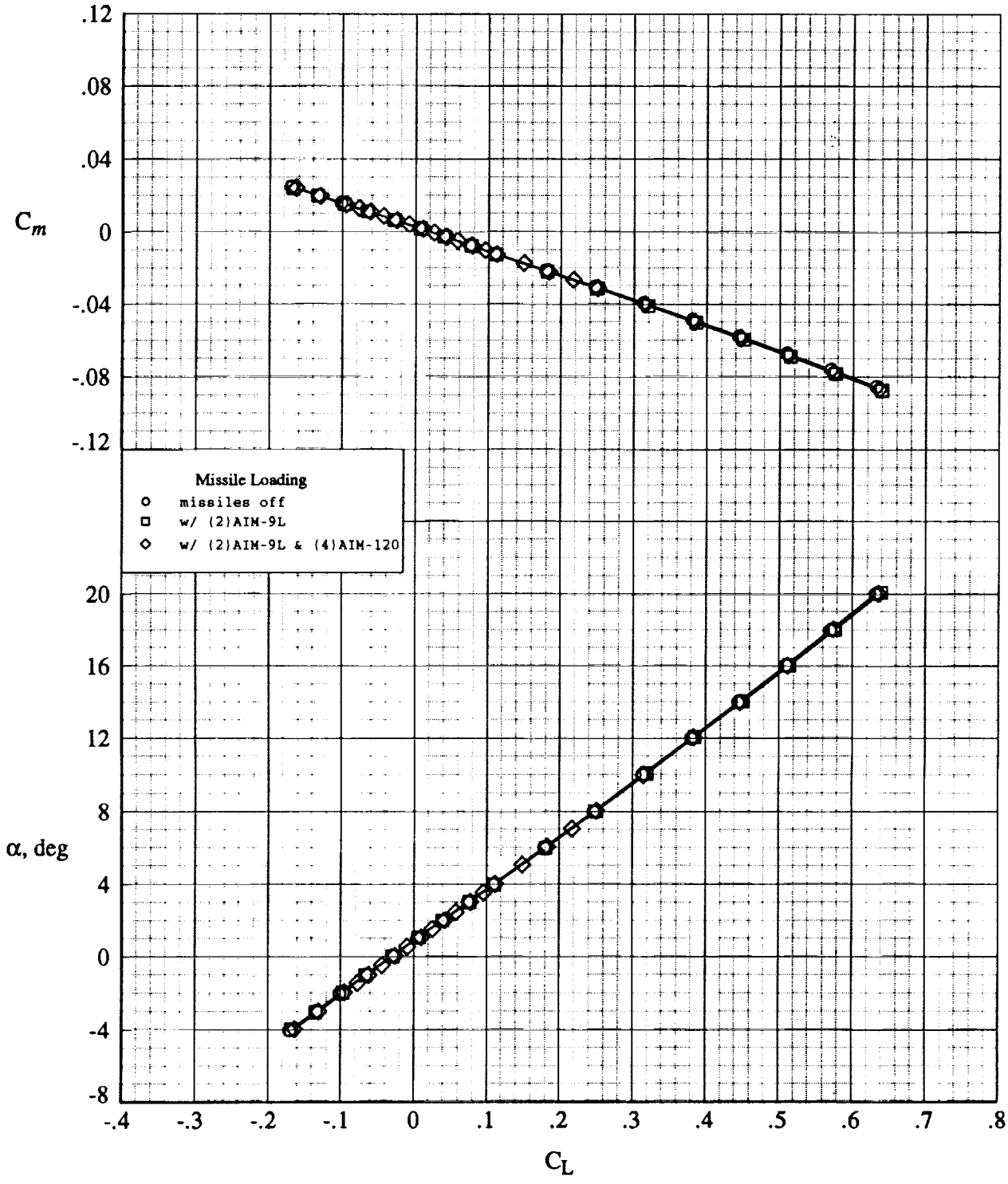

(c) $M = 2.00$.

Figure 20. Continued.

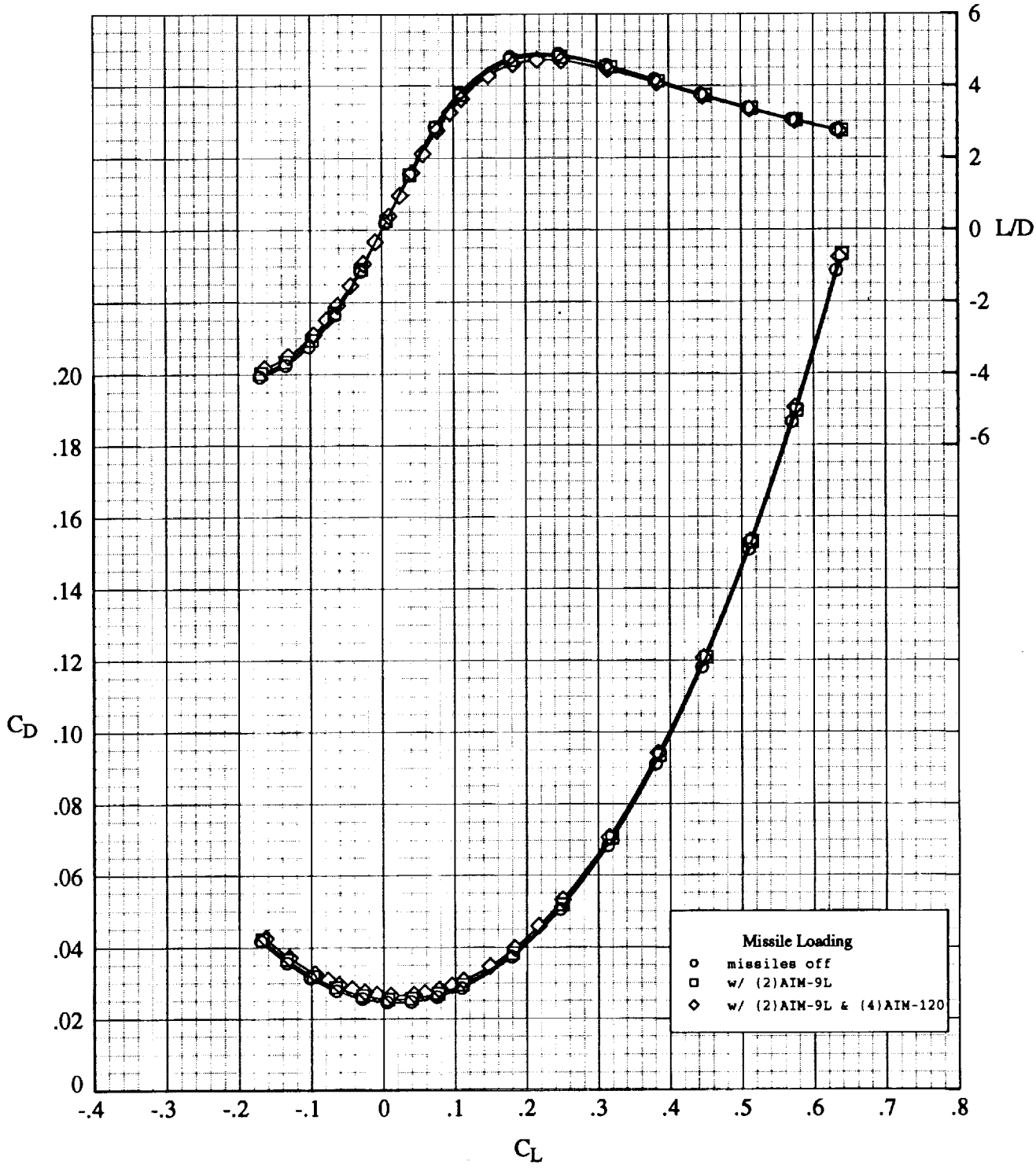

(c) Concluded.

Figure 20. Continued.

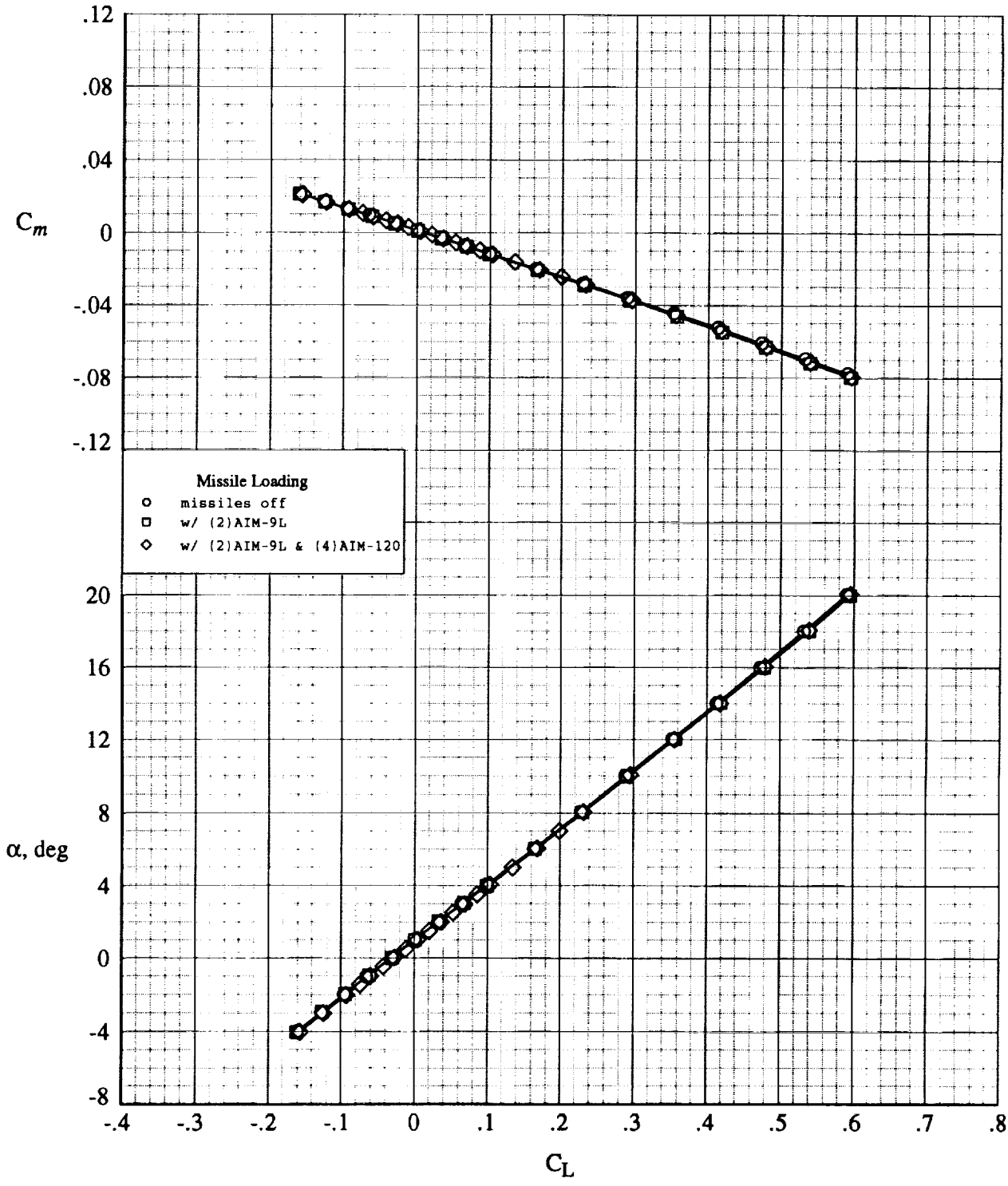

(d) $M = 2.16$.

Figure 20. Continued.

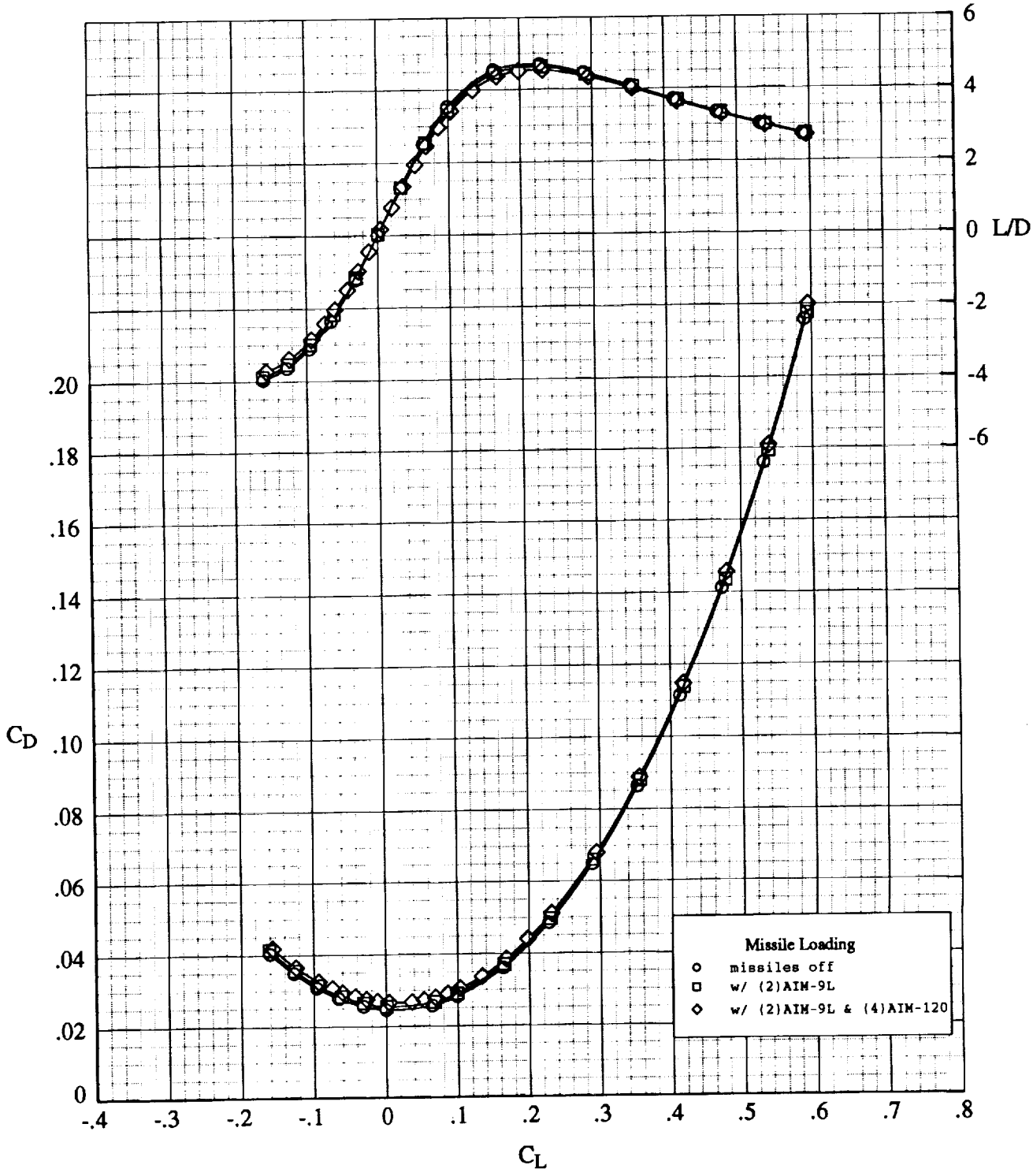

(d) Concluded.

Figure 20. Concluded.

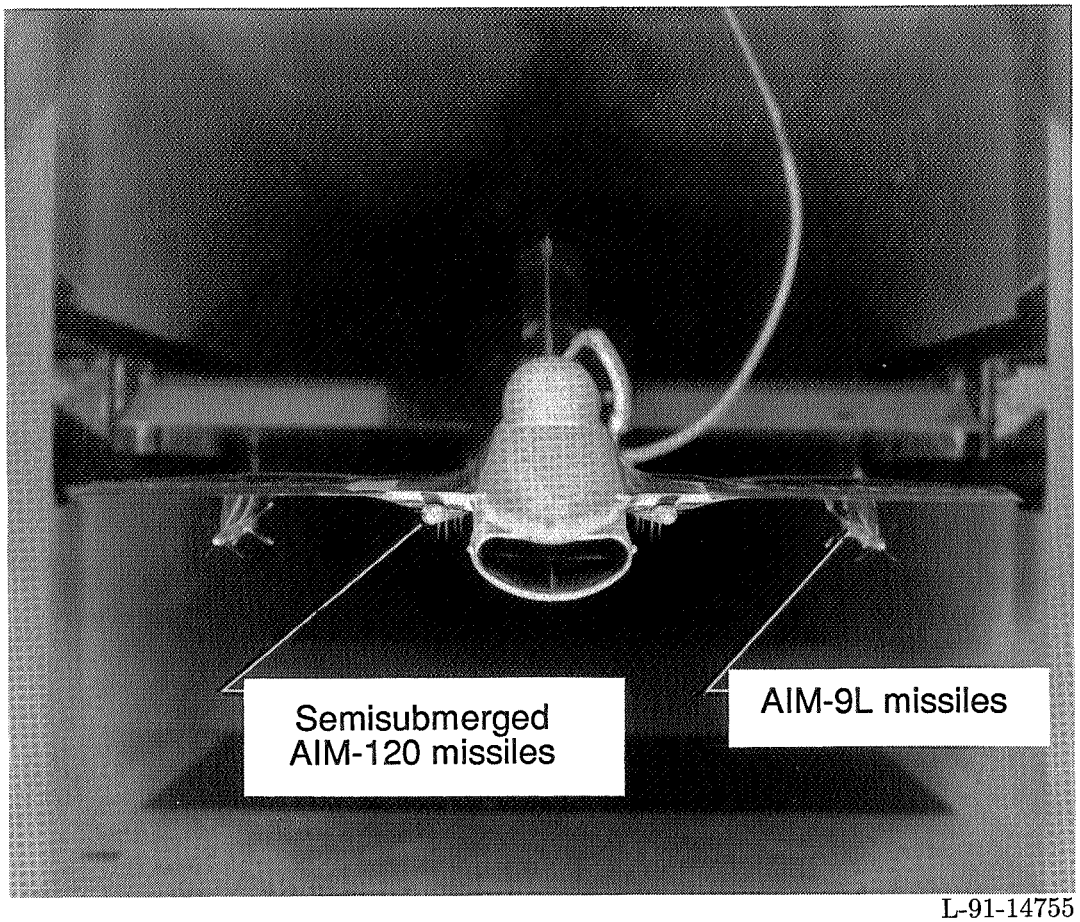

Figure 21. Frontal view of baseline model with basic air-to-air missiles installed.

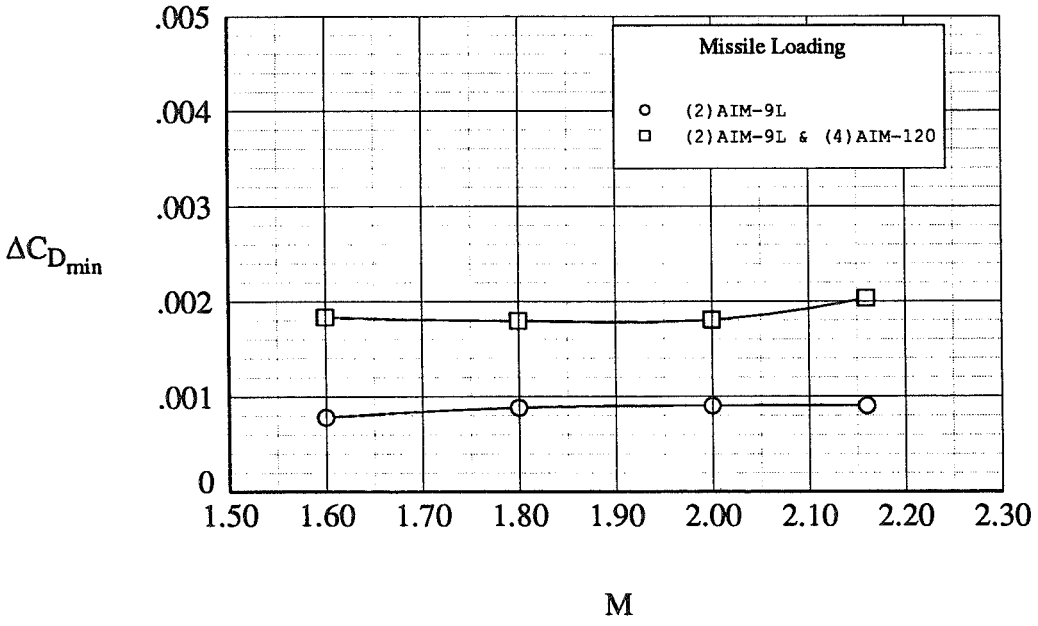

Figure 22. Effect on minimum drag of AIM-120 and AIM-9L missiles (baseline model).

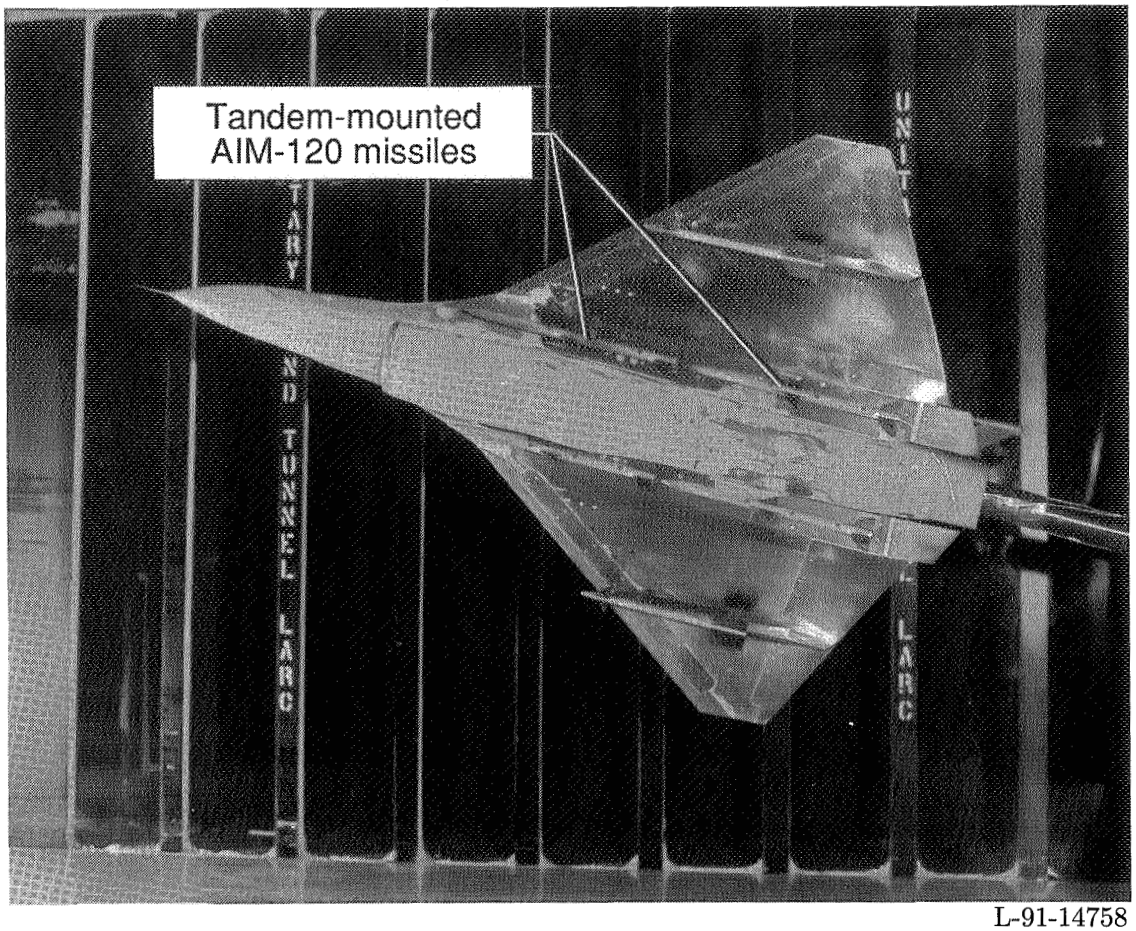

L-91-14758

Figure 23. Baseline model with tandem-mounted AIM-120 missiles.

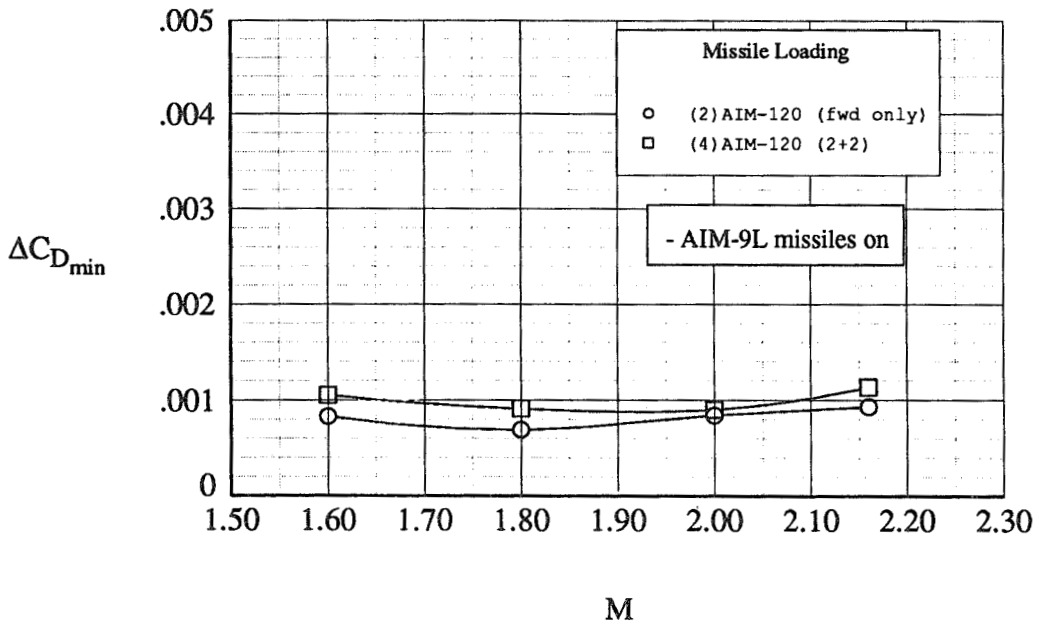

Figure 24. Effect on minimum drag with addition of AIM-120 missiles to baseline model.

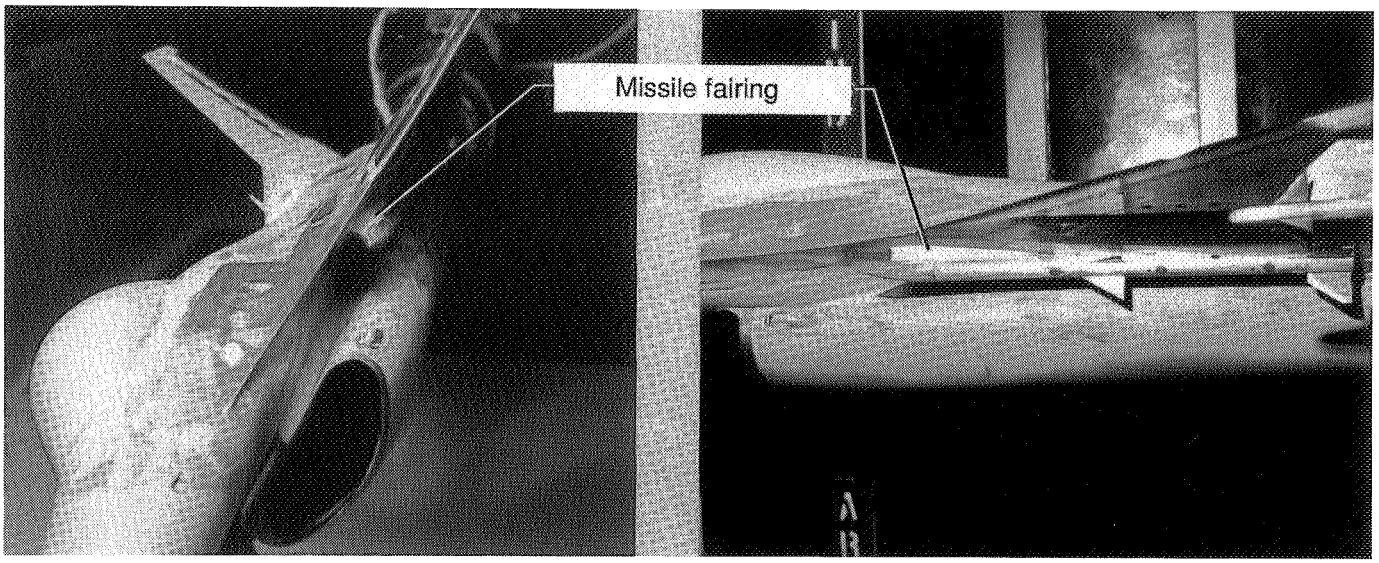

L-93-17

Figure 25. Baseline model with forward missile fairing.

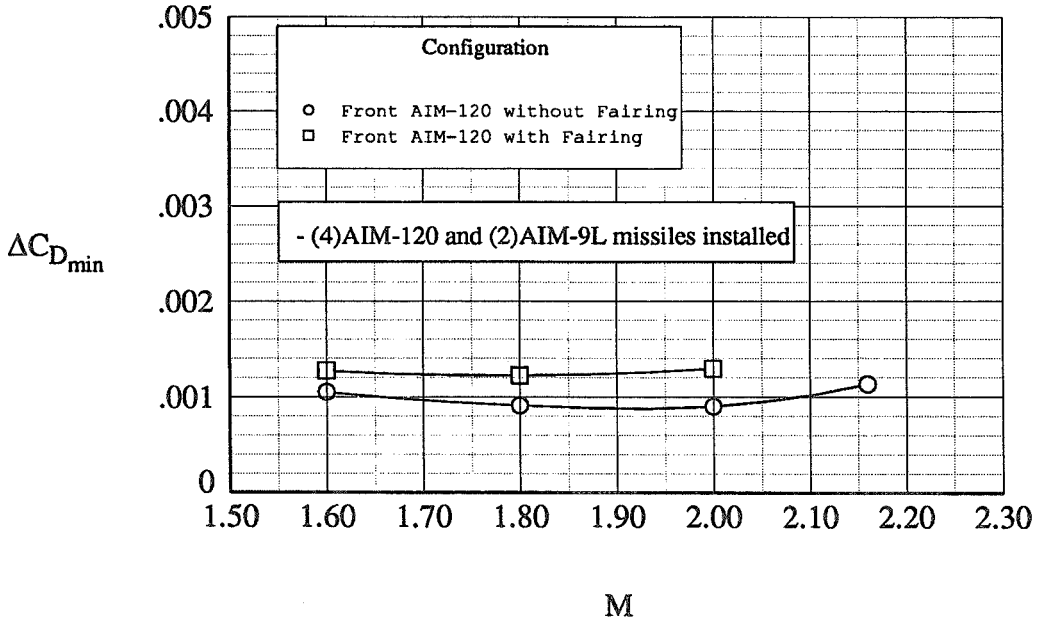

Figure 26. Effects on minimum drag of addition of AIM-120 missile fairing (baseline model).

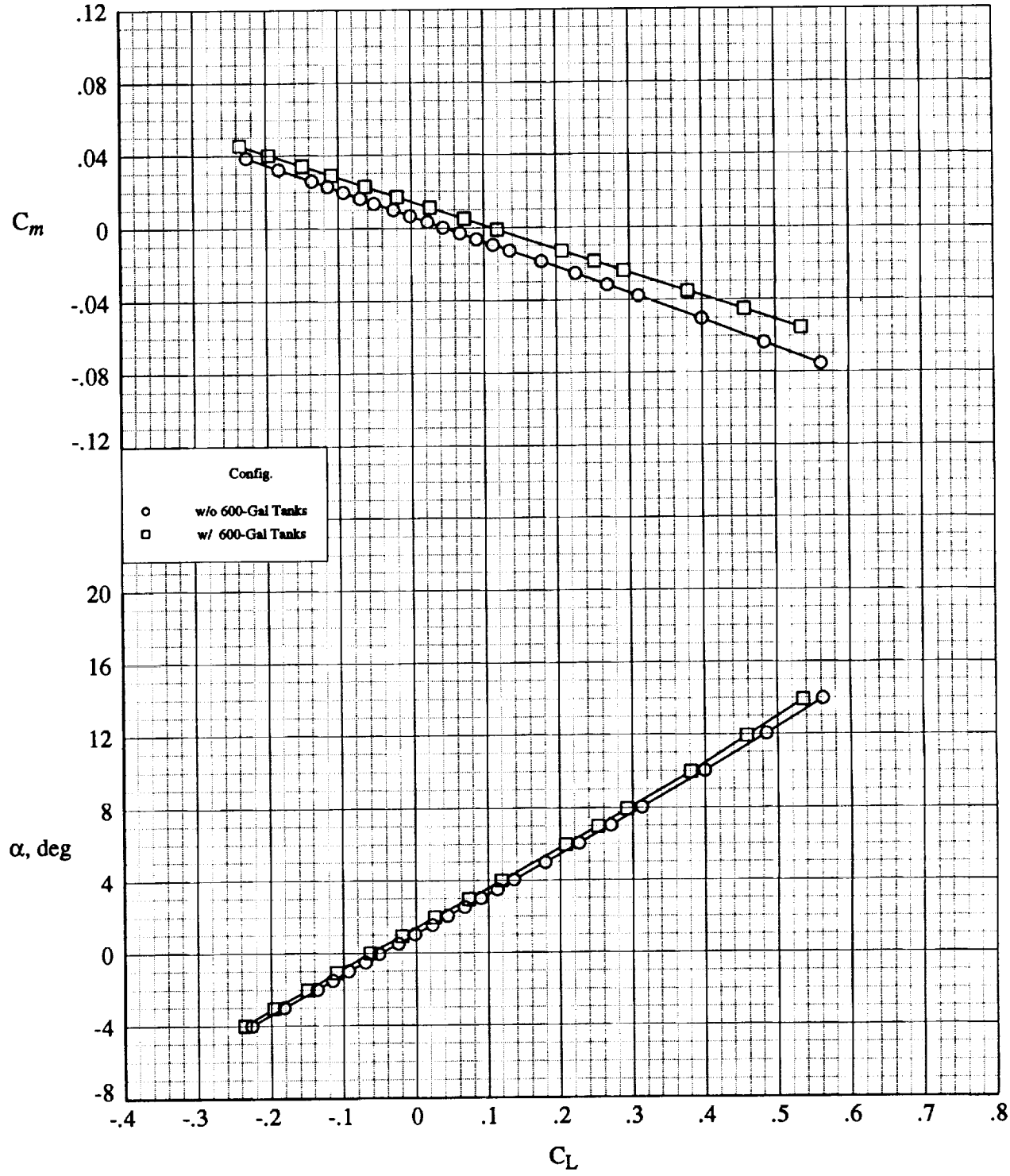

(a) $M = 1.60$.

Figure 27. Longitudinal aerodynamic effects of 600-gal fuel tanks on baseline model.

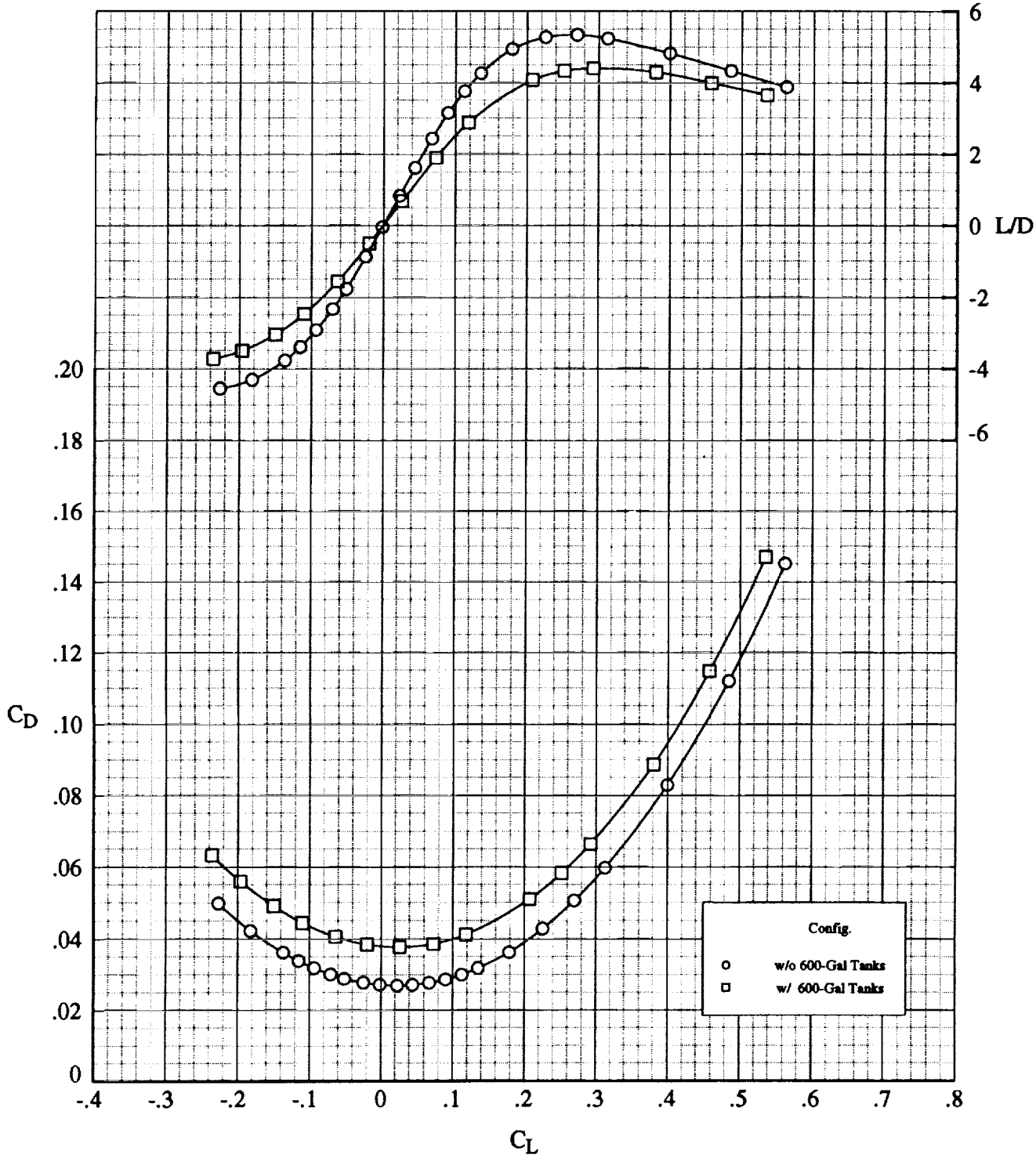

(a) Concluded.

Figure 27. Continued.

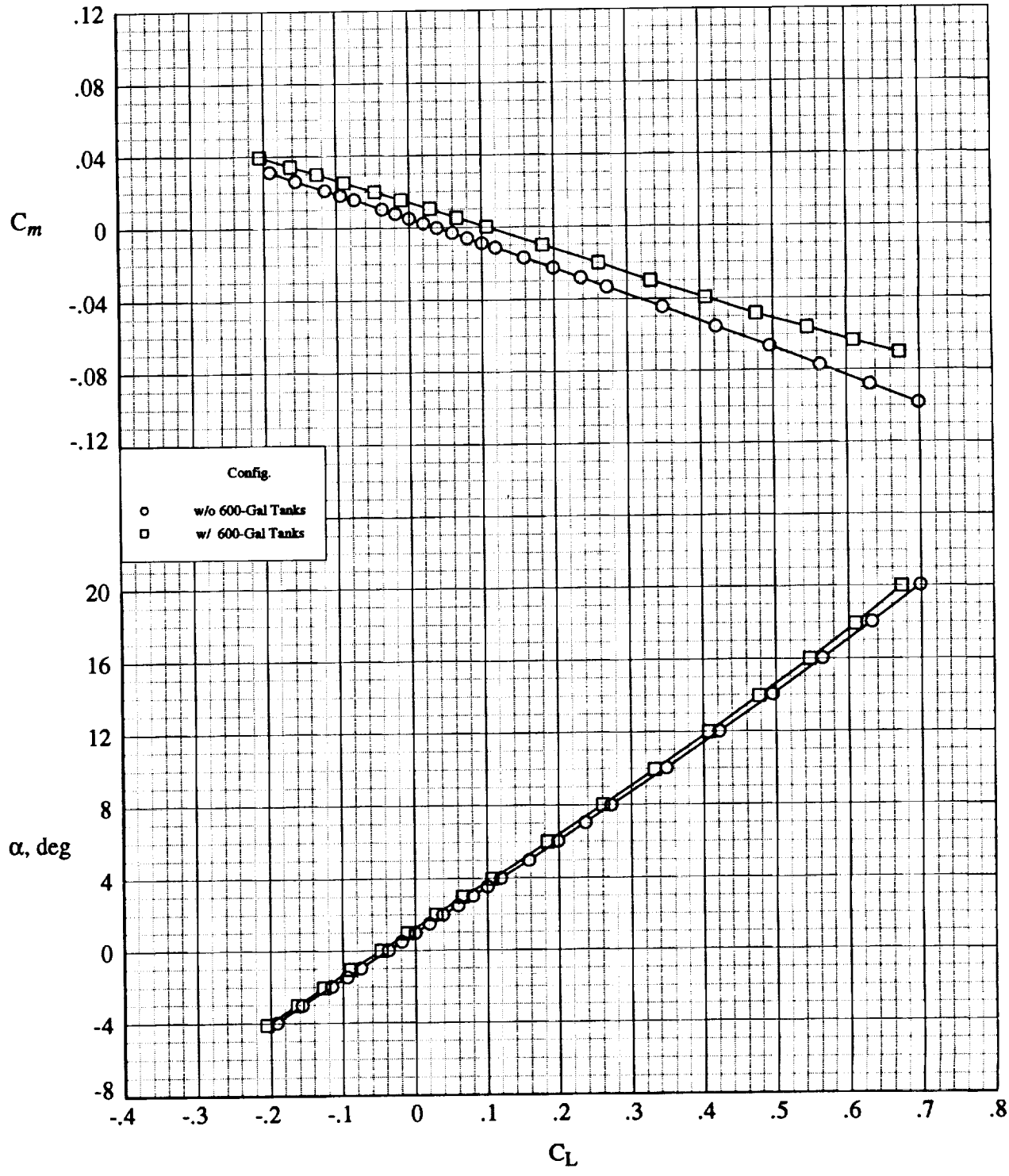

(b) $M = 1.80$.

Figure 27. Continued.

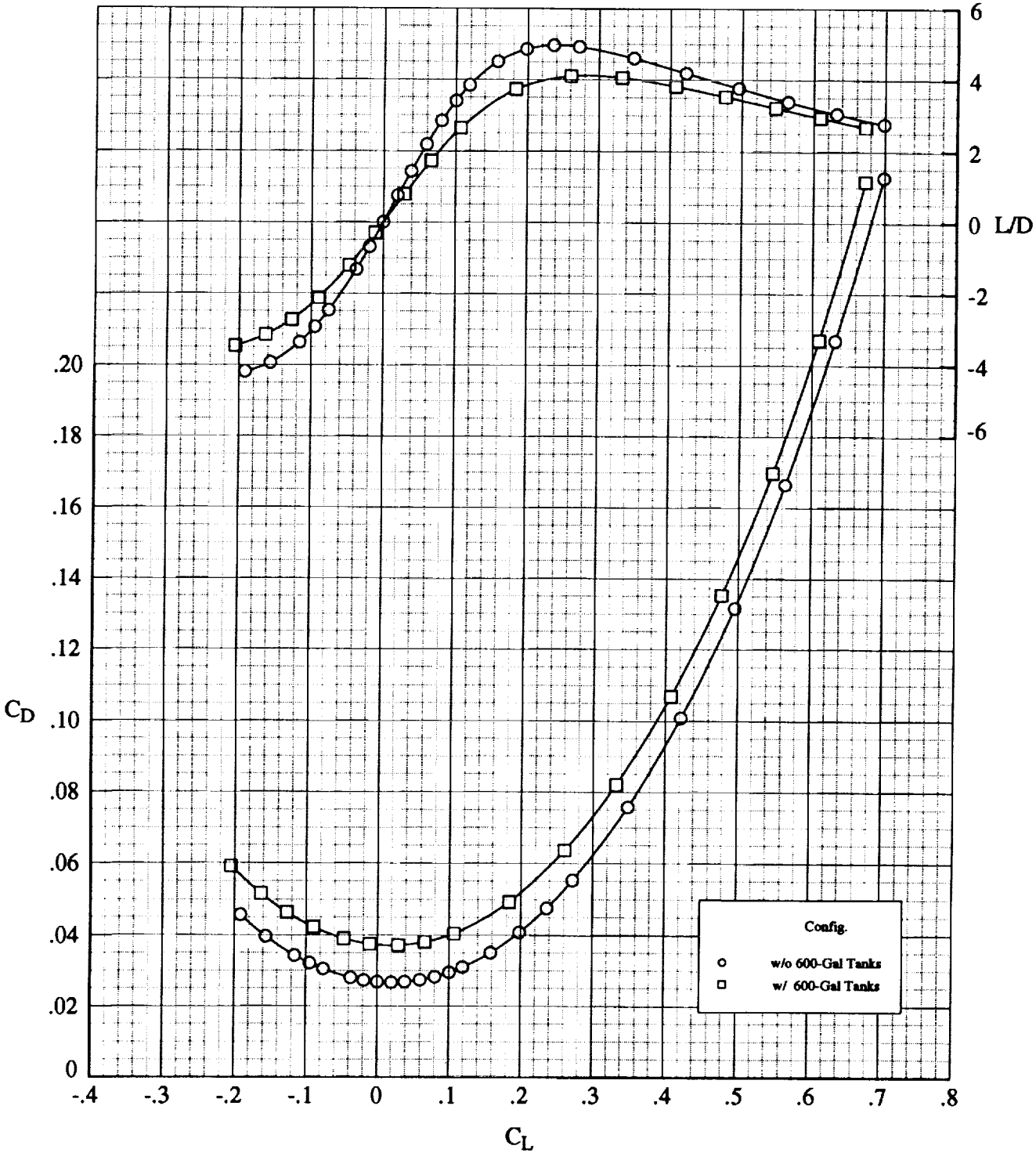

(b) Concluded.

Figure 27. Concluded.

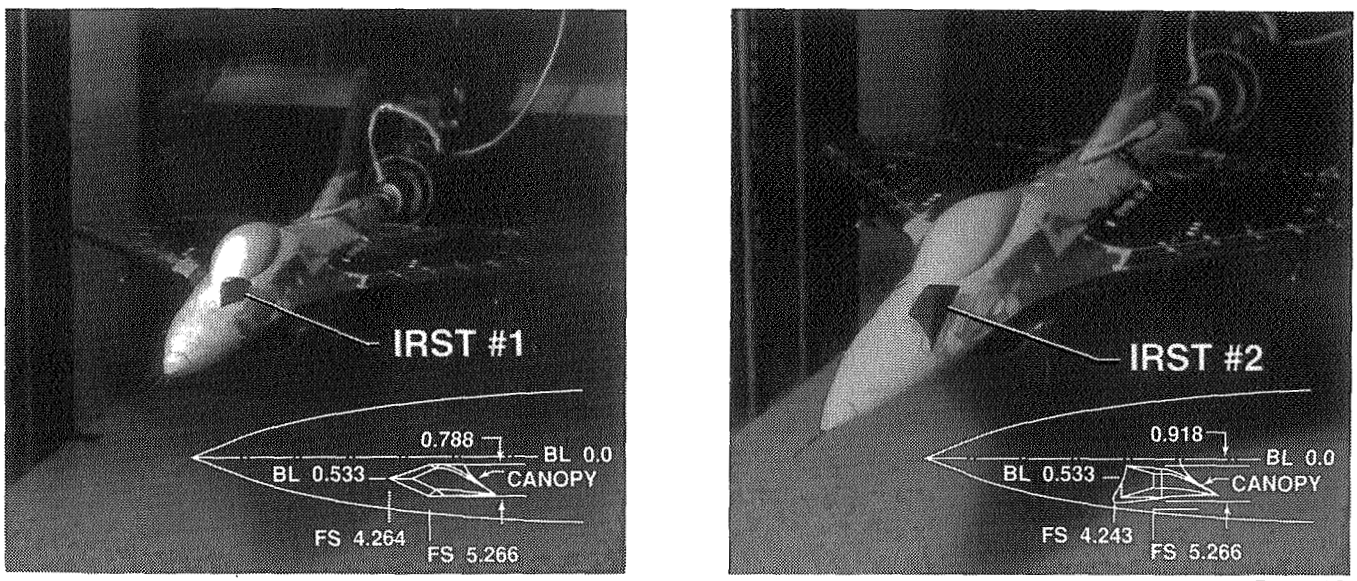

L-93-18

Figure 28. Baseline model with IRST fairings.

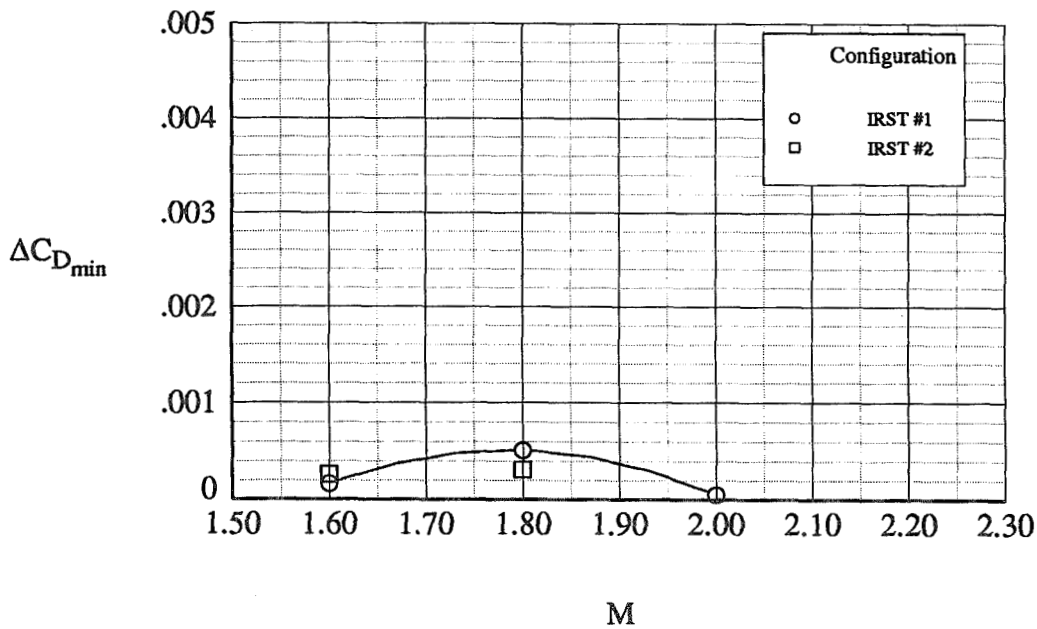

Figure 29. Minimum drag effects of IRST fairings installed on baseline model.

C-2

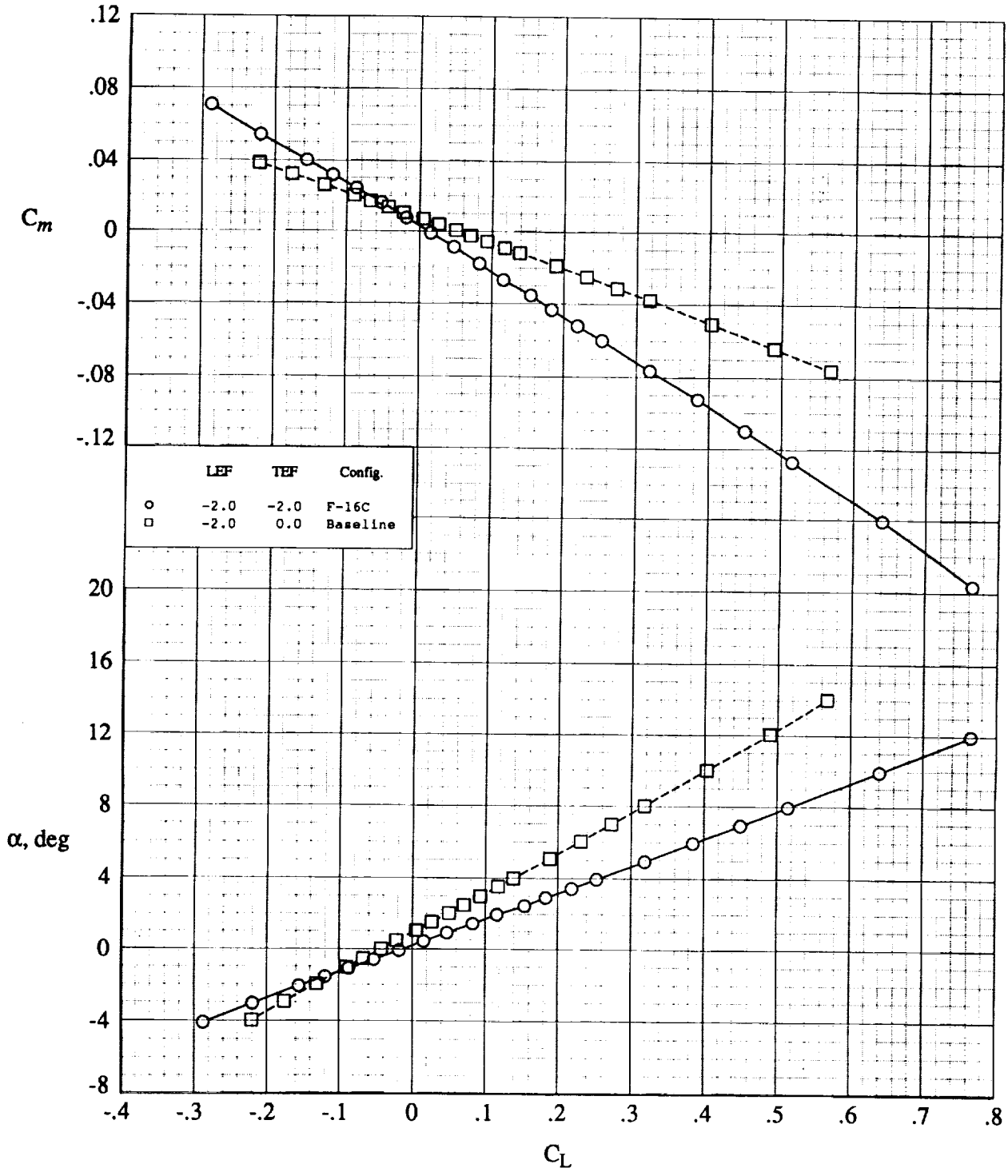

Figure 30. Longitudinal aerodynamic characteristics at $M = 1.60$ for baseline ($S_{\text{ref}} = 2.8$ ft^2; $\text{CG}_{\text{ref}} = 0.30\bar{c}$) versus F-16C ($S_{\text{ref}} = 1.333$ ft^2; $\text{CG}_{\text{ref}} = 0.35\bar{c}$).

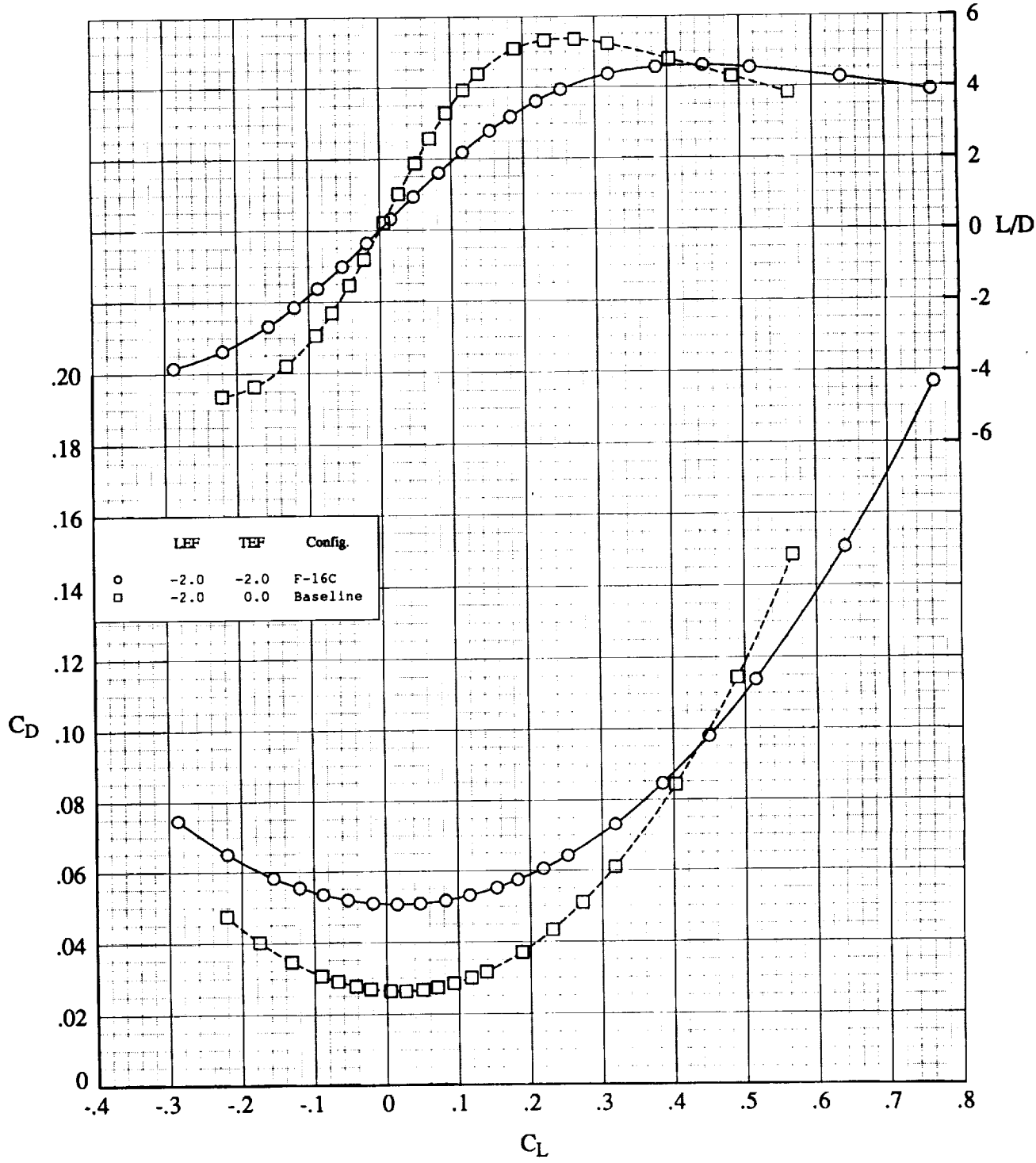

Figure 30. Concluded.

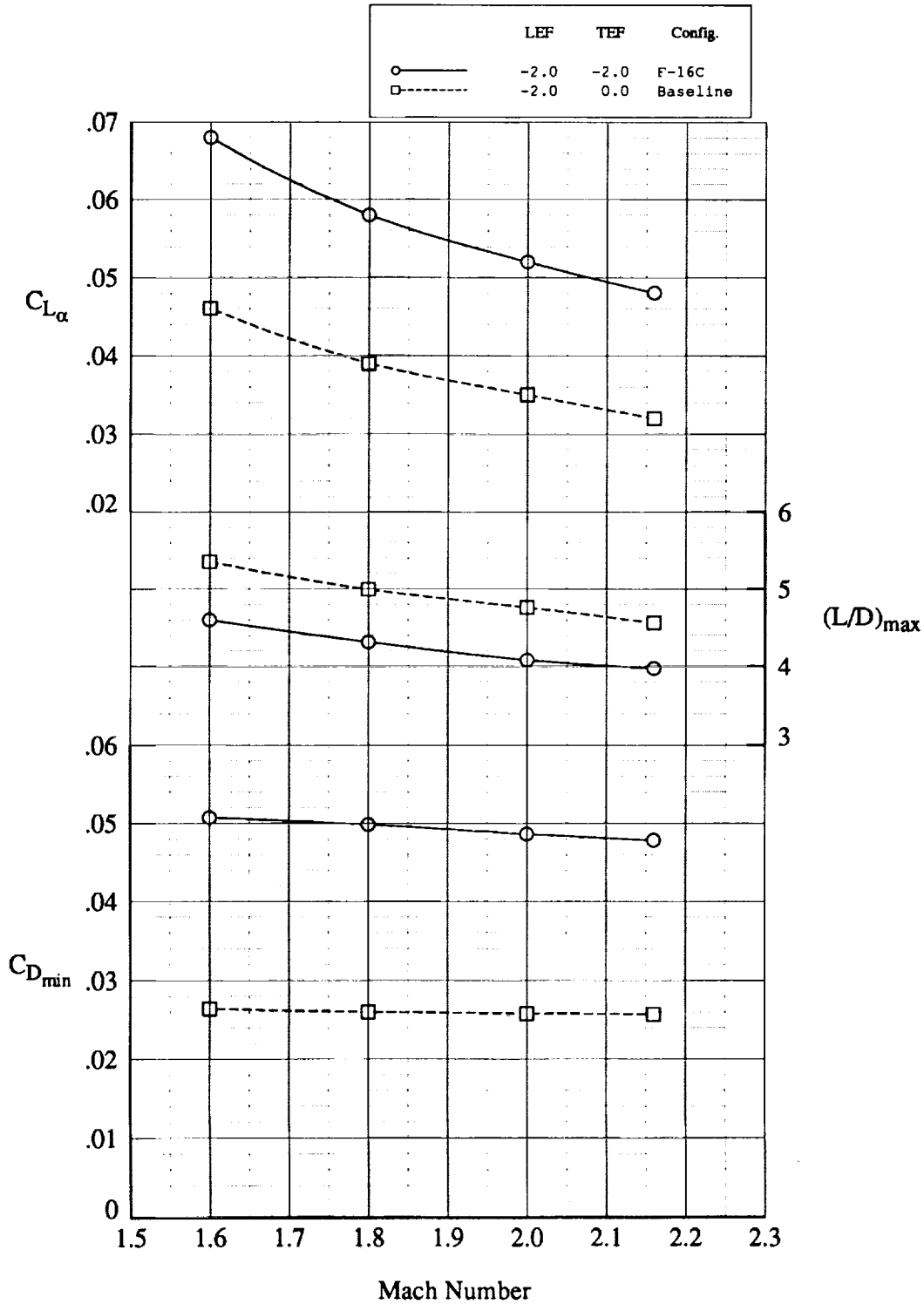

Figure 31. Longitudinal aerodynamic summary for baseline (S_{ref} = 2.8 ft^2; CG_{ref} = 0.30$\bar{c}$) versus F-16C (S_{ref} = 1.333 ft^2; CG_{ref} = 0.35$\bar{c}$).

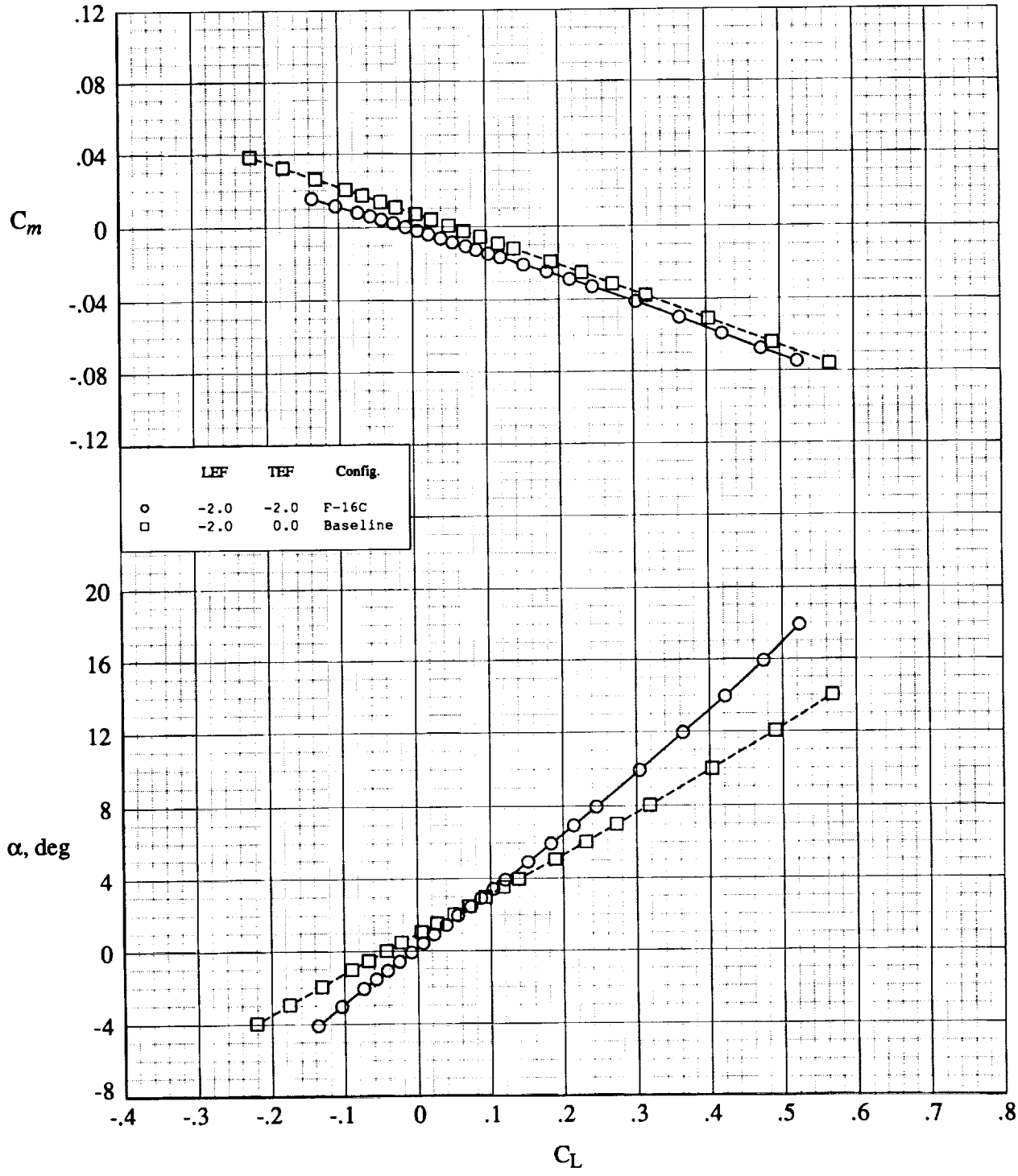

Figure 32. Longitudinal aerodynamic characteristics at $M = 1.60$ for baseline model ($CG_{ref} = 0.30\bar{c}$) versus F-16C ($CG_{ref} = 0.35\bar{c}$), based on common reference geometry.

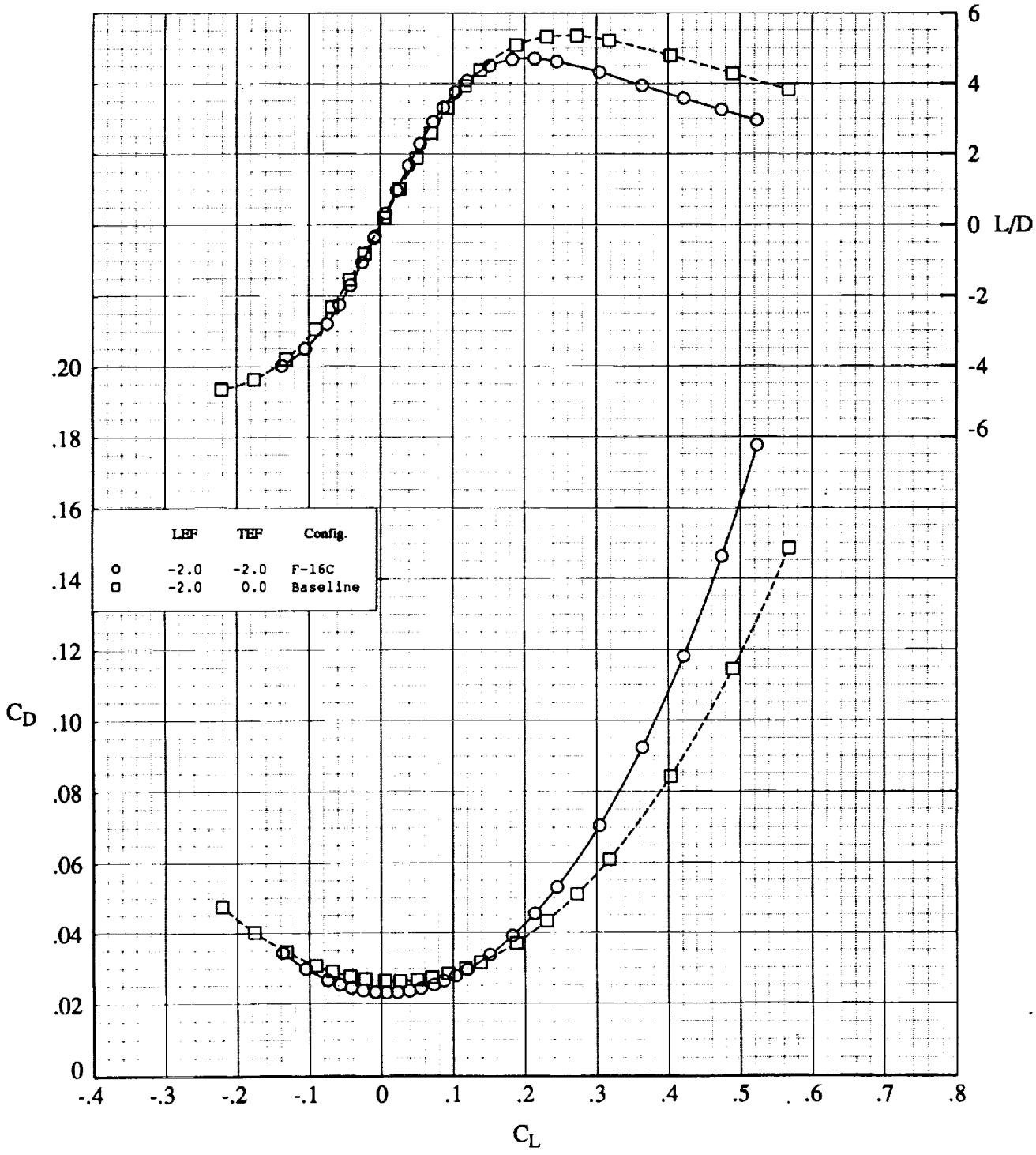

Figure 32. Concluded.

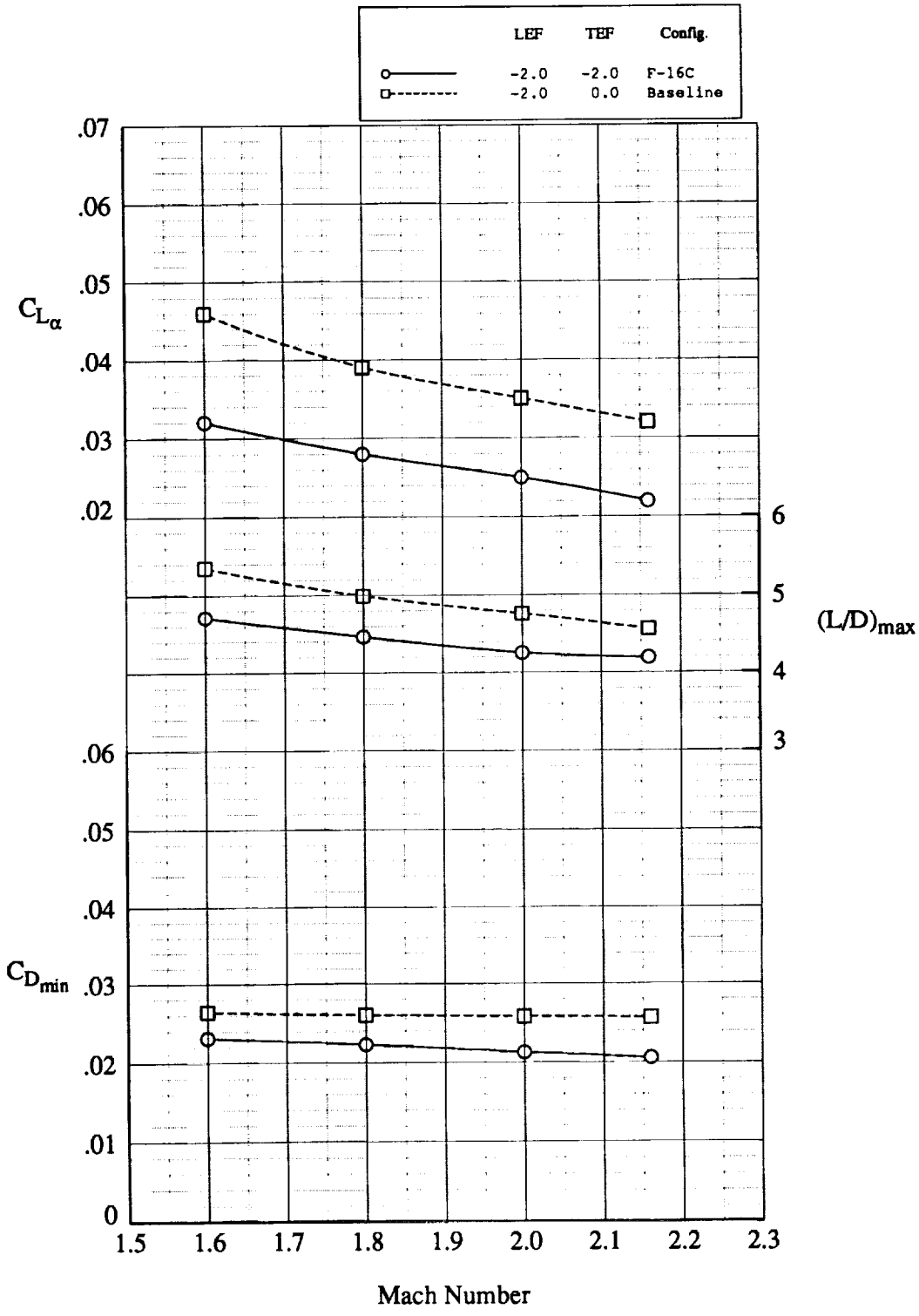

Figure 33. Longitudinal aerodynamic summary for baseline ($CG_{ref} = 0.30\bar{c}$) versus F-16C ($CG_{ref} = 0.35\bar{c}$), based on common reference geometry ($S_{ref} = 2.8$ ft^2; $\bar{c} = 17.555$ in.).

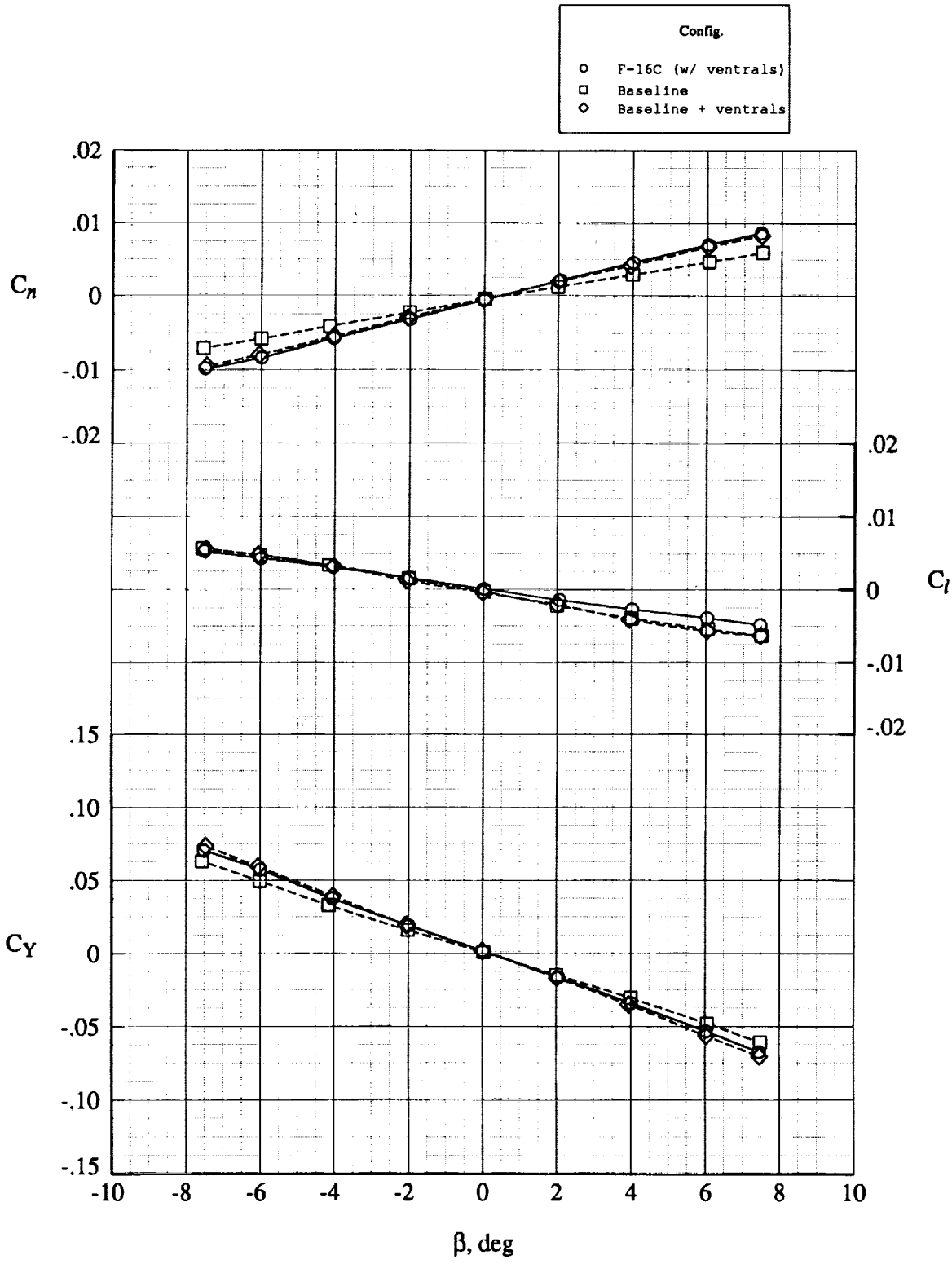

(a) $M = 1.60$.

Figure 34. Lateral-directional aerodynamic comparison for baseline model versus F-16C, based on common reference geometry ($S_{ref} = 2.8$ ft^2; $b = 27.753$ in.) with CG_{ref} = FS 21.683 and $\alpha = 0°$.

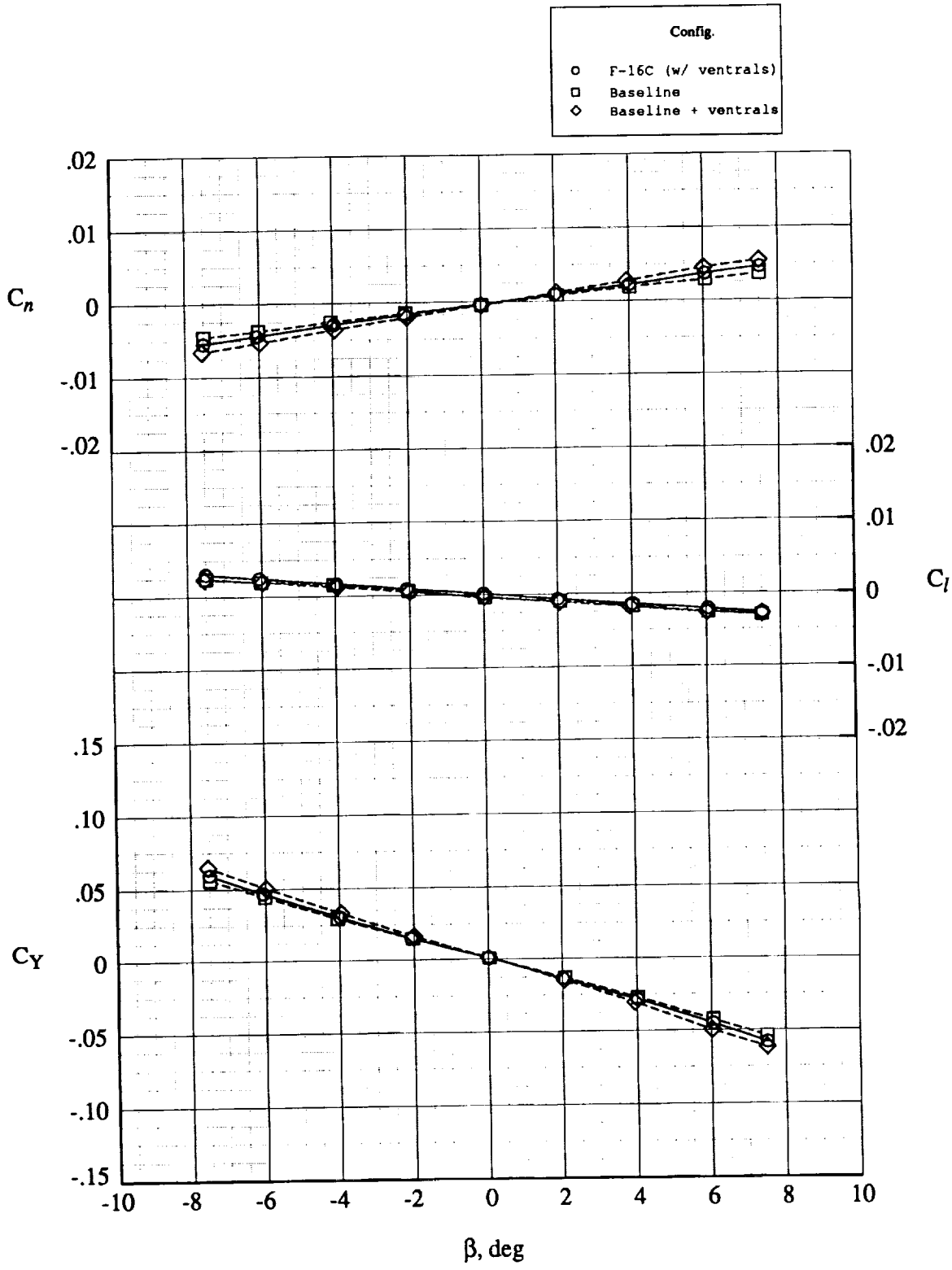

(b) $M = 2.00$.

Figure 34. Concluded.

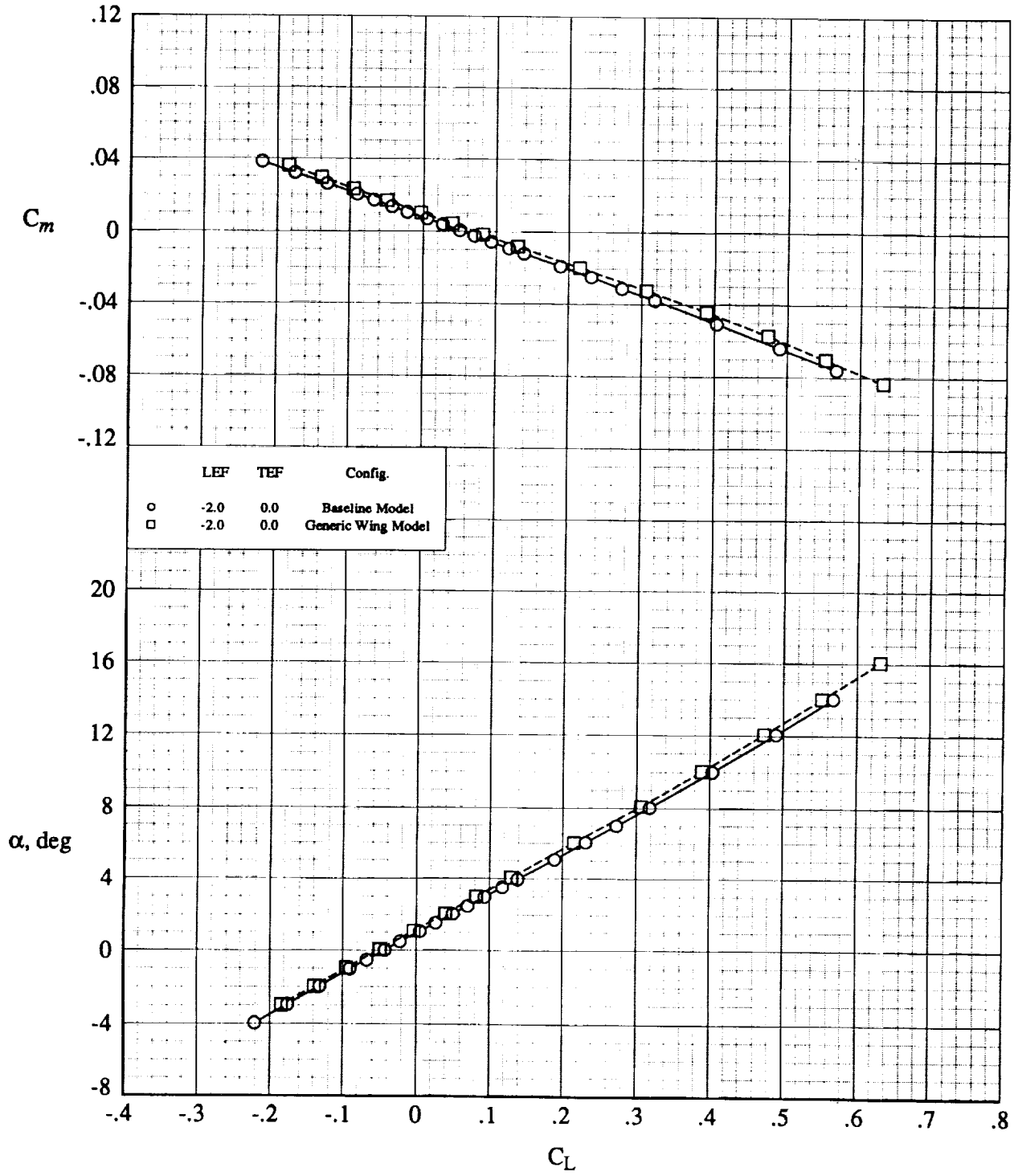

(a) $M = 1.60$.

Figure 35. Untrimmed longitudinal characteristics for baseline versus generic wing models. MRC $= 0.30\,\bar{c}$.

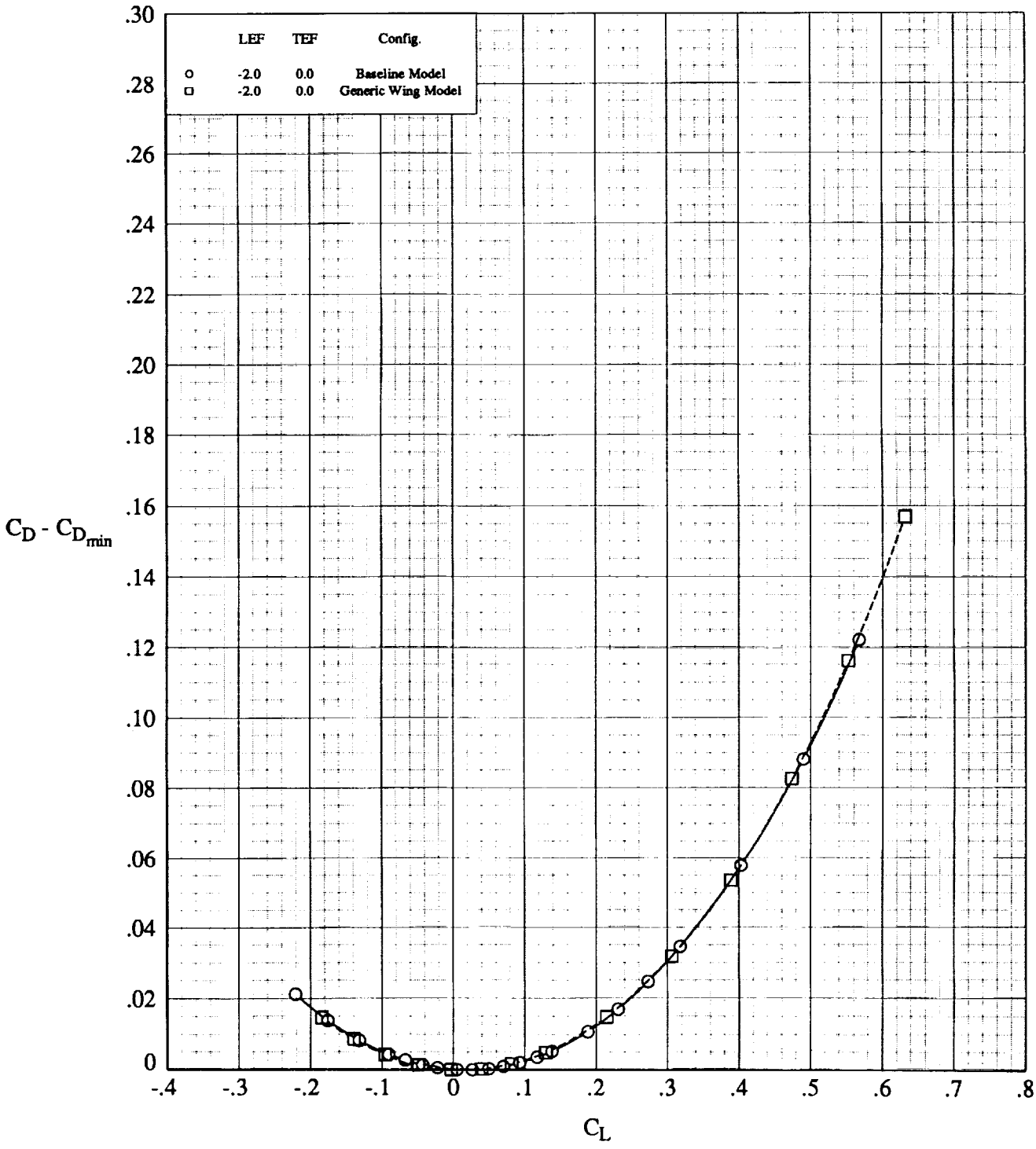

(a) Concluded.

Figure 35. Continued.

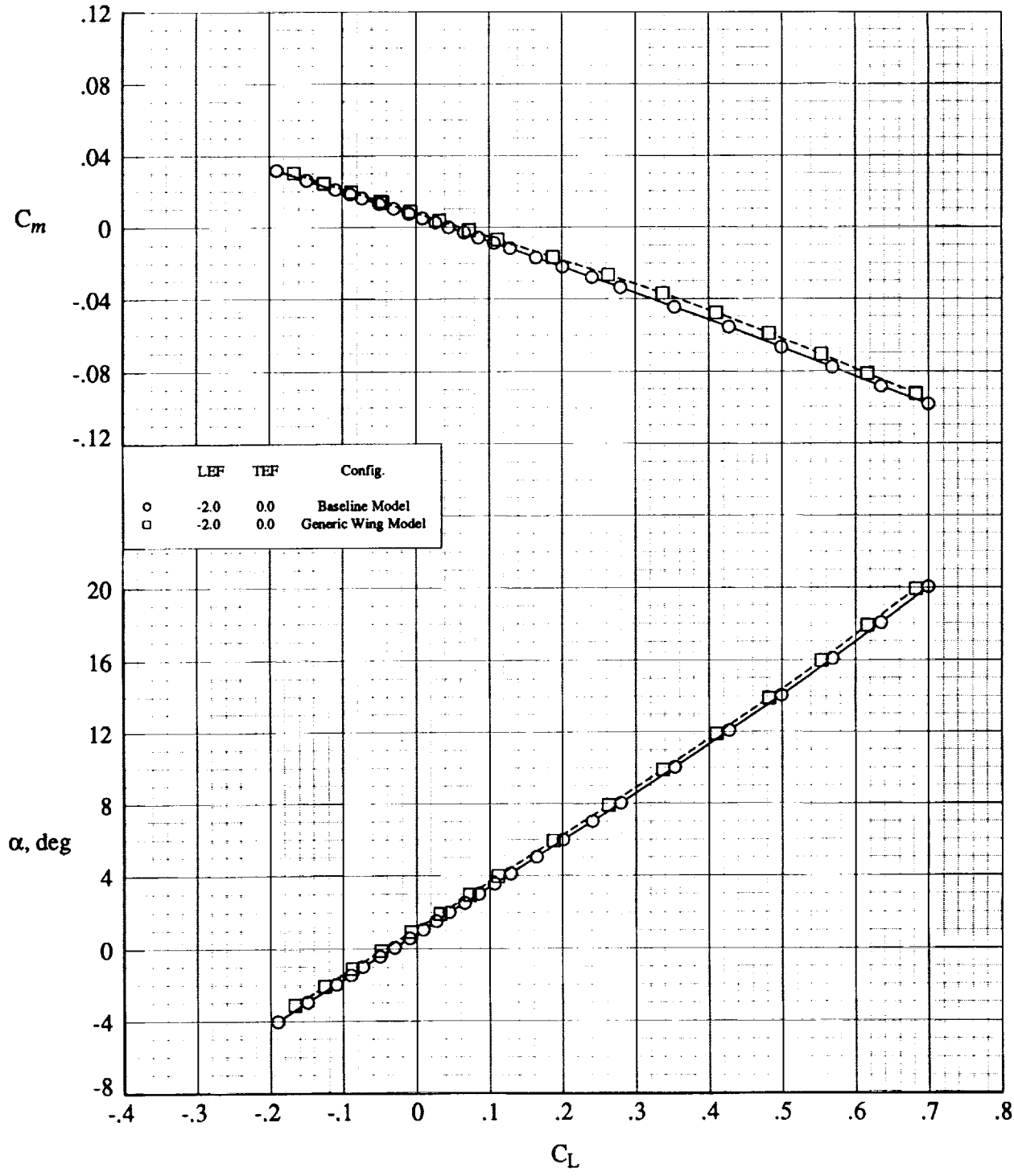

(b) $M = 1.80$.

Figure 35. Continued.

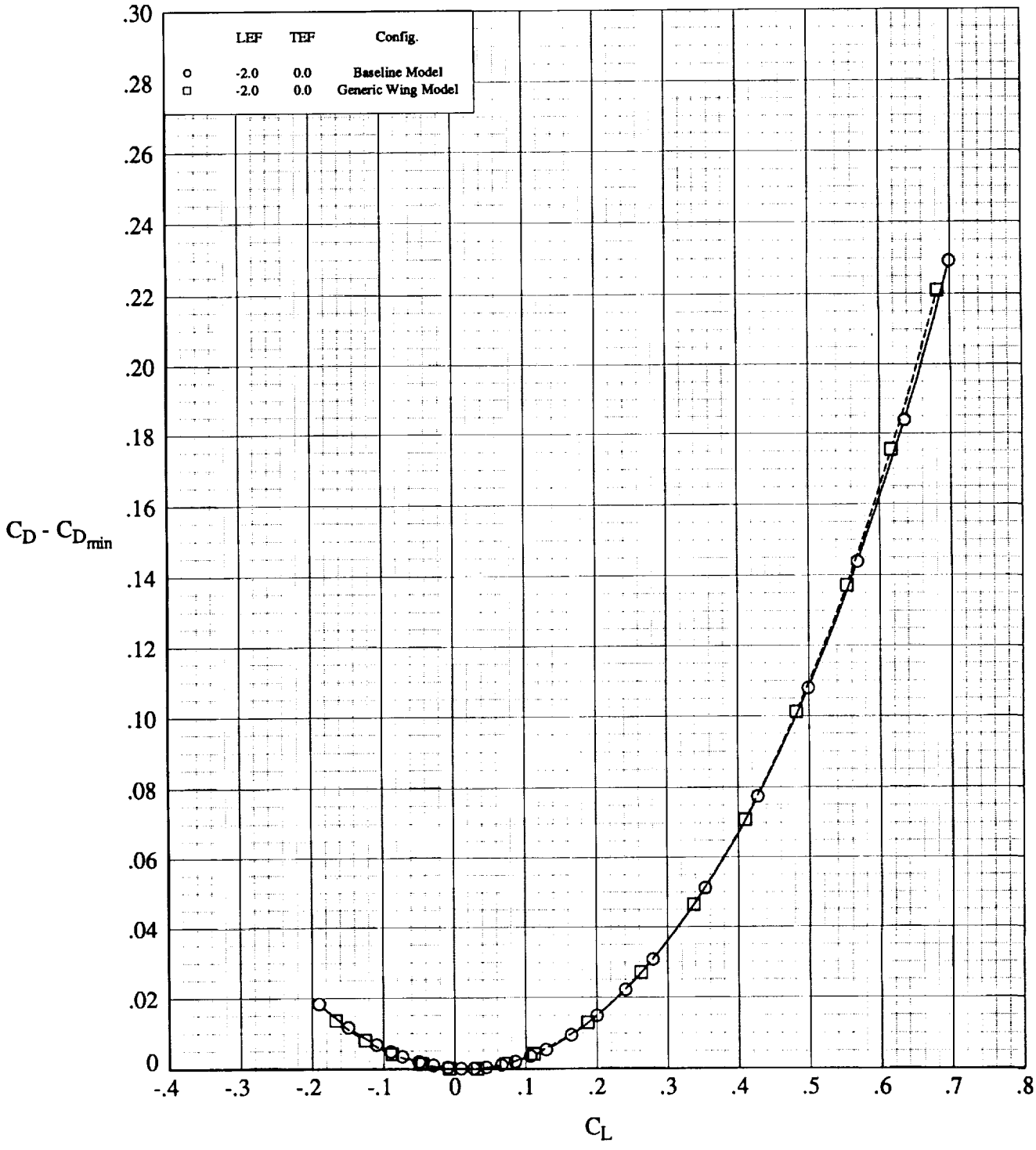

(b) Concluded.

Figure 35. Continued.

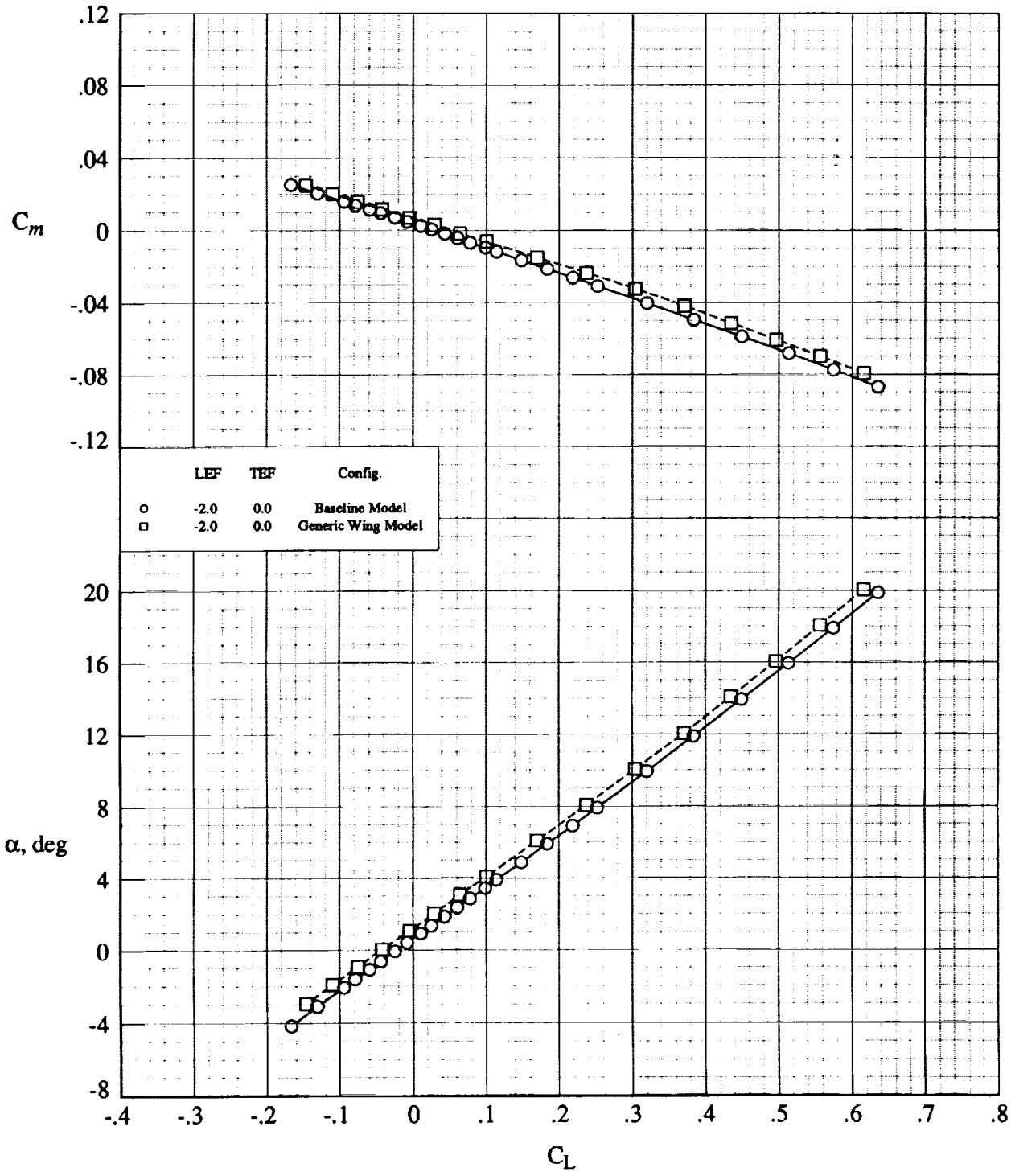

(c) $M = 2.00$.

Figure 35. Continued.

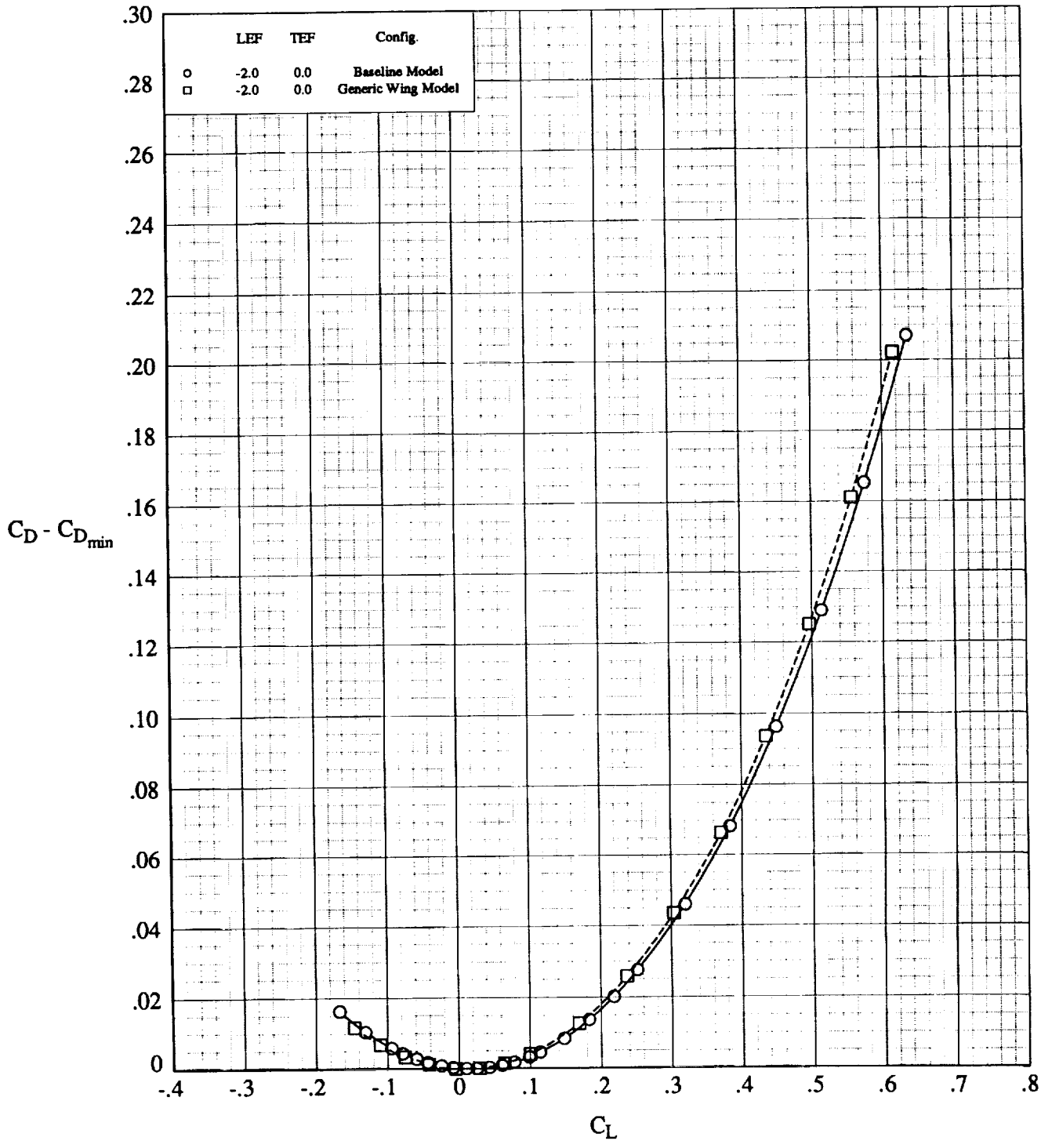

(c) Concluded.

Figure 35. Continued.

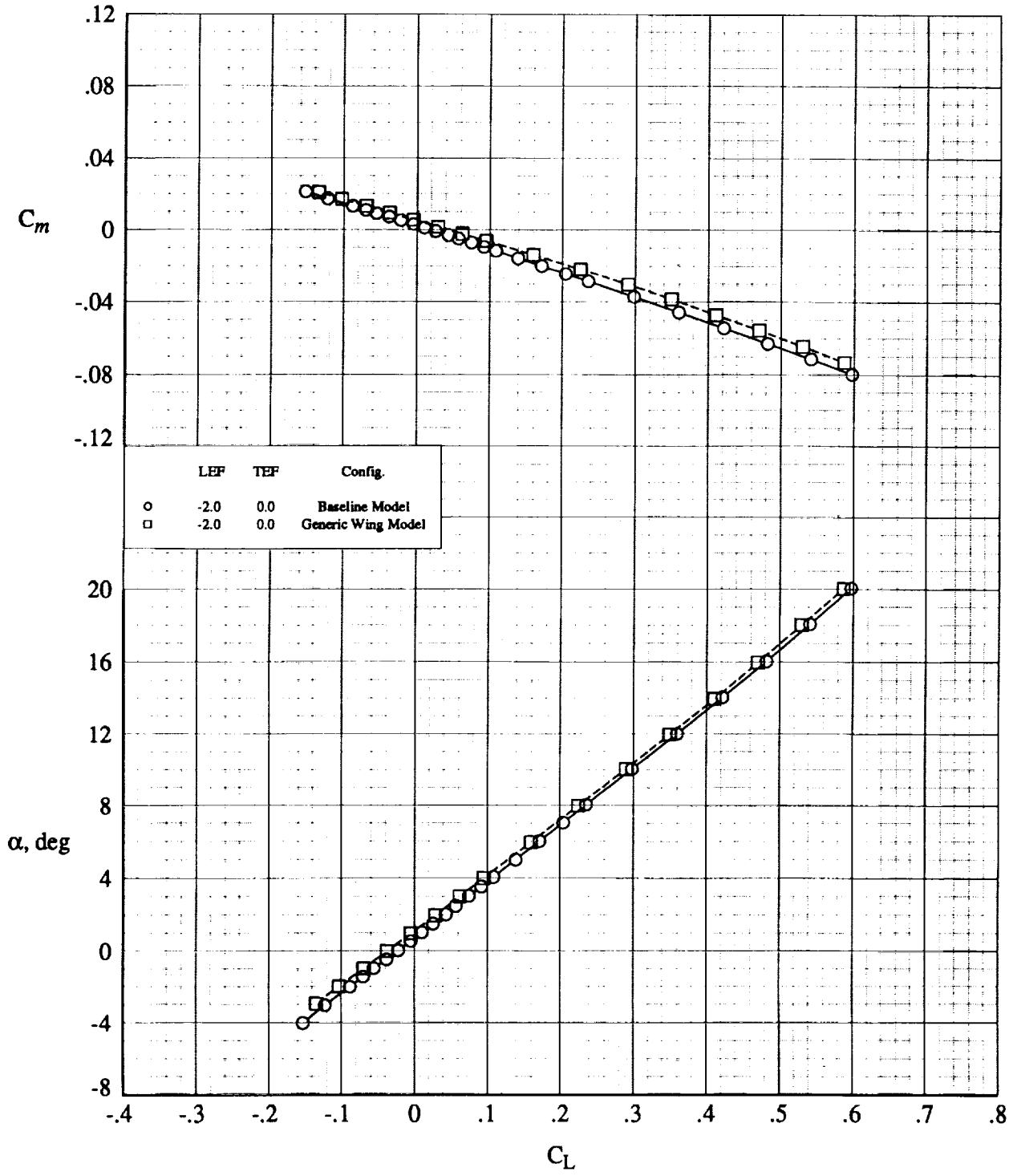

(d) $M = 2.16$.

Figure 35. Continued.

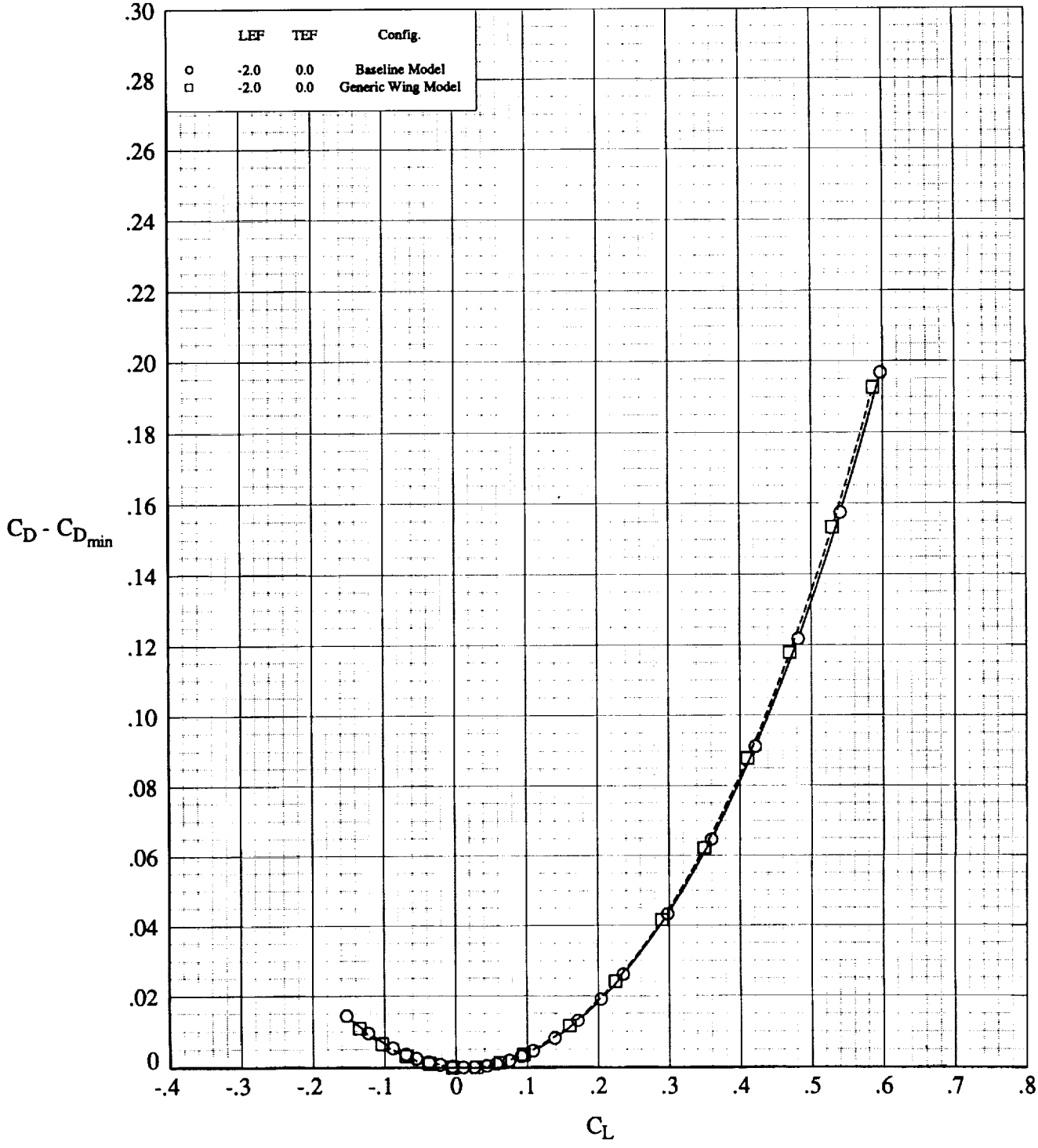

(d) Concluded.

Figure 35. Concluded.

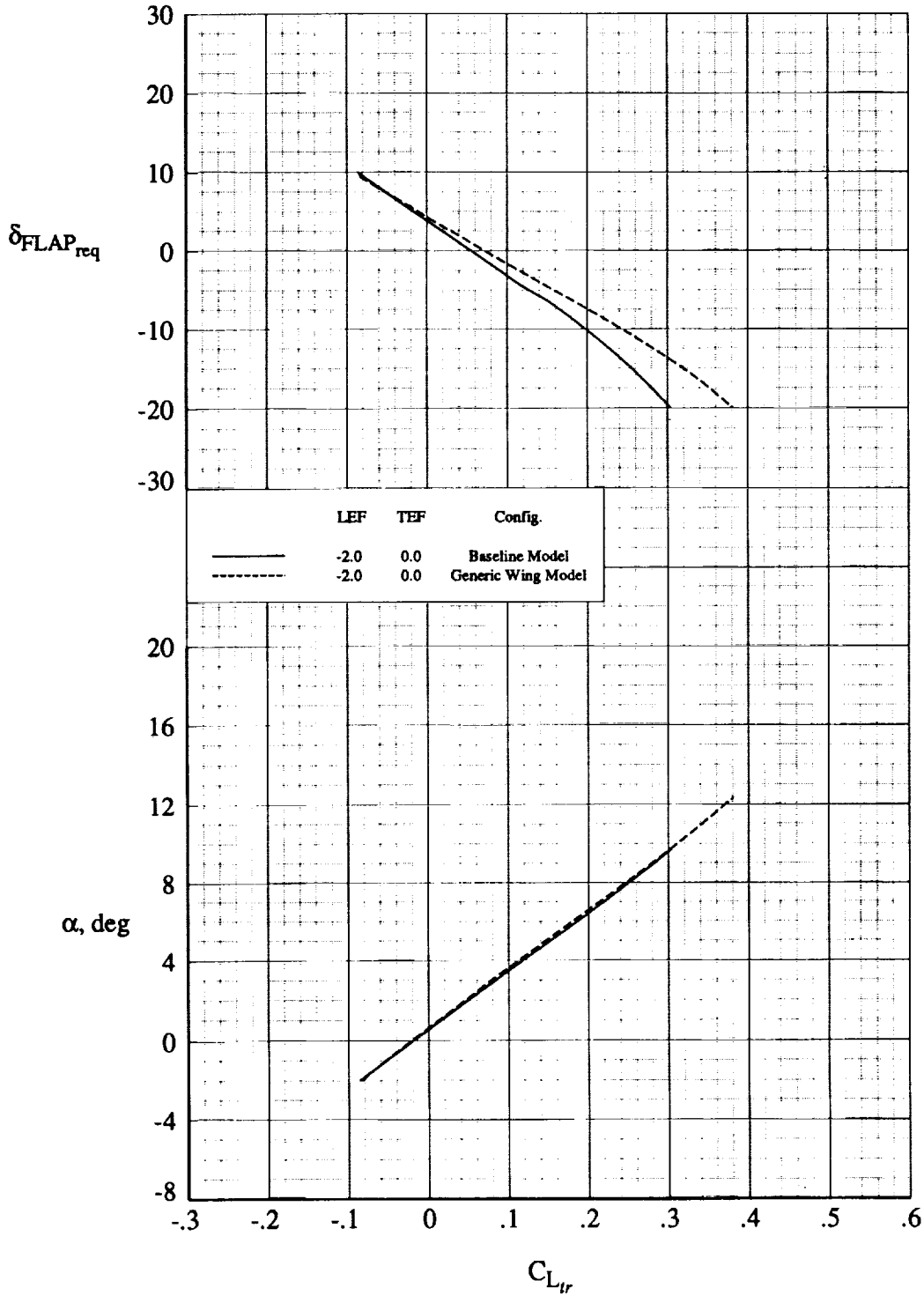

(a) $M = 1.60$.

Figure 36. Trimmed longitudinal characteristics for baseline versus generic wing models. MRC = $0.30\bar{c}$.

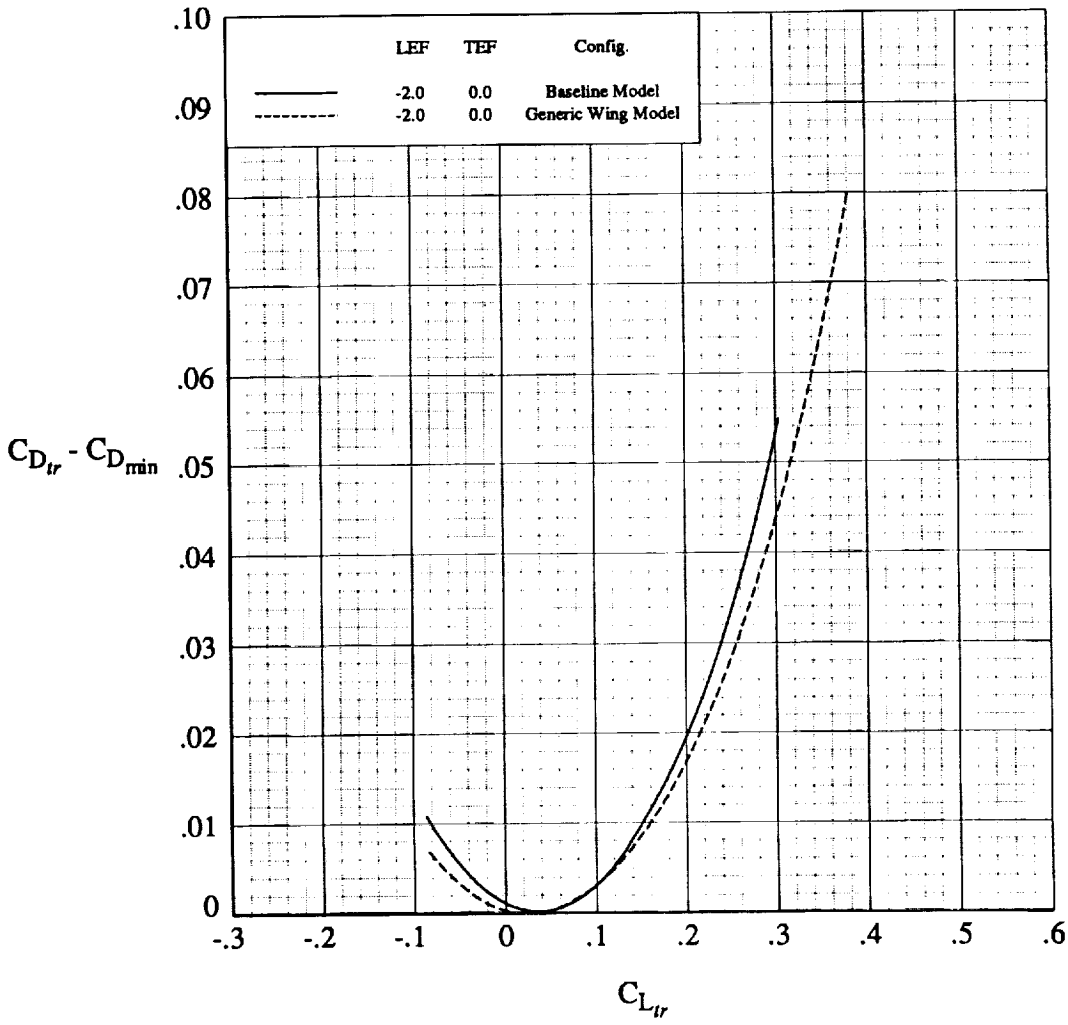

(a) Concluded.

Figure 36. Continued.

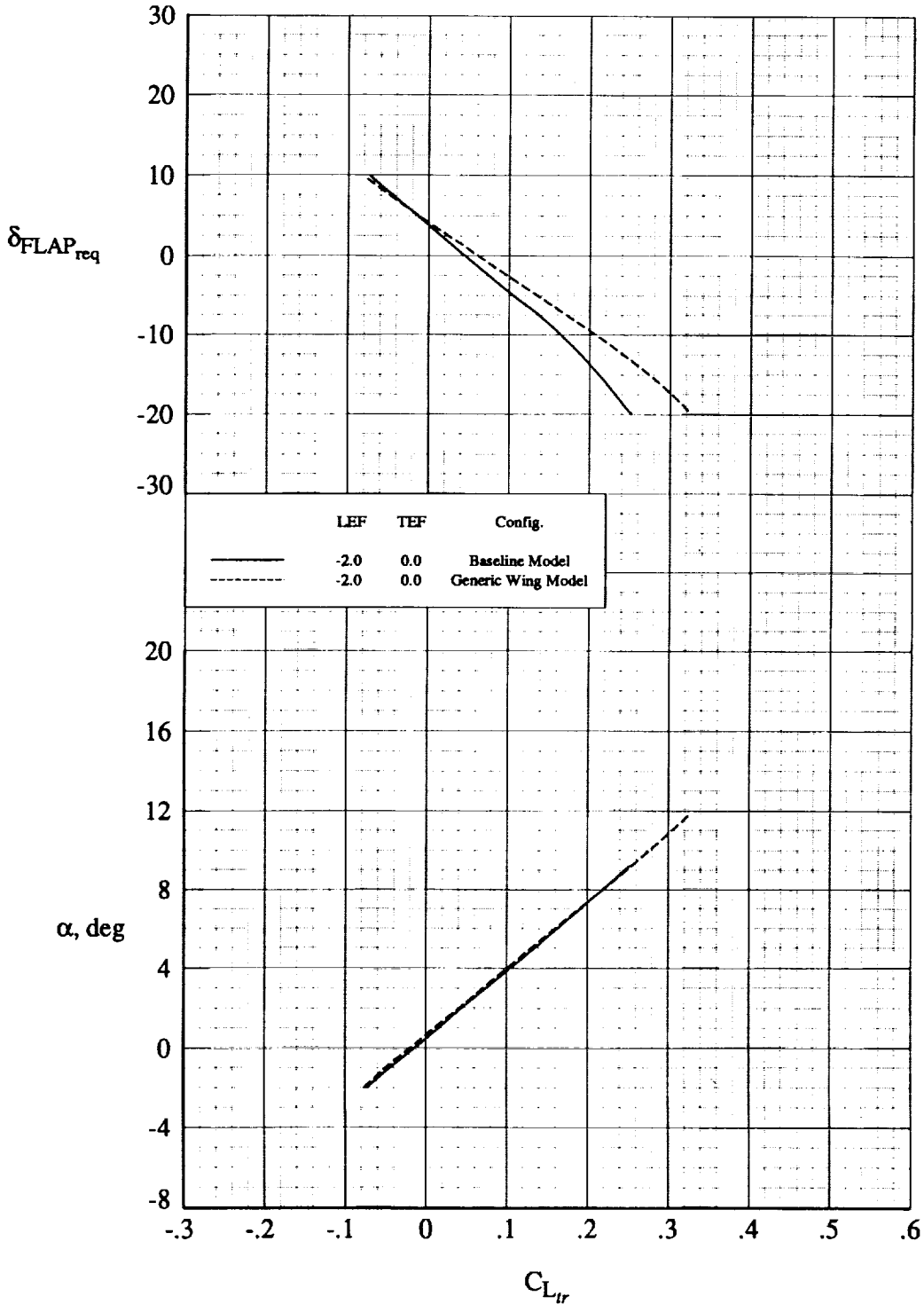

(b) $M = 1.80$.

Figure 36. Continued.

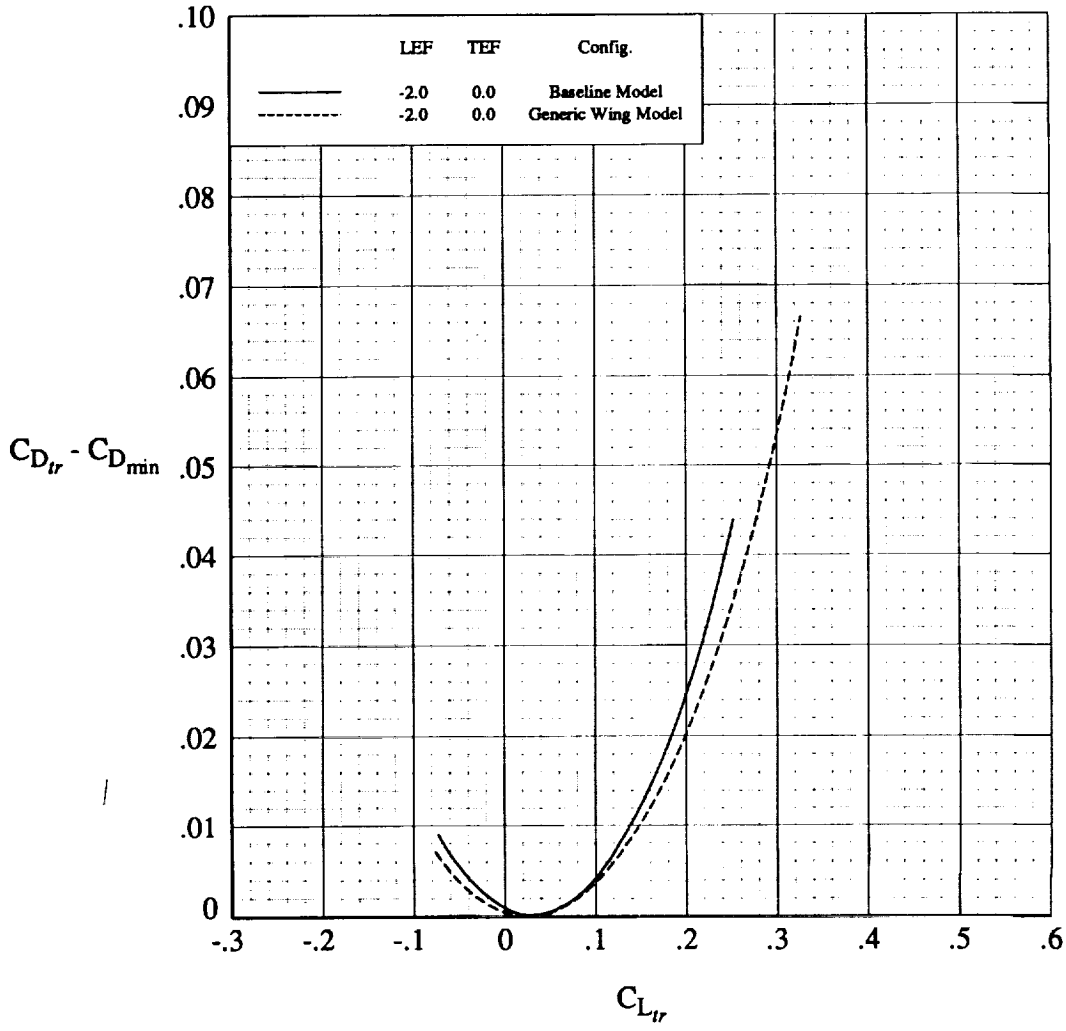

(b) Concluded.

Figure 36. Continued.

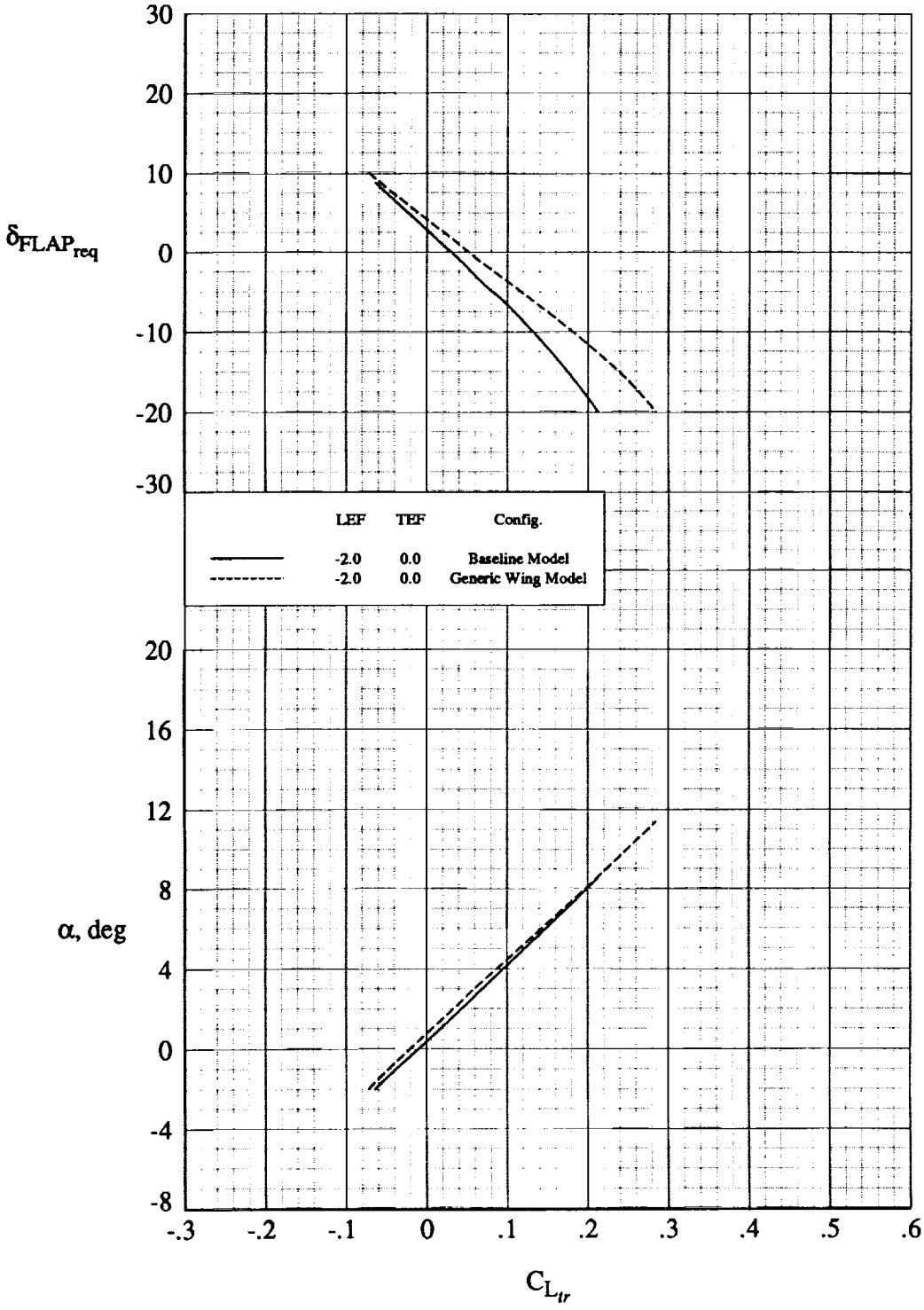

(c) $M = 2.00$.

Figure 36. Continued.

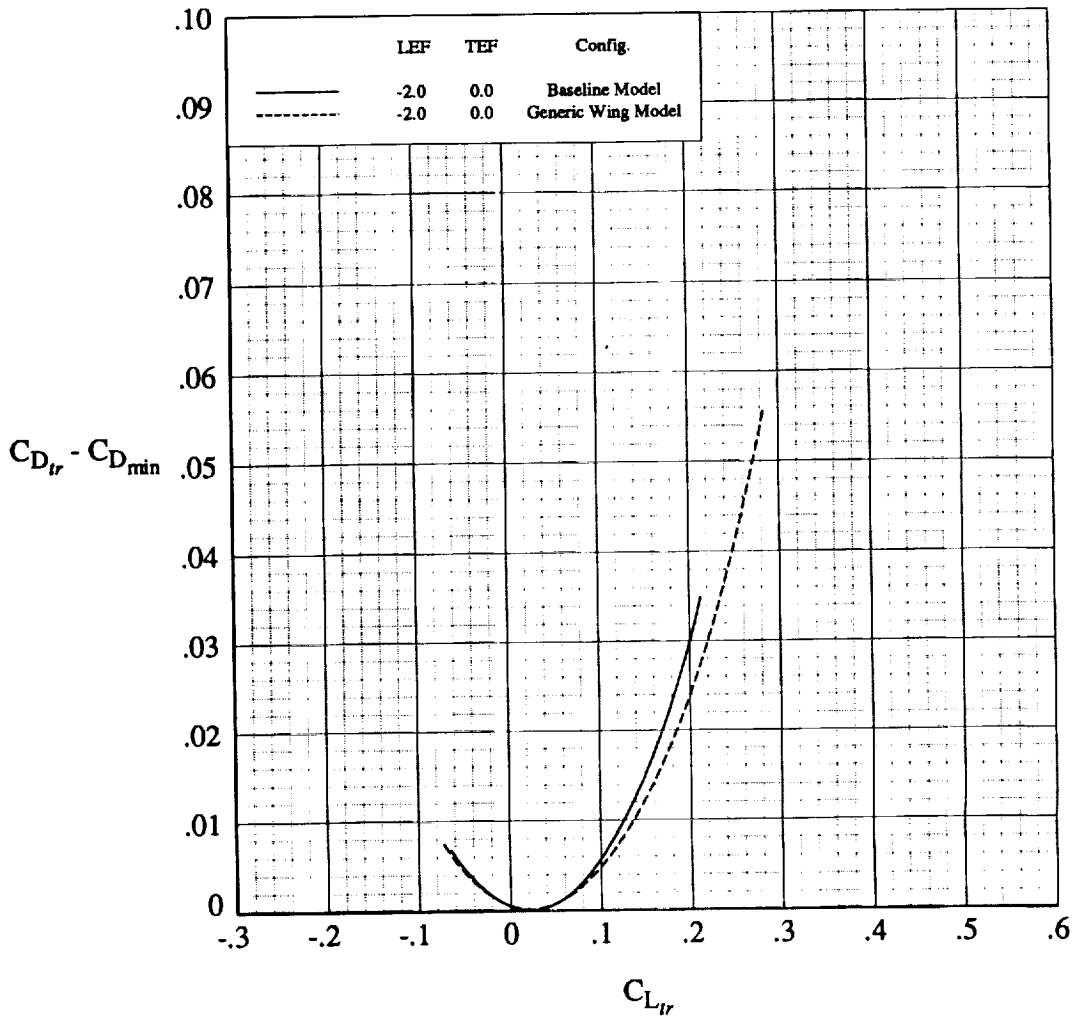

(c) Concluded.

Figure 36. Continued.

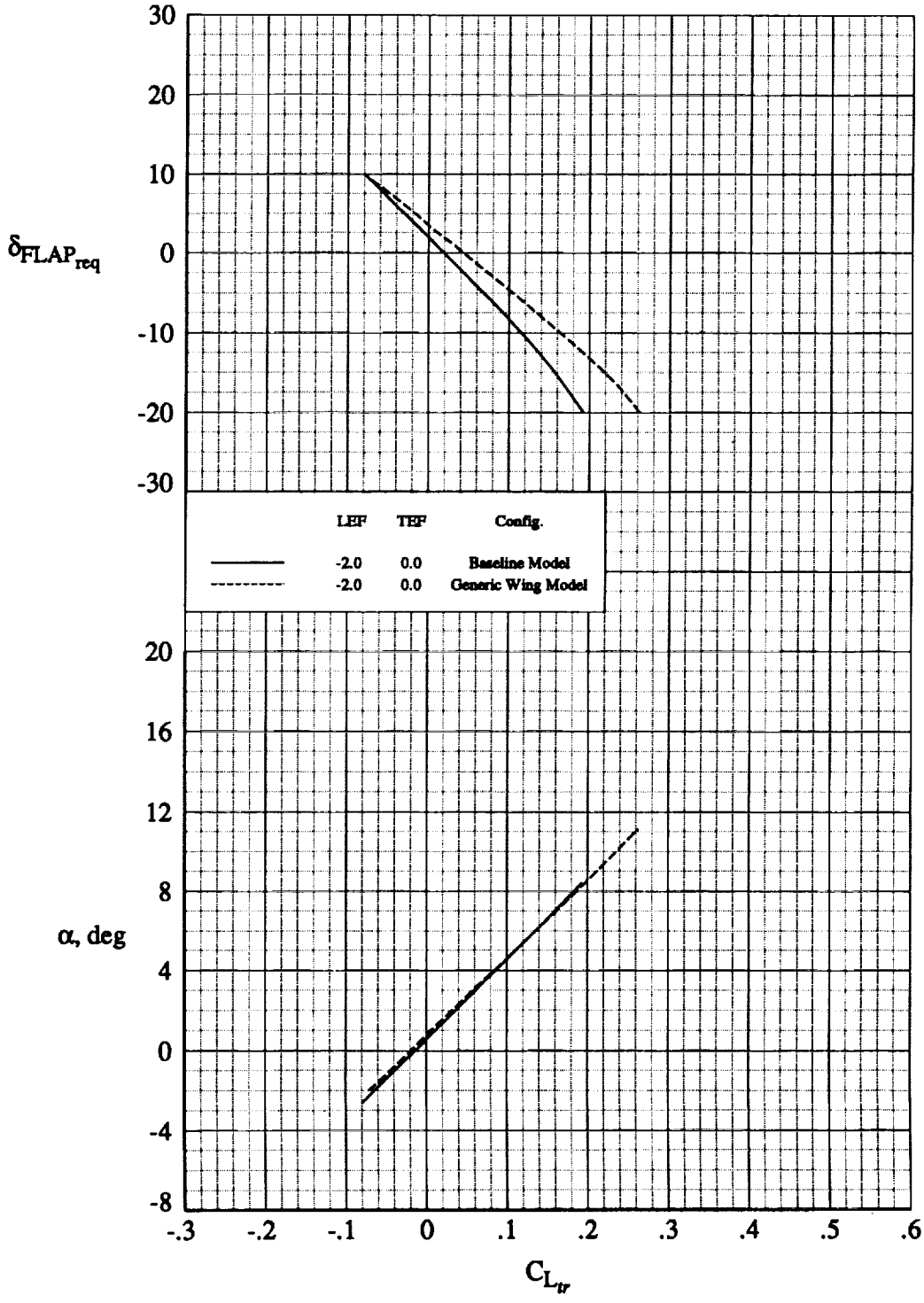

(d) $M = 2.16$.

Figure 36. Continued.

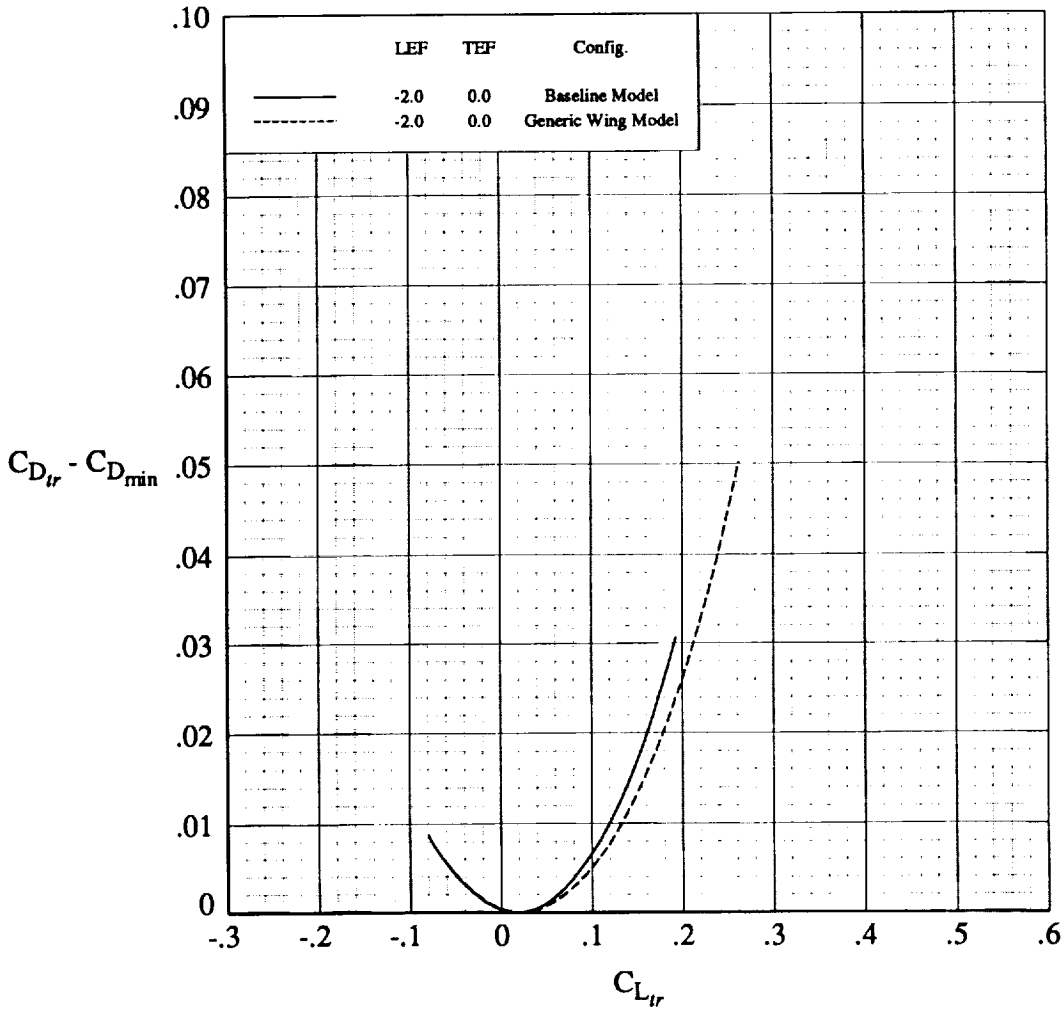

(d) Concluded.

Figure 36. Concluded.

*U.S. GOVERNMENT PRINTING OFFICE: 1993-728-150/60063

REPORT DOCUMENTATION PAGE

Form Approved
OMB No. 0704-0188

Public reporting burden for this collection of information is estimated to average 1 hour per response, including the time for reviewing instructions, searching existing data sources, gathering and maintaining the data needed, and completing and reviewing the collection of information. Send comments regarding this burden estimate or any other aspect of this collection of information, including suggestions for reducing this burden, to Washington Headquarters Services, Directorate for Information Operations and Reports, 1215 Jefferson Davis Highway, Suite 1204, Arlington, VA 22202-4302, and to the Office of Management and Budget, Paperwork Reduction Project (0704-0188), Washington, DC 20503.

1. AGENCY USE ONLY *(Leave blank)*	2. REPORT DATE	3. REPORT TYPE AND DATES COVERED
	July 1993	Technical Paper

4. TITLE AND SUBTITLE
Supersonic Aerodynamic Characteristics of an Advanced F-16 Derivative Aircraft Configuration

5. FUNDING NUMBERS
WU 505-59-30-01

6. AUTHOR(S)
Mike C. Fox and Dana K. Forrest

7. PERFORMING ORGANIZATION NAME(S) AND ADDRESS(ES)
NASA Langley Research Center
Hampton, VA 23681-0001

8. PERFORMING ORGANIZATION REPORT NUMBER
L-17143

9. SPONSORING/MONITORING AGENCY NAME(S) AND ADDRESS(ES)
National Aeronautics and Space Administration
Washington, DC 20546-0001

10. SPONSORING/MONITORING AGENCY REPORT NUMBER
NASA TP-3355

11. SUPPLEMENTARY NOTES
Fox: ViGYAN, Inc., Hampton, VA; Forrest: Langley Research Center, Hampton, VA.
This research was supported in part by the National Aeronautics and Space Administration under Contract NAS1-18585.

12a. DISTRIBUTION/AVAILABILITY STATEMENT
Unclassified Unlimited

Subject Category 02

12b. DISTRIBUTION CODE

13. ABSTRACT *(Maximum 200 words)*
A supersonic wind tunnel investigation was conducted in the NASA Langley Unitary Plan Wind Tunnel on an advanced derivative configuration of the United States Air Force F-16 fighter. Longitudinal and lateral-directional force and moment data were obtained at Mach numbers of 1.60 to 2.16 to evaluate basic performance parameters and control effectiveness. The aerodynamic characteristics for the F-16 derivative model were compared with the data obtained for the F-16C model and also with a previously tested generic wing model that features an identical planform shape and similar twist distribution.

14. SUBJECT TERMS	15. NUMBER OF PAGES
Supersonic aerodynamics; Fighter configurations; Delta wings; Wind tunnel tests	120
	16. PRICE CODE A06

17. SECURITY CLASSIFICATION OF REPORT	18. SECURITY CLASSIFICATION OF THIS PAGE	19. SECURITY CLASSIFICATION OF ABSTRACT	20. LIMITATION OF ABSTRACT
Unclassified	Unclassified		